THE NORDIC CONCRETE FEDERATION 1/2013 PUBLICATION NO. 47

Nordic Concrete Research

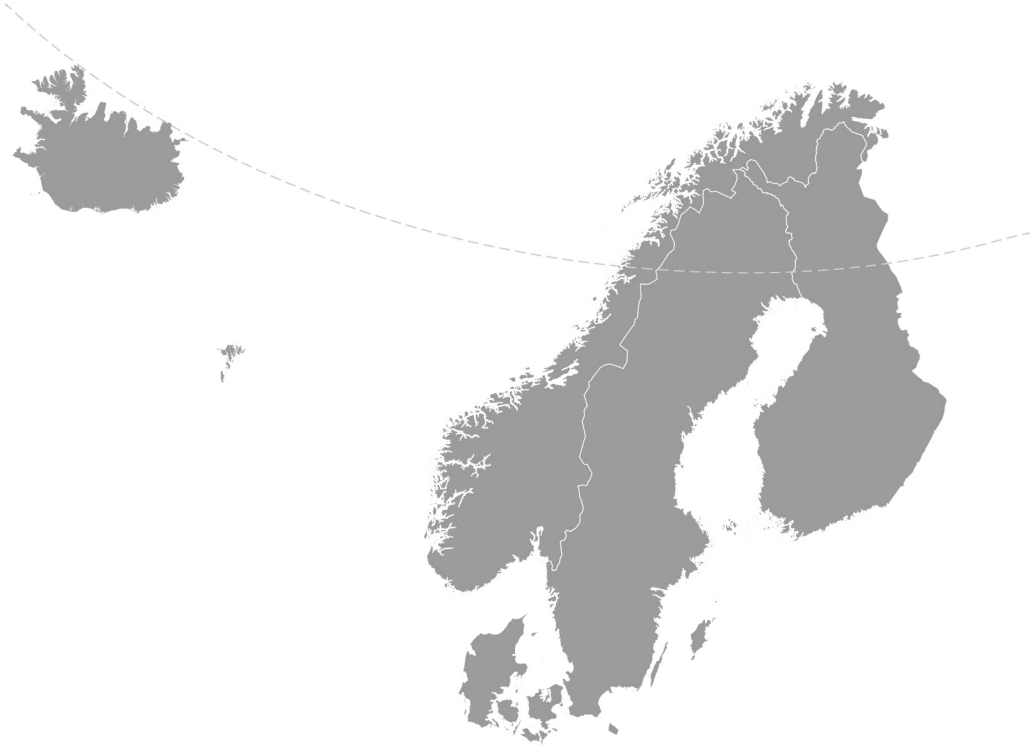

Nordic Concrete Federation

PUBLICATION NO. 47 1/2013

NORDIC CONCRETE RESEARCH

EDITED BY
THE NORDIC CONCRETE FEDERATION

CONCRETE ASSOCIATIONS OF: DENMARK
FINLAND
ICELAND
NORWAY
SWEDEN

PUBLISHER: NORSK BETONGFORENING
POSTBOKS 2312, SOLLI
N - 0201 OSLO
NORWAY

VODSKOV, JUNE 2013

Preface

Nordic Concrete Research is since 1982 the leading scientific journal concerning concrete research in the five Nordic countries, e.g., Denmark, Finland, Iceland, Norway and Sweden. The content of Nordic Concrete Research reflects the major trends in the concrete research.

Nordic Concrete Research is published by the Nordic Concrete Federation which also organizes the Nordic Concrete Research Symposia that have constituted a continuous series since 1953 in Stockholm. The Symposium circulates between the five countries and takes normally place every third year. The next symposium, no. XXII, will be held Reykjavik, Iceland 13 - 15 August 2014, in parallel with the ECO-CRETE conference. More information on the research symposium can be found on the webpage of the Nordic Concrete Federation; www.nordicconcrete.net

Since 1982, 397 papers have been published in the journal. Since 1994 the abstracts and from 1998 both the abstracts and the full papers can be found on the Nordic Concrete Federation's homepage: www.nordicconcrete.org. The journal thus contributes to dissemination of Nordic concrete research, both within the Nordic countries and internationally. We are very pleased, that during the latest years, growing interests in participating in the Nordic Concrete Research symposia, as well as for publishing in NCR have been observed.

The high quality of the papers in NCR are ensured by the group of reviewers presented on the last page. All papers are reviewed by three of these, chosen according to their expert knowledge.

Since 1975, 75 Nordic Miniseminars have been held – it is the experience of the Research Council of the Nordic Concrete Federation, that these Miniseminars have a marked influence on concrete research in the Nordic countries. In some cases, the information gathered during such Miniseminars has been used as Nordic input to CEN activities.

Vodskov, June 2013

Dirch H. Bager
Editor, Nordic Concrete Research

PUBLICATION NO. 47 1/2013

CONTENTS

Verification of Design Basis for a Foundation Slab Cast with SFRSCC – Results from Full Scale Beam Testing

Lars Nyholm Thrane
Consultant, M.Sc., Ph.D.
Danish Technological Institute
Gregersensvej, DK 2630 Taastrup
E-mail: lnth@teknologisk.dk

Jens Ole Frederiksen
Chief Consultant, M.Sc.
Danish Technological Institute
Gregersensvej, DK 2630 Taastrup
E-mail: jlf@teknologisk.dk

Thomas Pilegaard Madsen
Consultant, M.Sc.
Danish Technological Institute
Gregersensvej, DK 2630 Taastrup
E-mail: tpm@teknologisk.dk

Thomas Kasper
Chief Project Manager, Ph.D.
COWI
Parallelvej 2, DK 2800 Kgs. Lyngby
E-mail: tkas@cowi.dk

ABSTRACT

In 2011, the first demonstration project in the Danish steel fibre concrete consortium was carried out. A large foundation slab for a new rainwater basin was cast with steel fibre reinforced SCC (SFRSCC). Two designs were prepared in order to assess the potential benefits of a steel fibre concrete solution i) a conventional reinforcement solution without steel fibres and ii) a combined reinforcement solution including both conventional reinforcement and steel fibres. Both were designed to fulfil the maximum crack width requirement of 0.2 mm, however, the total amount of steel was reduced by 40 % in the combined reinforcement solution. This paper presents results from 4 point bending of full scale beams comparing these two reinforcement solutions. The results verified that the combined reinforcement solution provides similar or enhanced crack control up to crack widths of 0.2 mm.

Key words: steel fibre concrete, scc, mechanical properties, crack width.

1. INTRODUCTION

Combining steel fibres with concrete – resulting in Steel Fibre Reinforced Concrete (SFRC) – has been known since the sixties and the structural use of SFRC has been known and applied for the past 30 years. Steel fibres introduce a ductile behaviour of the concrete and contribute to the load bearing capacity [1-6]. Thus, it may be possible to reduce some of the conventional reinforcement, and obtain steel savings, reduced costs, and improved working environment for the concrete workers on site.

Unfortunately, common European design rules and standards do not exist to account for the ductility of steel fibre reinforced concrete, which is one of the main barriers to overcome for a more common use of steel fibres in structural applications. However, a number of different national and international guidelines have been proposed; see Gylltoft et al. [7] for an overview and comparison of these.

In 2010, a Danish innovation consortium on sustainable concrete structures with steel fibre reinforced concrete was initiated in order to prepare Danish guides on design and execution of SFRC based on the German guideline DAfStb 2010 [8]. The German guideline was selected because it has recently been published as a supplement to the German code DIN1045 and contains detailed design rules in line with Eurocode. The Danish consortium focuses in particular on steel fibre reinforced SCC (SFRSCC), which is potentially an attractive building material and not covered by DAfStb. Firstly, because SCC is known to improve the working environment and productivity [9-11]. Secondly, because the flow of SFRSCC causes fibres to rotate and the fibre orientation can be significant leading to significant anisotropy in the strength, which can be viewed as both a strength and a weakness of the material [12-18]. For instance, Døssland [18] compared the load carrying capacity of beams with SFRC and SFRSCC and found quite a significant increase in moment capacity going from SFRC to SFRSCC due to fibre orientation.

Thus, if flow induced fibre orientation is taken into account, the strength of SFRSCC in a certain direction may be significantly higher than that of conventional SFRC. The positive effect of fibre orientation may be utilised in some types of applications such as beams and walls. However, in slabs, significant fibre orientation in one direction is often not preferred, but SFRSCC is still an attractive building material from an overall sustainability point of view. Therefore, to study the applicability of SFRSCC for load carrying foundations slabs, a large foundation slab for a new rainwater basin was selected as the first full scale demonstration project (Figure 1). The slab dimensions were 50 m x 20 m x 0.4 m and it was cast with a C40/50 SFRSCC. The total amount of concrete was 380 m^3.

Figure 1 – Construction of the foundation slab cast with SFRSCC.

To assess the benefits of a steel fibre concrete solution two designs were prepared, a conventional solution without steel fibres and a combined reinforcement solution including both conventional reinforcement and steel fibres. The crack width requirement w_{max} = 0.2 mm for cracks resulting from restrained shrinkage was governing for the reinforcement design. The crack width equation for conventional reinforcement according to the German code DIN1045:2008

$$w_k = s_{r,\max} \cdot \left(\varepsilon_{sm}^{f} - \varepsilon_{cm}\right) \quad (1)$$

is amended for steel fibre reinforced concrete in the German DAfStb by

$$w_k = \left(1-\alpha_f\right) \cdot s_{r,\max} \cdot \left(1-\alpha_f\right) \cdot \left(\varepsilon_{sm}^{f} - \varepsilon_{cm}\right) \text{ with } \alpha_f = f_{ctR,s} / f_{ctm} \quad (2)$$

where α_f is the ratio between the residual uniaxial post crack strength provided by the steel fibres $f_{ctR,s}$ and the uniaxial first crack strength f_{ctm}. The calculated crack widths were 0.196 mm and 0.206 mm for the conventional and the combined reinforcement solutions, respectively. As SFRSCC is not covered by DAfStb due to the risk associated with fibre orientation, the combined reinforcement solution was designed under the assumption of a 3D random fibre orientation, which is typically assumed for normal vibrated SFRC. The conventional reinforcement solution consisted of Y16 at 100 mm in both directions at top and bottom (in total 157 kg steel per m^3 of concrete) and the combined reinforcement solution consisted of Y10 at 100 mm welded mesh reinforcement in both directions at top and bottom and 30 kg/m^3 Dramix® RC-80/60-BN fibres (in total 92 kg steel per m^3 of concrete).

In order to verify the design basis and assess the applicability of SFRSCC for slabs, four full scale beams were produced and subjected to identical loading conditions. Four point bending was chosen as it is very difficult from an experimental point of view to establish a loading condition including restrained shrinkage.

This paper presents the results from mechanical testing and subsequent evaluation of fibre orientation and distribution from drilled core samples. The details of the structural design and simulation of fibre orientation and distribution will be the subject of future papers. For the latter, a newly developed tool to predict fibre orientation and distribution is used [19].

2. EXPERIMENTAL

2.1 Casting of full scale beams

A total of four full scale beams were produced as part of a trial casting, three of these with a combined reinforcement solution and the last beam with a conventional reinforcement solution without steel fibres. The dimensions of the beams were 5000 mm x 1000 mm x 400 mm. The concrete cover was 35 mm. The same concrete mix, but without fibres, was used for the beam without steel fibres.

The flow properties were measured using the so-called 4C-Rheometer, an alternative to classical concrete rheometers, which is designed to measure the rheological properties yield stress and plastic viscosity from the slump flow test [20]. The yield stress of the SFRSCC was in the range of 80-100 Pa, corresponding to slump flow values from 500 to 540 mm, and the plastic viscosity was in the range from 60-100 Pa·s corresponding to a medium viscosity according to the definition given in [20].

To assess the effect of flow on fibre orientation and distribution, the casting conditions were not the same for the beams with a combined reinforcement solution. Two of the beams were cut out from the middle of a trial slab the size of 5000 mm x 5000 x 400 mm. The trial slab casting was representative of the full scale casting procedure i.e. the inlet was continuously being moved back and forth in a quite random way (Figure 2). The last two beams, one with the combined reinforcement and one with only conventional reinforcement, were cast directly in a beam formwork (Figure 3 and 4). The concrete was poured into the mould by placing the inlet at one end and then slowly moving it forward as the concrete reached the beam height. During casting, it was observed that the fibres had a tendency to accumulate on top of the reinforcement mesh when the inlet was kept for too long in the same position. Therefore the inlet was also moved from side to side and manual scraping was also applied. This was not as pronounced in the trial slab casting where it was possible to move the inlet more easily and avoid this phenomenon. Furthermore, the spacers between the top and bottom mesh affected the flow to some extent i.e. the velocity field was not complete unidirectional in the longitudinal direction.

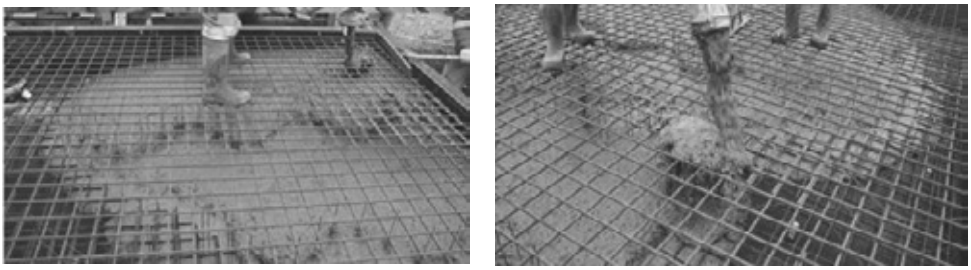

Figure 2 – Casting of trial slab with SFRSCC. Combined reinforcement solution.

Figure 3 – Casting of full scale beam with SCC. Conventional reinforcement solution.

Figure 4 – Casting of full scale beam with SFRSCC. Combined reinforcement solution.

2.2 Mechanical testing

Figure 5 shows the setup for four point bending with a constant moment section of 2.4 m assuming that the self-weight of the concrete has only little effect on the resultant moment curve in the load range considered.

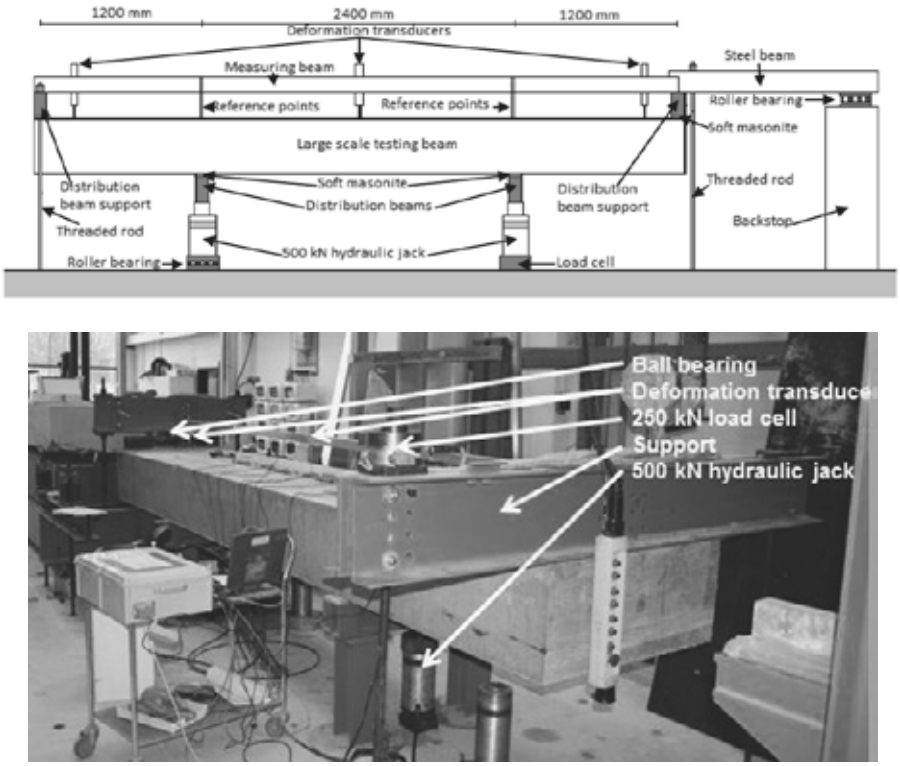

Figure 5 – Full scale beam testing. Four point bending setup.

2.3 Fibre orientation and distribution

The foundation slab design assumes a 3D random fibre orientation and one way to characterise fibre orientation is by the fibre count per unit area following the well-known equation derived by Krenchel [21]:

$$n_f = \alpha \frac{V_f}{A_f} \tag{3}$$

where n_f = number of fibres per unit area, α = orientation factor, V_f = fibre volume fraction, and A_f = cross section area of a fibre. The orientation factor varies from 0.0 to 1.0 referring to fibres parallel and orthogonal to the cross-section, respectively. The orientation factor is equal to 0.5 for a perfect 3D random orientation. For the used fibre type and volume fraction, 1D fully aligned and 3D random orientation of fibres correspond to fibre counts of 8646 and 4323 m^{-2}, respectively.

After mechanical testing, drilled core samples were taken from one of the cut beams and from the cast beam with combined reinforcement. The drilled cores were located as shown in Figure 6. Unfortunately, only five cores were obtained from the cut beam due to problems with the drilling equipment.

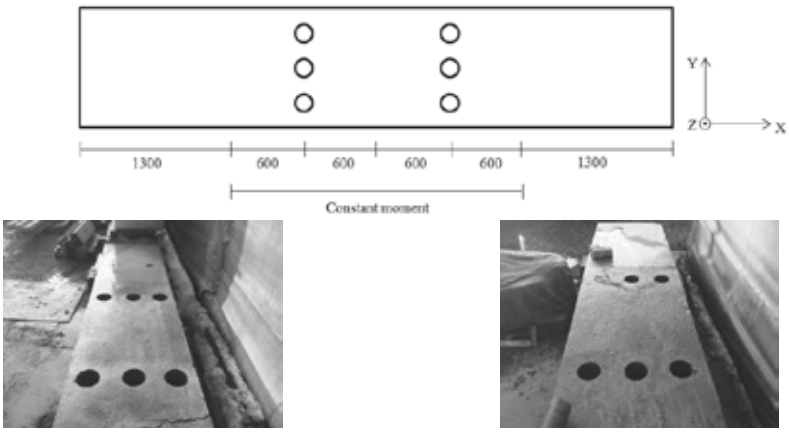

Figure 6 – Location of drilled cores (top). Cast beam (bottom/left). Cut beam (bottom/right).

Subsequently, each core was split in sections as shown in Figure 7 to measure the fibre count in the x (longitudinal), y (transverse) and z (vertical) direction. The top and bottom sections represent the cover layer zones and the section was split on the inside of the inner reinforcement bars located 55 mm from the surface (35 mm cover layer + 2 times bar diameter of 10 mm). The diameter of each cylinder was 150 mm.

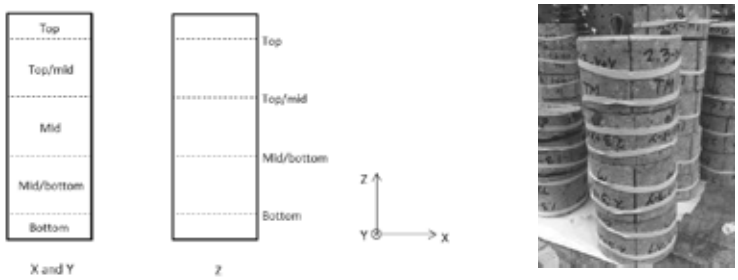

Figure 7 – Sectioning of drilled cores.

3. RESULTS AND DISCUSSION

For each beam, the crack pattern was monitored at different load steps. At each load step, all the cracks were detected, and the crack width and crack distance were measured (Figure 8). Figure 9 shows the maximum crack width detected at different load levels. The results show that the cracks widths in the combined reinforcement solution are somewhat lower than or equal to the conventional solution up to a moment of approximately 150 kNm/m. This indicates that the combined reinforcement solution provides similar or enhanced capacity in the serviceability limit state (SLS) compared to the conventional solution without steel fibres. The average distance between the cracks in the combined and conventional reinforcement solution was approximately 100 and 150 mm, respectively.

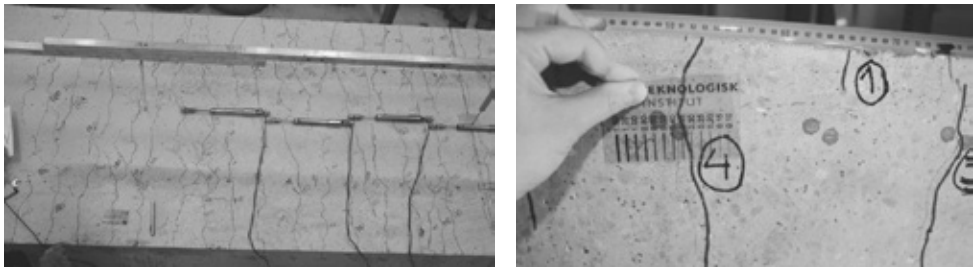

Figure 8 – Crack detection.

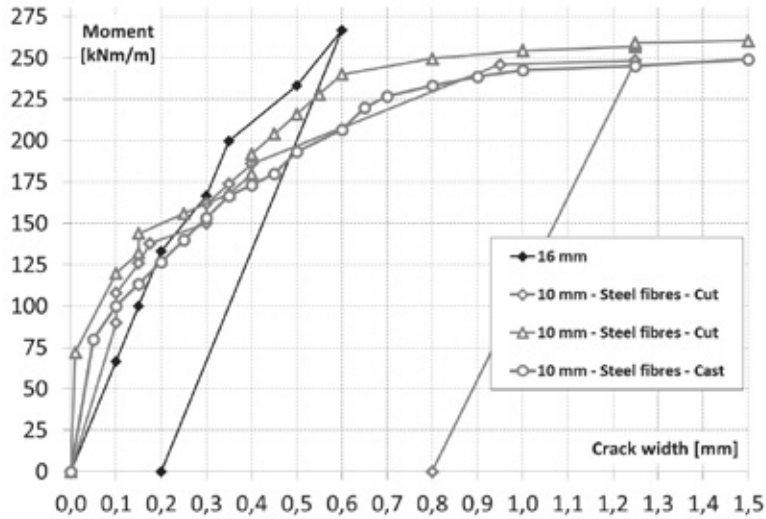

Figure 9 – Manually measured crack widths.

The full moment-deflection curves are shown in Figure 10. The deflection represents vertical deflection at the centre of the constant moment section. The behaviour of the two solutions is quite similar up to a moment of approximately 180 kNm/m. The beams with the combined reinforcement solution were loaded until failure occurred at approximately 240 kNm/m. If fibres had not been included, the calculated yield moment with 10 mm bars is 154 kNm/m. Thus, the addition of steel fibres increased the load bearing capacity with approximately 56 %. In all the three beams with steel fibres, failure occurred just above one of the loading points where the moment is approximately 3% higher than in the centre of the "constant moment section" due to self-weight of the beam.

As expected, the ultimate load carrying capacity of the conventional solution is larger than the combined reinforcement solution, however, to avoid damages to the equipment, the load was released after yielding had occurred but before failure. Yielding appeared at a moment of approximately 375 kNm/m which is in very good agreement with the calculated value of 379 kNm/m.

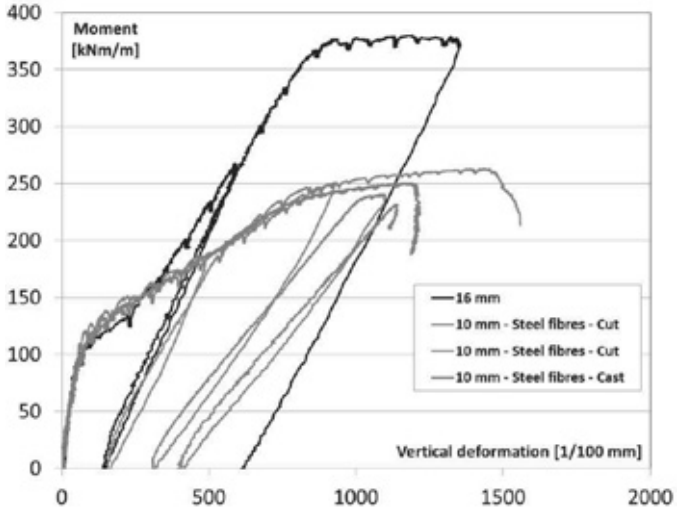

Figure 10 – Moment versus vertical deflection over the constant moment section.

Figure 11 shows the average fibre counts on the drilled cores from the cast and the cut beam, respectively. The red dashed lines represent theoretical fibre counts for 3D random and 1D full alignment. Comparing the fibre counts in the x-direction shows that the highest values are obtained for the cast beam except for the top section. This may explain why the cut beams exhibit a slightly better moment - crack width performance.

Importantly, the fibre counts show that the values in the x and y-direction are close, in particular for the cut beam, and that these values are close to the 3D random value assumed in the design. Thus, it may be assumed that the slab performance is the same in both directions (x and y).

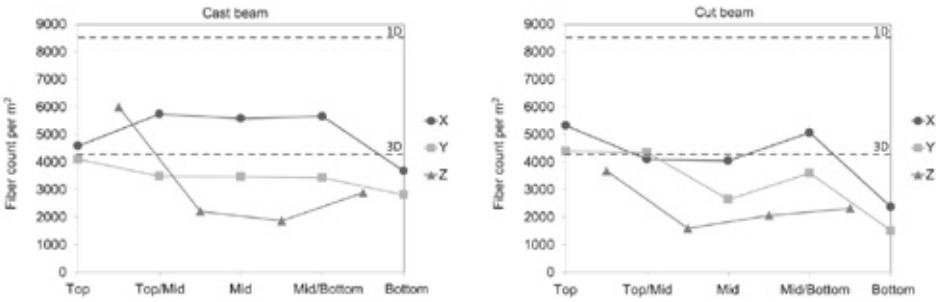

Figure 11 – Average fibre counts on drilled cores from the cast and the cut beam, respectively.

For the cast beam, the x-direction shows the highest values followed by the y- and z-direction. This corresponds to the x-direction being the dominant flow direction; however, for the top section the highest value is found in the z-direction. This may reflect the challenges observed during casting i.e. the tendency for fibre accumulation on the top mesh and the subsequent manual operations to avoid fibre balling.

For the cut beam the trend is somewhat similar with the lowest fibre counts found in the z-direction. Due to the much more random casting procedure, a dominant direction is not expected and the values x and y-direction are more similar. The bottom fibre count is somewhat lower, which may indicate that fibres in some places had difficulties penetrating into the cover layer zone.

Compared to conventional SFRC, the tendency for higher fibre counts in the x and y-direction may be an advantage over conventional SFRC. For the latter, one of the problems seem to be the tendency of steel fibres to orientate in the z-direction close to the poker vibrator.

The comparison of fibre counts to the theoretical 3D and 1D values has assumed a constant fibre concentration of 30 kg/m^3. To validate this assumption, the samples need to be crushed. These particular core samples have not been crushed, however, prior to cutting the beams out of the trial slab, another five core samples were drilled from the trial slab and crushed. Fibre concentrations from 28 to 31 kg/m^3 were obtained with an average value 29 kg/m^3. In the up-coming work, the drilled cores from the full scale beams will also be crushed both to validate the overall fibre concentration but also to study the fibre concentrations from top to bottom. In this way, it will be possible to study fibre orientation from top to bottom in more detail as the fibre count is a function of both fibre orientation and fibre concentration according to equation 3.

The results of mechanical performance combined with fibre counts indicate that SFRSCC is applicable for this type of structure. Local variations in fibre counts will occur, which reflect variations in fibre orientation and/or concentration, but it is expected that over a larger area these are leveled out and as a result the mechanical performance is more or less the same in the two load carrying directions (x and y).

4. CONCLUSION

A large foundation slab was selected as the first demonstration project in the Danish innovation consortium on sustainable concrete structures with steel fibre reinforced concrete. The slab was cast using SFRSCC, which has some advantages over conventional SFRC in terms of working environment and productivity. However, the main question was whether existing design rules for SFRC also apply to SFRSCC where flow induced fibre orientation and distribution can be significant. Two designs were prepared, one without steel fibres and one with a combined reinforcement solution. Both were designed to obtain the same performance in the serviceability limit state i.e. a maximum crack width of 0.2 mm caused by restrained shrinkage. In the combined reinforcement solution the total amount of steel was reduced by 40 % compared to the conventional solution. As part of a trial casting, four full scale beams were produced in order to verify the design basis. The results show that the combined reinforcement provides a) similar or enhanced performance up to crack widths of 0.2 mm and b) lower ultimate bearing capacity. Results from fibre counts on drilled cores indicate that it is possible to cast SFRSCC in slabs and produce a similar performance in both of the two load carrying directions (x and y). Local variations in fibre counts will occur due to variations in fibre orientation and/or fibre concentration, however, seen over a larger area it is expected that these are leveled out.

5. ACKNOWLEDGEMENTS

The authors acknowledge funding from the Danish Agency for Science, Technology and Innovation, "Sustainable Concrete Structures with Steel Fibres - The SFRC Consortium".

REFERENCES

1. Altun, F., Haktanir, T., Kamura, A., "Effects of steel fibre addition on mechanical properties of concrete and RC beams", *Construction and Building Materials*, 21, 2007, pp. 654–661.
2. Purkiss, J. A., Wilson, J., Blagojevii, I, "Determination of the load-carrying capacity of steel fibre reinforced concrete beams", *Composite Structures*, Vol. 38, No. 1-4, 1997, pp. 111-117.
3. Khaloo, A. R., Afshari M., "Flexural Behaviour of Small Steel Fibre Reinforced Concrete Slabs*", Cement and Concrete Composites*, 27 (1), 2005, pp. 141-149.
4. Jansson, A, Gylltoft, K, Löfgren, I, "Flexural behavior of members with a combination of steel fibres and conventional reinforcement", *Nordic Concrete Research*, No. 42, 2010, 155-172.
5. Ferrara, L., Meda, A., "Relationships between fibre distribution, workability and the mechanical properties of SFRC applied to precast roof elements", *Materials and Structures*, 39, 2006, pp. 411-420.
6. Dupont, D., Vandewalle, L., "Bending capacity of steel fibre reinforced concrete (SFRC) beams", *Proceedings of the International congress on challenges of concrete construction*, Dundee, 2002. p. 81–90.
7. Jansson, A., Gylltoft, K., Löfgren, I., "Design methods for fibre-reinforced concrete: a state-of-the-art review", *Nordic concrete research*, No. 38, 2008, pp. 21-36.
8. Deutscher Ausschuss für Stahlbeton, DAfStb Richtlinie Stahlfaserbeton, March 2010.
9. Emborg, M., Simonsson, P., "Industrial concrete construction for a better economy and working environment – possibilities and obstacles with self compacting concrete", *Nordic concrete research*, No. 38, 2008, pp. 37-50.
10. Nielsen, C, "Does SCC really improve the working environment?" *5th International Rilem SCC Conference*, 2007, pp. 967-974.
11. Nielsen, C, Thrane, L. N., Pade, C., "Danish experience with self compacting concrete", *Journal of Concrete Plant International*, no 1, 2008, pp. 60-68.
12. Boulekbache, B., Hamrat, M., Chemrouk, M., Amziane, S., "Flowability of fibre-reinforced concrete and its effect on the mechanical properties of the material", *Construction and Building Materials*, 24, 2010, pp. 1664-1671.
13. Martinie, L., Roussel, N., "Fibre Reinforced Cementitious Materials: From Intrinsic Isotropic Behaviour to Fibre Alignment", *Proceedings of Design, Production, and Placement of SCC*, Montreal, 2010, pp. 407-415.
14. Dupont, D. and Vandewalle, L., "Distribution of steel fibres in rectangular sections", *Cement and Concrete Composites* 27, 391-398, 2005.
15. Torrijos, M. C., Barragan, B. E., Zerbino, R., L., "Placing conditions, mesostructural characteristics and post-cracking response of fibre reinforced self-compacting concretes", *Construction and Building Materials*, 24, 2010, pp. 1078–1085.
16. Carlswärd, J., "Shrinkage cracking of steel fibre reinforced self compacting concrete overlays: test methods and theoretical modelling", *PhD Thesis 2006:55, Luleå University of Technology*, 266 pp. (http://epubl.ltu.se/1402-1544/2006/55/LTU-DT-0655-SE.pdf).

17. Groth, P., “Fibre reinforced concrete: fracture mechanics methods applied on self-compacting concrete and energetically modified binders”, *PhD Thesis 2000:04, Luleå University of Technology*, 237 pp. (http://epubl.luth.se/1402-1544/2000/04/LTU-DT-0004-SE.pdf).
18. Døssland, Å. L., “Fibre Reinforcement in Load Carrying Concrete Structures”, *Phd thesis, NTNU, Department of Structural Engineering*, 2008, pp. 288.
19. Svec, O., Skocek, J., Stang, H., Olesen, J. F., Thrane, L. N., “Application of the fluid dynamics model to the field of fibre reinforced self-compacting concrete”, *Proceedings of the International Conference on Numerical Modelling Strategies for sustainable concrete structures*, Aix en Provence, 2012.
20. Thrane, L. N., Nielsen, C. V., Pade, C, ”Determination of Rheology of Self-Consolidating Concrete Using the 4C-Rheometer and How to Make Use of the Results”, *Journal of ASTM International*, Vol. 7 (1), 2010, pp. 10.
21. Krenchel, H., Fibre spacing and specific fibre surface, *Proceedings of the RILEM Conference on Fibre Reinforced Cement and Concrete*, 1975, pp. 69–79.

Comparison of durability parameters of self-compacting concrete and conventional slump concrete designed for marine environment

Martin Kaasgaard
M.Sc., Consultant
Danish Technological Institute
Gregersensvej 4
DK - 2630 Taastrup
E-mail: mkaa@dti.dk

Claus Pade
M.Sc., Team Leader
Danish Technological Institute
Gregersensvej 4
DK - 2630 Taastrup
E-mail: cpa@dti.dk

Ulf Jönsson
M.Sc., Construction Manager
Femern A/S
Vester Søgade 10
DK - 1601 København V
E-mail: ujo@femern.dk

Christian Munch-Petersen
M.Sc., Concrete Expert
Emcon A/S
Ordrupvej 60
DK - 2920 Charlottenlund
E-mail: cmp@emcon.dk

ABSTRACT

In this study fly ash concrete, 3-powder concrete (Portland cement, fly ash, silica fume) and concrete based on slag cement have been investigated. Self-compacting and slump concretes were designed using the same aggregate materials and to have as similar compositions as possible. The main differences between the self-compacting concretes and corresponding slump concrete mix compositions were that the self-compacting concretes had a slightly higher paste content, a higher dosage of superplasticizer and maximum aggregate size of 16 mm compared to 22 mm for slump concrete. The compositions of the slump concretes were selected as to meet the typical Danish requirements to concrete structures exposed to marine conditions, i.e. the concrete was air entrained and having a w/c-ratio of 0.40. The concretes were batched and mixed using an industrial scale concrete mixing station applying special procedures that ensured high batching

accuracy and identical mixing sequence. The fresh concrete properties of air content, density, slump, slump flow, plastic viscosity and initial setting time were measured and a suite of test specimens were cast comprising cylinders and cubes as well as larger size blocks for long term exposure testing. The strength development and accelerated durability parameters such as frost resistance and chloride migration coefficient were assessed. Chloride penetration profiles were obtained after 6 months of exposure to sea water. The results indicate that self-compacting concrete performs similar to the conventional slump concrete in all aspects of durability.

Key words: Self-compacting concrete, slump concrete, supplementary cementitious materials, durability.

1. INTRODUCTION

Self-consolidating concrete (SCC) is widely used in DK. The majority of precast plastic concrete is SCC and close to 40 % of the ready-mixed concrete production is SCC. However, even if SCC in Danish regulations is fully allowed for any exposure, SCC is generally not used under severe exposure conditions such as marine environments, the purpose for which it was originally developed in Japan in the late 1980's [1].

One reason for the limited use of SCC might be a lack of economic benefit. It is easy for the contractor to see the benefit from needing only two people to do the job that with conventional concrete would require six people. This is typically the case for simple slabs on ground when comparing the required manpower of a SCC solution compared to a slump concrete solution, and therefore the extra cost per cubic meter of SCC pays off [2]. For the more complicated and perhaps vertical formwork often required for structures exposed to severe environmental conditions the picture can be less evident. The benefit of using SCC may be reduced for a number of reasons:

- the labor cost for the actual casting process is relatively low
- the cost of formwork is increased as hydrostatic pressure needs to be accounted for
- the need for more careful control of concrete workability
- the need for more careful planning and control of the concrete casting
- the geometrical accuracy of free surfaces is not as good as can be achieved with slump concrete.

However it must be realized, that even if SCC is allowed in any exposure class only limited documentation exists that SCC based on local materials and traditions will perform just as good in service in terms of durability as a conventional solution using slump concrete. This is obviously not an optimal situation for the promotion of SCC.

Consequently, in Denmark there is a need for documentation of durability properties of SCC mix designs having comparable materials cost to conventional concrete mix designs. This was among the reasons why Femern A/S as owner of the coming Fehmern Belt Fixed Link between Denmark and Germany initiated laboratory and field tests on the durability of a variety of

concrete compositions - including SCC - all potentially suitable for marine structures. Selected durability parameters from accelerated testing as well as parameters from large marine exposure test specimens are presented and compared for SCC and conventional slump concrete with three different binder systems Portland cement (CEM I) + fly ash, Portland cement (CEM I) + fly ash + silica fume, and blast furnace slag cement (CEM III/B).

2. EXPERIMENTIAL WORK

The concrete compositions and the testing program were designed in a co-operation between Femern A/S and Danish Technological Institute. The experimental work comprised mixing, casting and testing of six types of concrete, three self-compacting and three conventional slump concretes of similar binder compositions; Portland cement (CEM I) + fly ash, Portland cement (CEM I) + fly ash + silica fume, blast furnace slag cement (CEM III/B). For each concrete type two concrete blocks with dimensions 2000 x 1000 x 200 mm and 1000 x 1000 x 200 mm respectively were produced and furthermore a number of cylinders and cubes were cast. The large blocks were exposed to the marine conditions at the Fehmern Belt exposure site at Rødbyhavn, while the smaller block, the cylinders and the cubes were used for initial characterization of the different concrete types.

The test program comprised the measurement of fresh concrete properties (air content, density, slump/slump flow, air void distribution, setting time, bleeding and for SCC furthermore yield stress, plastic viscosity and t_{500}) on each batch of concrete. The cylinders were used for determination of compressive and splitting tensile strength developments (EN 12390-3, EN 12390-6, EN 12390-7) and the cubes were used for determination of frost resistance according to SS 13 72 44-IA. Cores were drilled from the smaller elements after 28 maturity days and used for determination of compressive strength (EN 12504-1) and frost resistance (SS 13 72 44-IIIA), air void analysis (EN 480-11), petrographic analysis (DS 423.41, DS 423.42, DS 423.43, DS 423.44, DS 423.45) and measurement of chloride migration coefficient after 28 as well as 180 maturity days according to NT Build 492.

Cores were drilled from the large elements after 6 months of exposure and used for determination of compressive strength (EN 12504-1), air void analysis (EN 480-11), petrographic analysis (DS 423.41, DS 423.42, DS 423.43, DS 423.44, DS 423.45) and measurement of chloride profiles from 1m below the water level according to the principles of NT Build 443. Based on the chloride profiles the diffusion coefficient and surface concentration was estimated.

Only selected important durability related parameters from the test program are presented in this article. More data on the six concrete types presented in this study as well as nine other concrete types can be found at www.concreteexpertcentre.dk.

2.1 Materials and mix proportions

The cementitious materials used were a CEM I 42.5 N Portland cement (low alkali sulfate resisting cement) from Aalborg Portland, class F fly ash (Emineral B4) from the coal-fired power plant in Asnæs, silica fume from Elkem in aqueous suspension (EMSAC 500S) and a CEM III/B 42.5 N slag cement from CEMEX's plant in Schwelgern Germany.

The fine aggregate used was Storebæltssand 0/2 mm obtained by sea dredging at "Rønne Banke" near the Danish island of Bornholm in the Baltic Sea. The Storebæltssand was used back in the early 1990's for the production of the tunnel lining elements for the Great Belt Link. The fine aggregate does primarily consist of quartz.

The coarse aggregate used was crushed granite from Rønne on the Danish island of Bornholm in the fractions 4/8, 8/16 and 16/22 mm. The Rønne granite has a long track record in Danish infrastructure projects and was e.g. used for the concrete for the East Bridge of the Great Belt Link.

Air entraining agent (Amex SB 22) and superplasticizer (Glenium SKY 532-SU) from BASF were used. In order to simultaneously meet the requirements to air content (3-5 %) and air void distribution (spacing factor below 0.2 mm) additional defoamer had to be added to the superplasticizer to minimize its entrainment of relatively large air voids.

The slump concretes were proportioned to meet the typical Danish requirements to concrete structures exposed to marine conditions, i.e. the concretes were air entrained with a target air content of 4.5 % and having a w/c-ratio of 0.40. The w/c-ratio was calculated using activity factor of 2 for silica fume and 0.5 for fly ash according to the Danish concrete standard DS 2426. The self-compacting concretes were proportioned based on the slump concretes, but with slightly higher paste content. Furthermore the maximum aggregate size was reduced from 22 mm for the slump concretes to 16 mm for the self-compacting concretes. Target slump for the slump concretes was 160 mm and target slump flow for the self-compacting concretes was 580 mm. The mix proportions of the six types of concrete are presented (without admixture content) in Table 1.

2.2 Mixing, casting and curing of concrete

The mixing of the concretes was performed in an industrial 375 liter counter-current panmixer with a capacity of 250 liter ready mixed concrete. The mixing station was equipped with 5 aggregate silos and 4 powder silos. The use of an industrial mixing station ensures the applicability of the results to actual full scale concrete production. In order for the concretes to be produced with precisely the desired water/cement ratio (within ± 0.002 of the target 0.400), a special batching procedure was adopted, involving very accurate determination of moisture content of the aggregates. Each aggregate was weighed separately onto the conveyor belt, and samples were taken for determination of moisture content using microwave ovens, before the aggregate was transferred to the mixer. After determination of moisture content, the appropriate amount of water to be added to obtain a water/cement ratio of 0.400 was calculated and subsequently weighed into the mixing stations water tank. The mixer, already containing the aggregates, was started and the powder was added followed by water, air entraining agent and finally superplasticizer. The superplasticizer was added with a delay of 30 seconds from the addition of water and the final mixing time after dosage of all materials was 120 seconds. After mixing, the concrete was discharged to a 500 liter crane bucket and fresh concrete properties were determined.

For the casting of cylinders/cubes and the small concrete blocks, batches of 230 liter concrete were produced. The cylinders/cubes were cast using a vibration table for the slump concretes, while no compaction was applied for the self-compacting concretes. For the casting of the larger concrete blocks, two batches of 230 liter concrete were produced. The blocks were cast from the

crane bucket into the formwork. The slump concretes were cast in 3 and 6 layers of 30-40 cm for the small and large blocks respectively and each layer was compacted using a Ø40 mm poker vibrator according to HETEK report no. 74 [3]. The self-compacting concretes were cast through an Ø100 mm fire hose mounted at the bottom of the crane bucket using a casting rate of approximately 20 meters per hour.

Table 1 — Composition and fresh concrete properties of the six concrete types tested.

Concrete ID				Fly ash	Fly ash SCC	3-powder	3-powder SCC	Slag cement	Slag cement SCC
Powder composition	Portland cement	%-wt		75	75	84	84		
	Slag cement	%-wt						100	100
	Fly ash	%-wt		25	25	12	12		
	Silica fume, solid	%-wt				4	4		
Concrete composition	Portland Cement	kg/m^3		300	336	300	350	360	410
	Fly ash	kg/m^3		100	112	43	50	-	-
	Silica fume, solid	kg/m^3		-	-	14	17	-	-
	Water content	l/m^3		140	157	140	163	144	164
	Aggregate 0/2	kg/m^3		642	678	677	687	689	686
	Aggregate 4/8	kg/m^3		367	349	377	354	373	353
	Aggregate 8/16	kg/m^3		271	704	272	713	263	712
	Aggregate 16/22	kg/m^3		541	-	543	-	525	-
Cylinders and cubes	Slump	mm		160	-	160	-	140	-
	Slump flow	mm		-	570	-	540	-	580
	t_{500}	s		-	4.5	-	6.0	-	3.5
	Yield stress	Pa		-	51	-	63	-	45
	Plastic viscosity	Pa·s		-	58	-	47	-	62
	Density	kg/m^3		2340	2350	2380	2340	2360	2310
	Setting time,	hr:min		04:50	05:10	05:00	06:20	05:40	08:20
	Air content	%		5.4	4.2	4.9	4.3	4.4	5.2
Small block	Slump	mm		180		180	-	160	-
	Slump flow	mm		-	570	-	550	-	560
	t_{500}	s		-	5.0	-	4.5	-	4.5
	Yield stress	Pa		-	49	-	60	-	53
	Plastic viscosity	Pa·s		-	70	-	55	-	59
	Density	kg/m^3		2340	2390	2360	2349	2360	2340
	Setting time,	hr:min		-	-	-	-	-	-
	Air content	%		5.3	3.2	5.4	4.0	4.0	4.4
	Spacing factor	mm		0.12	0.24	0.15	0.18	0.19	0.15
Large block	Slump	mm		110	-	140	-	160	-
	Slump flow	mm		-	620	-	590	-	610
	t_{500}	s		-	5.0	-	3.5	-	3
	Yield stress	Pa		-	34	-	41	-	35
	Plastic viscosity	Pa·s		-	91	-	38	-	59
	Density	kg/m^3		2330	2360	2350	2370	2320	320
	Setting time,	hr:min		-	-	-	-	-	-
	Air content	%		5.5	4.3	5.2	3.5	4.8	4.8

Demolding of the cylinders/cubes and concrete blocks was carried out 24 hours after casting. The cylinders/cubes were placed in a 20 °C water curing tank until test, while the blocks were wrapped in plastic and placed indoors until a maturity of at least 14 days was reached for the larger elements and 28 days for the smaller elements. Thermocouples cast into the blocks were used to monitor the maturity. In early April 2010 the large concrete blocks were placed at the exposure site in Rødbyhavn when they had reached a maturity of approximately 45 days (43-49 days).

3. RESULTS AND DISCUSSION

3.1 Compressive strength development

The compressive strength developments of the six different concrete types are presented in Table 2 and Figure 1. Each data point represents the average of two measurements on Ø150 mm cylinders.

The strength development of SCC and slump concrete are similar for concrete with corresponding binder systems. The 3-powder concretes and slag cement based concretes have very similar compressive strengths at all maturities. For the fly ash concretes the rate of strength development is the same for SCC and slump concrete, however, the SCC consistently exhibit roughly 10-20 % higher strength at all maturities than the slump concrete. This difference cannot readily be explained even with the 1.2 % lower air content of the fly ash SCC.

Table 2 ─ Compressive strength development (Ø150 mm cylinders) of the six different concrete types tested.

Fly ash		Fly ash SCC		3-powder		3-powder SCC		Slag cement		Slag cement SCC	
Maturity (hours)	Strength (MPa)	Maturity (hours)	Strength (MPa)	Maturity (hours)	Strength (MPa)	Maturity (hours)	Strength (MPa)	Maturity (hours)	Strength (MPa)	Maturity (hours)	Strength (MPa)
13.4	4.5	16.1	7.5	13.2	5.3	15.7	6.8	15.8	1.9	20.8	2.3
25.4	10.9	25.6	12.8	26.4	14.7	22.1	10.1	23.1	3.6	27.9	3.6
48.8	17.6	48.5	21.1	48.6	20.1	45.9	19.0	41.1	11.2	51.2	13.7
76.2	22.1	72.1	26.1	75.4	25.5	69.6	23.4	62.5	17.6	75.9	22.6
168	29.7	168	36.8	168	35.4	168	37.6	168	36.0	168	38.9
672	43.8	672	52.7	672	56.2	672	59.5	672	55.6	672	52.9
1344	50.8	1344	55.4	1344	61.3	1344	61.5	1344	59.8	1344	59.0
Air, fresh (%)	5.4		4.2		4.9		4.3		4.4		5.2

3.2 Frost resistance and air void analysis

The results from testing of frost resistance of the different concretes are presented in Figures 2 and 3 for cast cubes and drilled cores from the small blocks respectively.

For the cast cubes the frost resistance of slump concrete and SCC are virtually identical. The fly ash and 3-powder concretes have “very good” frost resistance (< 0.10 kg/m^2 scaling after 56 freeze/thaw cycles), while both the CEM III/B concretes have only what corresponds to “good”

frost resistance according to the SS 13 72 44 test method. The finding that concrete containing blast furnace slag has a reduced salt scaling frost resistance is in agreement with previously reported results [4], [5].

The results for the drilled cores again characterize the CEM III/B concretes as having as a "good" frost resistance. For the fly ash concretes the SCC exhibits significantly poorer frost resistance, "acceptable" as compared to "very good", than the slump concrete, while the opposite trend although less pronounced is the case for 3-powder binder system. For the fly ash concretes, the observed difference might be explained by a low air content (2.8 %) and high spacing factor (0.24) in the hardened SCC compared to the slump concrete (see Table 2). Generally, the spacing factor should be below 0.2 to achieve good frost resistance. The air void analysis can however not explain why the 3-powder SCC concrete has a better frost resistance compared to the slump concrete.

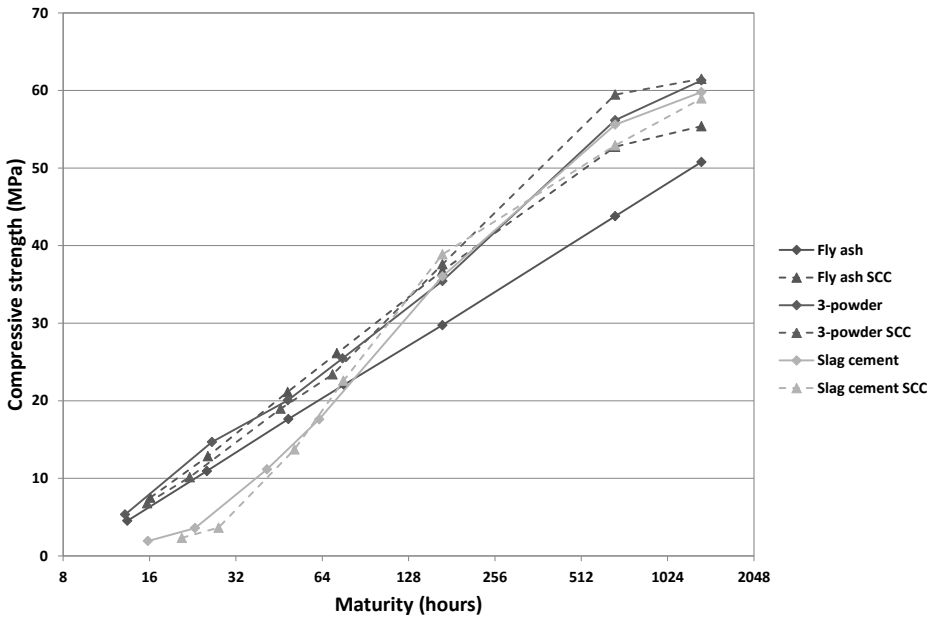

Figure 1 — Compressive strength development (Ø150 mm cylinders) of the six different concrete types tested.

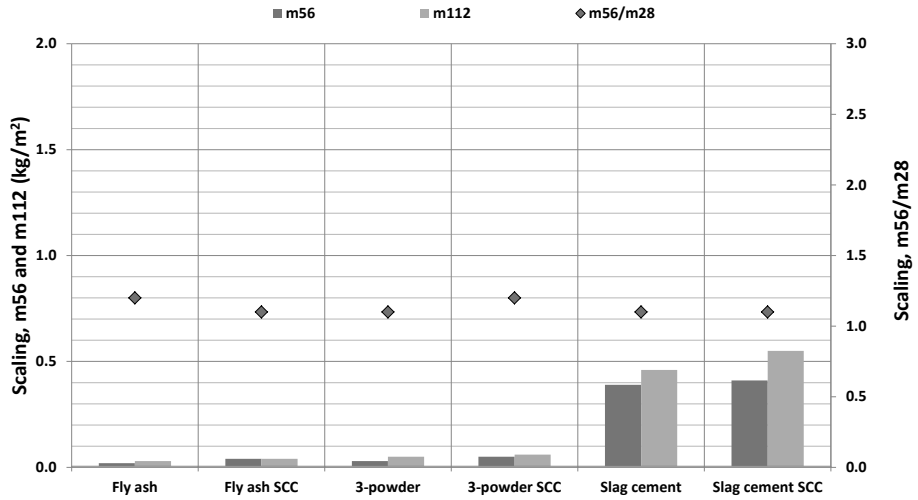

Figure 2 — Frost resistance of cast cubes representing the six different concrete types tested.

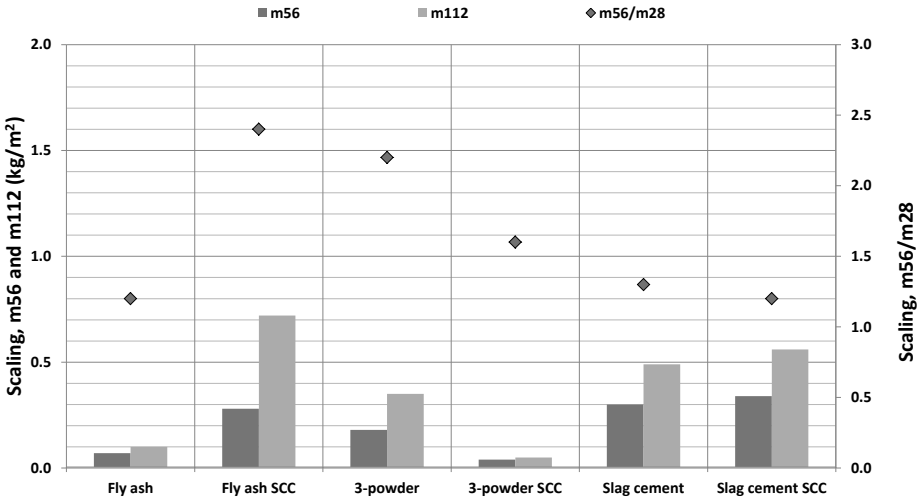

Figure 3 — Frost resistance of drilled cores taken from the small blocks.

In general the results seem to suggest that there is no difference in the frost resistance between slump concrete and SCC of comparable air void structure provided that both types of concrete have been cast properly. Although not supported by any referenced results this was also the conclusion by the recent RILEM TC 205-DSC [6].

3.3 Chloride ingress

The results from testing of chloride ingress parameters are presented in Table 3. The measured NT Build 492 migration coefficients from drilled cores taken from the small block are also presented graphically in Figure 4, whereas the obtained chloride profiles after 180 days of exposure to sea water at Fehmern Belt exposure site at Rødbyhavn are shown in Figure 5.

Table 3 — Chloride ingress parameters measured for the six different concrete types.

Concrete type	NT Build 492, 28 days	NT Build 492, 180 days	Chloride ingress profiles, 6 month exposure		
	Migration coefficient ($x10^{-12}$ m^2/s)	Migration coefficient ($x10^{-12}$ m^2/s)	Diffusion coefficient ($x10^{-12}$ m^2/s)	C_S (%-wt)	K $(mm/(years)^{0.5})$
Fly ash	27.5	2.3	2.93	0.35	19.9
Fly ash SCC	23.3	2.9	3.11	0.40	21.6
3-powder	9.7	2.8	2.76	0.44	20.9
3-powder SCC	9.9	3.1	1.68	0.46	16.6
Slag cement	2.5	1.3	0.61	0.29	8.5
Slag cement SCC	2.3	1.0	0.33	0.31	6.4

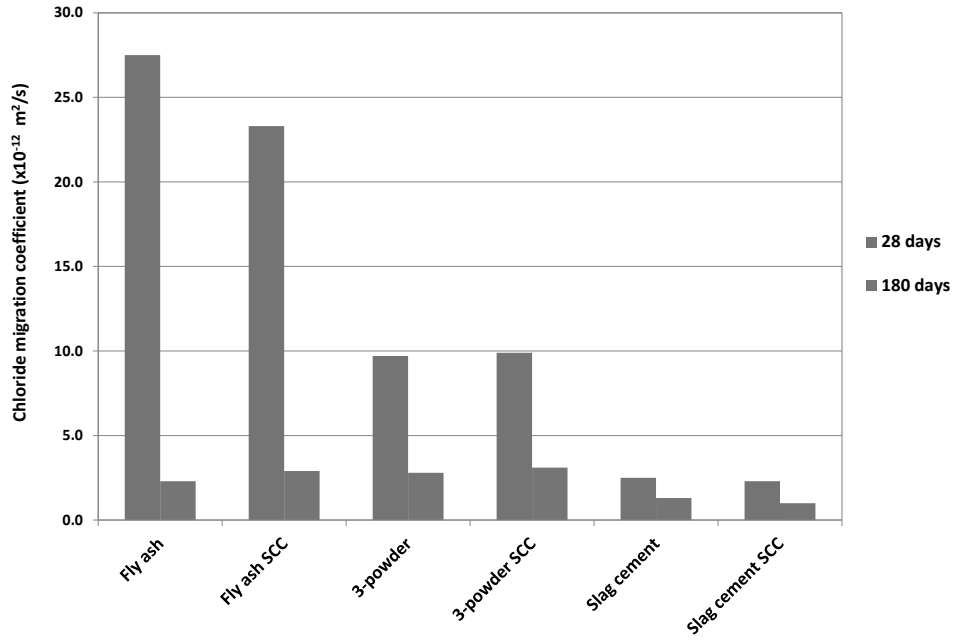

Figure 4 — Chloride migration coefficients of drilled cores taken from the small blocks.

No difference between slump concrete and SCC could be recognized in the chloride ingress parameters recorded.

Quite similar chloride migration coefficients were obtained for the respective slump and SCC concretes with same binder systems at 28 maturity days as well as after 180 maturity days. The development in the migration coefficient over time is markedly different for the three binder systems investigated. At early stages (28 days) as expected the slag cement concretes have the lowest values, the 3-powder concretes have intermediate values, and the fly ash concretes the higher values. After 180 days the slag concretes still exhibit the lowest migration coefficients, but the fly ash concretes have "caught up" with the 3-powder mixtures; both binder systems having migration coefficients in the range 2 to 3 $x10^{-12}$ m^2/s or about twice that of the slag cement concretes.

The chloride profiles of cores drilled below sea level from the larger blocks after six months of exposure are presented in Figure 5. As seen from the figure the ingress profiles of the SCC and slump concretes with similar binder systems are fairly similar. These similarities are also expressed in the diffusion coefficients, surface concentrations and K value parameters estimated from the best fit Fick's second law solution to the profiles (Table 3). For the 3-powder and slag cement concretes, the SCCs generally have lower chloride contents at all depths than their slump counter parts, whereas the opposite is the case for the fly ash concretes. However, the differences are quite small and presumably within what can be expected between two profiles from the same level of the same concrete specimen.

Only limited information has until now been made available in the literature concerning chloride ingress in SCC [6]. However, a recent Swiss study [7] investigating the chloride ingress into concrete by three different accelerated methods of four different binder systems at different water/powder ratios ranging from 0.35 to 0.60 supports the findings of the current study, i.e. that the chloride resistance of SCC is similar to that of slump concrete with corresponding binder.

Likewise, Zhu and Bartos [8] found that the chloride migration coefficients of fly ash SCC and fly ash slump concrete with water to powder ratios of 0.35 and 0.36 respectively were almost identical, i.e. 6.3 and 6.6 x 10^{-12} m^2/s.

A discussion of the reasons behind the observed differences between the chloride ingress parameters of the three investigated binder systems is beyond the scope of this paper.

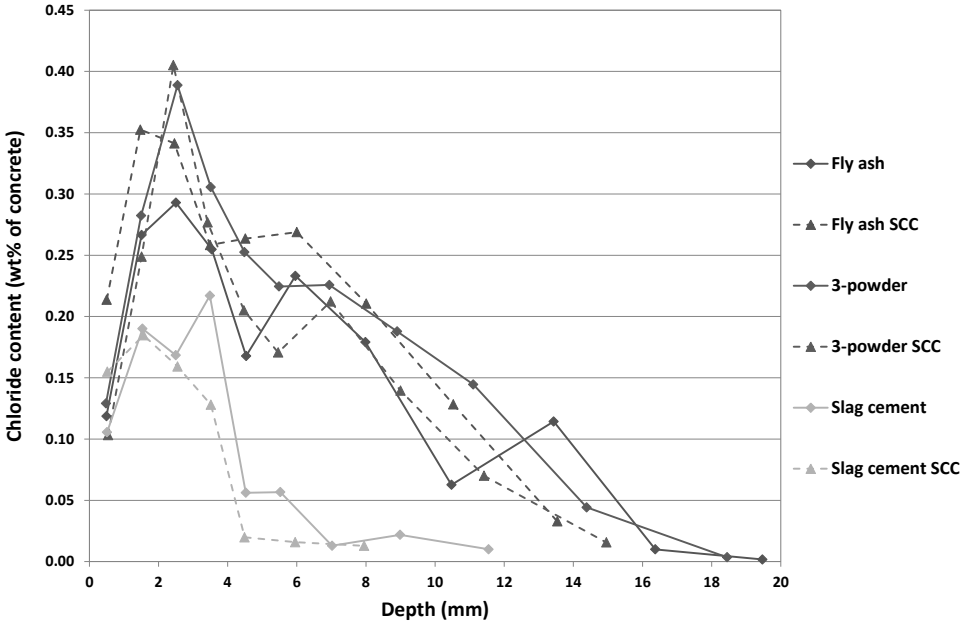

Figure 5 — Chloride profiles from 1m below the waterline after 6 months exposure of large blocks at the Fehmern Belt exposure site at Rødbyhavn.

4. CONCLUSIONS

For the three investigated binder systems Portland cement (CEM I) + fly ash, Portland cement (CEM I) + fly ash + silica fume and slag cement (CEM III/B) it may be concluded that self-compacting concrete performs similar to conventional slump concrete with respect to the durability parameters investigated.

The following sub-conclusions can be drawn:

1) The compressive strength development up to 56 days of maturity when stored immersed in water are very similar.

2) The frost resistance of slump and SCC concrete is similar provided that the air void structure of the concretes is fairly similar. The investigated fly ash and 3-powder concretes had good frost resistance, whereas the slag cement based concretes exhibited somewhat more scaling than the two other binder systems.

3) The slump and SCC concretes have very similar chloride migration coefficient after both 28 and 180 days. The slag cement concretes have the lowest chloride migration coefficients at both ages, while the fly ash concretes have the far largest reduction in migration coefficient from 28 to 180 maturity days.

4) The chloride profiles are similar for the respective slump and SCC concretes after 6 months of exposure with some minor fluctuations. As a direct result of the profile similarities the estimated parameters (diffusion coefficient, surface concentration and K value) of the Fick's second law solutions to the recorded profiles reveal no differences between SCC and slump concrete.

The above conclusions are valid for well-proportioned concrete that has been correctly batch, mixed, cast and cured into a concrete body of homogeneous character. For such concrete it seems, perhaps not surprising, evident that the durability is governed by the binder composition, while the workability of the concrete in the fresh state has no influence.

5. ACKNOWLEDGEMENTS

The authors gratefully acknowledge Femern A/S and the Danish Expert Centre for Infrastructure Construction, without their support this paper would not have been possible.

REFERENCES

1. Okamura, H.; and Ouchi, M., "Self-Compacting Concrete," *Journal of Advanced Concrete Technology*, V. 1, No. 1, Apr. 2003, pp. 5-15.

2. Poulsen, Aage, "Cost savings by use of SCC in floors," *Nordic SCC Net Workshop, Copenhagen,* 19 June, 2006. (Powerpoint presentation at http://www.scc-konsortiet.dk/12180).

3. Vejdirektoratet, "Stavvibrering, Højkvalitetsbeton, Entreprenørens teknologi - nvisning," *HETEK rapport 74,* 1997, pp. 31, in Danish. (http://www.hetek.teknologisk.dk/16228).

4. Utgenannt, P., "Frost resistance of concrete – Experience from three field exposure sites," *SP report 2001:30*, Swedish National Testing Institute, Borås, Sweden, 2001.

5. Valenza II, J.J.; and Scherer, G.W., "A review of salt scaling: I. Phenomenology," *Cement and Concrete Research*, V. 37, 2007, pp. 1007-1019.

6. RILEM Technical Committee 205-DSC, "Durability of self-compacting concrete", *Materials and Structures*, V. 41, 2008, pp. 225-233.

7. Loser, R.; Lothenbach, B.; Leeman, A.; and Tuchschmid, M., "Chloride resistance of concrete and its binding capacity – Comparison between experimental results and thermodynamic modeling," *Cement and Concrete Composites*, V. 32, 2010, pp. 34-42.

8. Zhu, W.; and Bartos, P.J.M, "Permeation properties of self-compacting concrete," *Cement and Concrete Research*, V. 33, 2003, pp. 921-926.

Concrete Sandwich Panel Structure without Traditional Diagonal Trusses

Petri Annila
Researcher, M.Sc.
Tampere University of Technology
Tekniikankatu 12, P.O. Box 600
FI – 33101 Tampere
E-mail: petri.annila@tut.fi

Jommi Suonketo
Project Manager, M.Sc.
Tampere University of Technology
Tekniikankatu 12, P.O. Box 600
FI - 33101 Tampere
E-mail: jommi.suonketo@tut.fi

Jukka Lahdensivu
Research Manager, Dr. Tech.
Tampere University of Technology
Tekniikankatu 12, P.O. Box 600
FI - 33101 Tampere
E-mail: jukka.lahdensivu@tut.fi

ABSTRACT

A typical concrete sandwich panel consists of an outer layer, thermal insulation and an inner layer. Traditionally, the outer and inner layers have been connected by trusses. Our objective was to study a new kind of sandwich concrete panel structure without diagonal trusses. In the studied sandwich panels the traditionally used mineral wool boards were replaced with stone wool lamella insulation. Long-term tests (2700 hours) showed that the shear stiffness of stone wool lamellas was extremely high and that no significant displacement occurred even at relatively high stress levels.

The safety of the structure must, however, be ensured by stainless steel connection pins. Tensile strength tests showed that a small number of connection pins is enough to ensure attachment of the outer concrete layer to the inner layer.

Key words: Precast concrete panel, creep, long-term deformation, stone wool lamella, connection pin, diagonal truss

1. INTRODUCTION

1.1 General

Prefabricated concrete facades have been the most common facade type in residential buildings (at least blocks of flats) and office buildings in Finland since the late 1960's. A typical concrete sandwich panel consists of an outer layer, thermal insulation and an inner layer. The outer and inner layers are connected by steel trusses. The thickness of the outer layer has typically varied from 40 to 85 mm, and the compression strength of the concrete has typically been about C20/25. The thermal insulation has traditionally been mineral wool with a design thickness of 70 to 160 mm depending on the current building regulations. Traditionally, in sandwich panels has been used mineral wool boards and all strength related to outer concrete layer of the panel has been conducted to inner layer via trusses. The diagonals of the trusses have been made of stainless steel 5 mm in diameter since the early 1970's.

The Finnish requirement for thermal conductivity of external wall assemblies in regular buildings has been less than 0.17 W/Km^2 since the beginning of 2010 [1]. In most cases, that requires 240 mm of mineral wool in sandwich panels. The requirements for low energy buildings and passive houses are even higher. Thermal conductivity of 0.14 W/Km^2 (low energy) requires approximately 300 mm of mineral wool and 0.09 W/Km^2 (passive house) approximately 490 mm. The compression strength of the concrete typically used in facades today is C30/37 and thickness of the outer layer with a centric mesh (#3-150) is 80 mm [2].

It is clear that an increase in the thickness of thermal insulation has a strong effect on the dimensions of the sandwich panel and consequently also on the length of the diagonals of trusses. The compressed bars of trusses will become so slender due to the drying shrinkage of the outer concrete layer that they will buckle [3]. The traditional way of manufacturing precast concrete sandwich panels with trusses is not cost effective in the case of low energy buildings or passive houses.

The connectors between the concrete layers of concrete sandwich panels have been studied partly as a consequence of the cold bridge effect of the traditionally used steel and concrete connectors. The extra conductance caused by 5 mm connection pins (6 pcs/m^2) is 0.0035 W/K which means that the cold bridge effect of metal connectors is minor [4]. Yet, people have started examining the possibility of using fibre-reinforced plastic connectors instead of traditional ones. Salmon et al. [5] have studied fibre-reinforced plastic (FRP) connectors while Oh et al. [6] have studied glass fibre-reinforced polymer (GFRP) connectors. Results of both studies show that plastic connectors are worth considering as an alternative to traditional steel and concrete connectors.

Salmon et al. [5] found that some bonding occurs between the insulation and the concrete layers, but they also detected that it deteriorates over time and will not provide strength over the lifetime of a structure. However, they have not conducted any long-term tests.

Oh et al. [6] studied vertically cast concrete sandwich panel structures (60 mm outer layer, 100 mm insulation layer and 130 mm inner layer). The insulation layers were expanded polystyrene (EPS) and extruded polystyrene (XPS). Their results showed the shear strength of an EPS structure to be 135 kN/m² (same as kPa) and that of an XPS structure 168 kN/m².

Another study by Oh et al. [7] found that the casting position (horizontal or vertical) can significantly affect the ultimate shear strength of a structure. However, this series of tests was performed using only one test specimen and the natural variation of the results makes them uncertain. For example, since the shear strengths of the EPS structures were close to each other, it is difficult to estimate the effect of the casting position reliably. The weakest shear strength (66 kN/m²) of this study was reached with a horizontally cast XPS specimen.

In any case, these studies showed that it is possible to attain sufficient shear strength without steel, plastic or concrete connectors using EPS and XPS insulation. They also showed that long-term durability and long-term deterioration need to be studied further. It is also important to examine the use of other insulation materials (e.g. mineral wools).

1.2 Curving of concrete due to uneven shrinkage

The curving of the outer layer of a concrete sandwich panel is the result of uneven drying of concrete. A centrally placed mesh cannot prevent curving as traditionally used connection trusses can. The shrinkage of concrete is mostly caused by drying and hydration. Normally, drying shrinkage involves physical desiccation by evaporation without chemical drying due to the hydration. The influence of hydration on the external volume of a concrete body is called autogenous shrinkage, which is also caused mainly by desiccation.

Usually only drying shrinkage is worthy of consideration. In the case of typical concrete mixtures, autogenous shrinkage is normally insignificant, but can be a concern with high strength concrete with a low water-to-cement ratio. [8]

Concrete shrinkage can be divided into two parts: early age and long-term shrinkage. The mechanisms of both shrinkage stages are basically the same, but their influence is different because early age concrete has not yet gained much strength and stiffness.

Early age shrinkage
Early age shrinkage is caused by chemical reactions and drying. It is the part of total shrinkage that occurs before the concrete has gained much strength. This stage is critical because even the smallest stress during it can result in large shrinkage strains or cracking. Concrete also has the highest tendency to shrink at this stage because it contains a lot of free water and has no structure to prevent it from bleeding to the surface and evaporating, and because the hydration process is at its most intensive then.

There is no exact definition for which part of total shrinkage is early age shrinkage and which is long-term shrinkage. Often it is considered that early age shrinkage takes place between completion of casting and the age of 24 hours or demoulding. During that period, concrete starts to change from a fluid to a rigid stage (sets) and starts to gain strength (hardens). [9]

Long-term shrinkage
Long-term shrinkage can continue over many years. Usually, only drying shrinkage is considered long-term shrinkage. It consists of both physical drying by evaporation and chemical drying by hydration. In the case of modern high-strength concretes with a low water-to-cement ratio, chemical self-desiccation can be of great significance [8].

The pores of fresh concrete are water-filled. As the concrete desiccates, capillary stresses are generated at local water surfaces. The intensity of capillary stress is inversely proportional to pore size. Capillary stress pulls cement particles closer to each other causing shrinkage. Total shrinking stress depends on the size, number and humidity of pores in the concrete.

Aggregate particles restrain drying shrinkage in concrete. It has also been shown that the larger the maximum aggregate size, the lower the drying shrinkage strain [10]. Moreover, non-uniform drying causes internal stresses which partially restrain local shrinkage strain. Some restraint also arises from reinforcing bars and connections to adjacent structures. All restraints cause stresses to shrinkable concrete. If the induced tensile stresses are greater than the tensile capacity of the concrete, cracks will arise.

When shrinkage strains are restrained, partially or fully, creep causes internal stresses to decrease [11]. Therefore, the total shrinkage of a non-uniformly desiccated concrete body is less than that of a uniformly desiccated one.

Besides drying and autogenous shrinkage, also carbonation causes shrinkage in the long run. Yet, because carbonation normally develops slowly and its contribution to total shrinkage is insignificant, it is usually ignored as a shrinkage factor and only considered as a durability factor.

1.3 Objective

The objective was to study a new kind of sandwich concrete panel structure without diagonal trusses. In the examined sandwich panels the traditionally used mineral wool boards were replaced with stone wool lamella insulation.

The study consisted of two phases. The main objective of the first phase was to determine whether the shear stiffness of mineral wool lamellas can bear the weight of the outer concrete layer and the extent of long-term deformation. The second phase involving conducting tensile strength tests on connection pins had two main objectives: to determine the best connection pin types and to determine the tensile strength of the best connection pin type.

2. EXECUTION OF THE TESTS

The tests examined the tensile strength of connection pins and shear strength of mineral wool lamellas. Several test specimens were prepared for the various tests.

2.1 Test specimens

Specimens for long-term tests
A total of 18 specimens were made for long-term tests using the normal production line of a precast concrete panel factory. The concrete used was a typical façade concrete in use in Finland. It's design compressive strength was 35-40 MPa (C30/37). Actual compressive strength was not measured during the study because it was not considered very important for long-term tests.

The thickness of the inner layer, onto which the specimen was mounted, was 80 mm in all specimens corresponding to the thickness of the inner layer of a sandwich panel. The width of specimens was 200 mm and their height 500 mm. The thickness of the stone wool lamellas was 280 mm in all specimens. The thickness of the outer concrete layer of specimens was 40 mm, 70 mm or 100 mm. Six specimens of each outer concrete layer thickness were used. There were no mechanical connections (like diagonal trusses or connection pins) between the concrete layers. The specimen is shown in Figure 1.

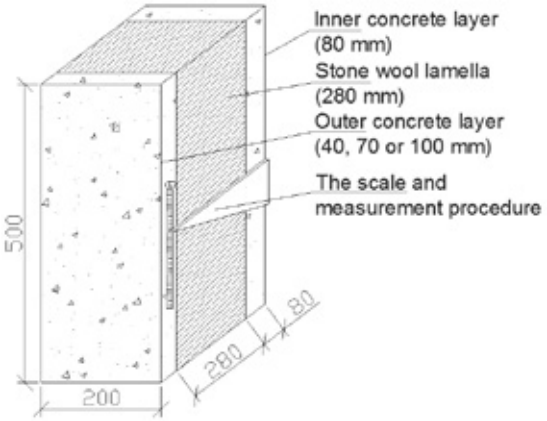

Figure 1 – Test specimen of long-term tests

Specimens for tensile strength tests on connection pins

The specimens for tensile strength tests on connection pins were cast concrete panels in which different types of connection pins had been installed immediately after casting. The diameter of the connection pins was 5 mm and they were installed to a depth of 20 mm. The thickness of the concrete panels used in connection pins type tests was 40 mm, and six (types A, C, D and E) or 10 (type B) connection pins of the same type were installed perpendicularly in each panel. Figure 2 shows the arrangement of the test specimens. Used connection pin types are presented in Figure 3.

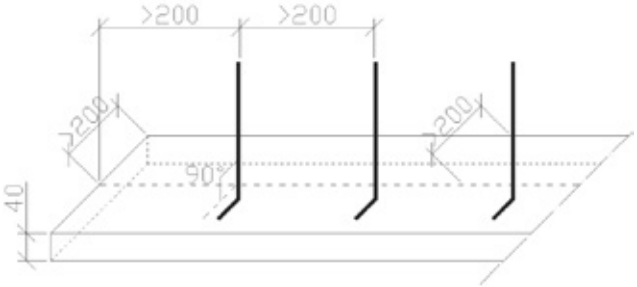

Figure 2 –Arrangement of test specimens

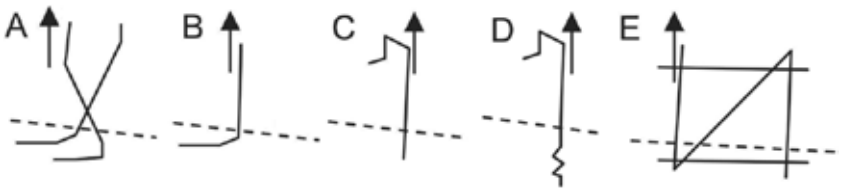

Figure 3 – Used connection pin types.

Only the 20 mm installation depth was used because a company participating in the study wanted to find out the tensile strength of connection pins in a structure where the outer concrete layer is only 40 mm thick. Manufacturers of connection pins have not given recommendations for that type of structure [12-14].

The thickness of the concrete panel in the tensile strength tests on the best connection pin type (type D) was 100 mm and the anchors were installed at 45 degrees. Connection pins were 410 mm long and 5 mm in diameter [12]. Installation depth was 50 mm. The test arrangement is shown in Figure 4. During the casting of the concrete panel, 150x150x150 mm³ concrete cubes were also cast for compression strength tests.

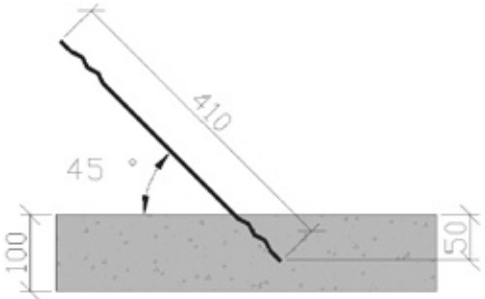

Figure 4 – Test specimen of final tensile strength test on type D connection pins.

2.2 Long-term tests

Specimens were mounted on special racks by the inner layer so that displacement of the outer layer could occur freely. Displacement was measured right after installing the specimen (short-term displacement due to own mass) and then daily for the first week, every other day for the second week, and once a week for the remaining period. Long-term tests were carried out from April 20th to August 10th 2009, for a total of 16 weeks (2700 hours).

All specimens were subjected to outdoor temperature and relative humidity conditions but sheltered from precipitation and sunshine. Temperature and relative humidity were measured automatically at one hour intervals during the tests at three points within the shelter. Figure 5 shows the long-term test specimens in the shelter.

Figure 5 – Long-term test specimens were mounted on special racks inside a well-ventilated shelter.

2.3 Tensile strength tests

Test specimens were attached to a floor in the laboratory hall of Tampere University of Technology (TUT). For testing, specimens of different types of connection pins were attached to the floor horizontally. To determine the best connection pin, the test specimen was attached to the floor at an angle of 45 degrees.

The tensile load test was carried out using a loading device. The loading rate was 10 mm/min. in connection pin type tests and 2 mm/min. when testing the best type of connection pin. The loading rate was measured by the loading device. A computer recorded the tensile load every second. At the beginning of the tests, the computer recorded the tensile load at least 45 times (type C tensile strength, test number 2) and typically 60-180 times (types A, B, D and E) before ultimate strength was reached. In all the tests, the tensile load grew almost linearly before ultimate strength was reached. The typical growth rate was about 20-30 N/s. This means that the measurement uncertainty due to the loading rate was trivial.

The principle of the second part of tensile strength tests (45 °) is shown in Figure 6.

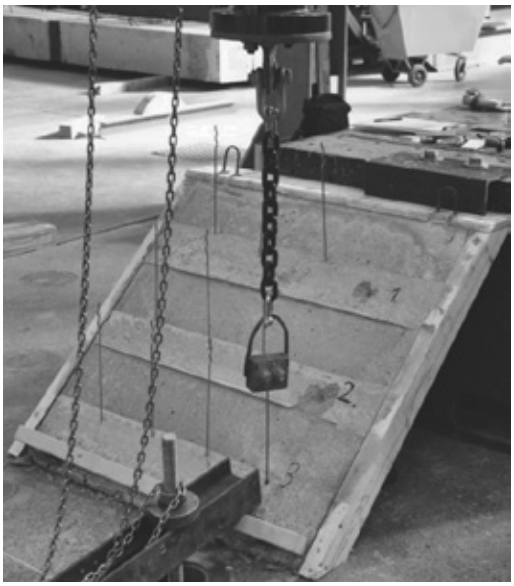

Figure 6 – Principle of 45 degree tensile strength tests.

3. RESULTS AND DISCUSSION

3.1. Shear strength tests on mineral wool lamellas

Short-term displacement occurred right after the specimens were lifted up and mounted on the racks. Average displacement was 0.27 mm in the specimen with an outer layer of 40 mm, 0.41 mm with a 70 mm layer and 1.31 mm with a100 mm layer, see Table 1. Initial displacement was small enough with all concrete outer layer thicknesses which makes them suitable for practical applications. The thickness of the outer layer of concrete sandwich panels used today is between 70 and 85 mm.

Table 1 – Average short- and long-time specimen displacements during the tests.

Thickness of outer layer [mm]	Short-time displacement [mm]	Long-time displacement (creep)				Total displacement after 16 weeks [mm]
		After 12 weeks [mm]	After 16 weeks [mm]	Highest measured displacement [mm]	Week	
40	0.27	0.37	0.29	0.50	12	0.56
70	0.41	0.37	0.32	0.49	15	0.73
100	1.31	0.46	0.49	0.68	14	1.80

Long-time specimen displacements as a function of outdoor temperature and relative humidity during the tests are shown in Figure 7. There were problems with the data logger that recorded outdoor air temperature and relative humidity. Data for May 11th to May 27th (17 days) is missing.

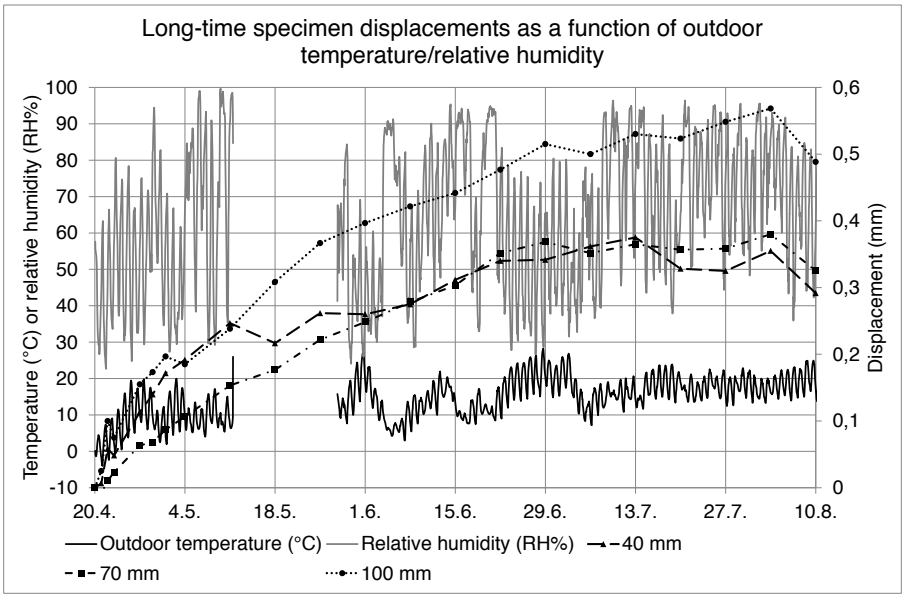

Figure 7 –Long-time specimen displacements as a function of outdoor temperature/relative humidity.

Primary creep occurred for 1500 hours in all specimens followed by a secondary creep phase. Average long-time displacement after 16 weeks was less than 0.50 mm with all specimens and outer layer thicknesses, see Table 1. Higher displacements were also measured during the tests, but they were the result of outdoor circumstances which were not constant during the test. The test period was from late spring to late summer. Temperatures varied from -4.0 °C to 28.2 °C, the average being 14.7 °C. Relative humidity varied from 22.6 RH % to 99.7 RH %, the average being 65.5 RH %.

The total displacement of a specimen is the sum of its short- and long-time displacement. The total displacement after 16 weeks of tests was 0.56 mm with an outer layer of 40 mm, 0.73 mm with a 70 mm outer layer, and 1.80 mm with a 100 mm outer layer. The behaviour of all specimens with an outer layer thickness of 40 mm and 70 mm was similar during the tests. The total displacement of specimens with an outer layer thickness of 40 mm and 70 mm was less than 1 mm. The total displacement of specimens with an outer layer thickness of 100 mm was almost 2 mm. It was more than double compared to thinner outer layer specimens, but still acceptable in practice.

In specimens with a 100 mm outer layer displacement was biggest during the first 24 hours and was thus short-time displacement. It was 4.8 times bigger compared to a specimen with a 40 mm outer layer, and the displacement of a specimen with a 70 mm outer layer was 1.5 times bigger than that of one with a 40 mm outer layer. The weight of the outer layer of a specimen with a 100 mm outer layer was 2.5 bigger and that of one with a70 mm outer layer 1.8 times bigger than the weight of a specimen with a 40 mm outer layer. The long-time displacements were much closer.

Some permanent deformation must have occurred in the mineral wool lamellas during the first 24 hours' displacement in specimens with a 100 mm outer layer but not in thicker specimens. The shear tension of the mineral wool lamellas was rather low with all specimens: 0.94 kPa (40 mm), 1.65 kPa (70 mm) and 2.35 kPa (100 mm). No signs of failure were found in the mineral wool lamellas after tests. However, the mechanical behaviour of mineral wool lamellas under stress is not linear.

3.2 Tensile strength tests on connection pins

The ultimate tensile strength of the connection pins was between 1.7 and 5.3 kN. The best connection pin was type D whose embedded part was wavy. The weakest type was the straight connection pin (type C). Average ultimate tensile strength and standard deviation of test results are presented in Table 2.

Table 2 – Tensile strength of different types of connection pins.

Type of connection pin	Number of tensile strength tests	Average ultimate tensile strength (kN)	Standard deviation of ultimate tensile strength (kN)
A	6	5.2	2.3
B	10	4.4	1.2
C	6	1.7	0.5
D	6	5.3	1.2
E	6	4.4	1.2

Figure 8 shows the normal test result distributions. There were only six (type A, C, D and E) and 10 tests results (type B) per connection pin type, which means that the normal distributions are just estimates of the results of larger scale tests. Despite the uncertainty of the mathematical distribution, it enabled determining a confidence level for the tensile strength of connection pins.

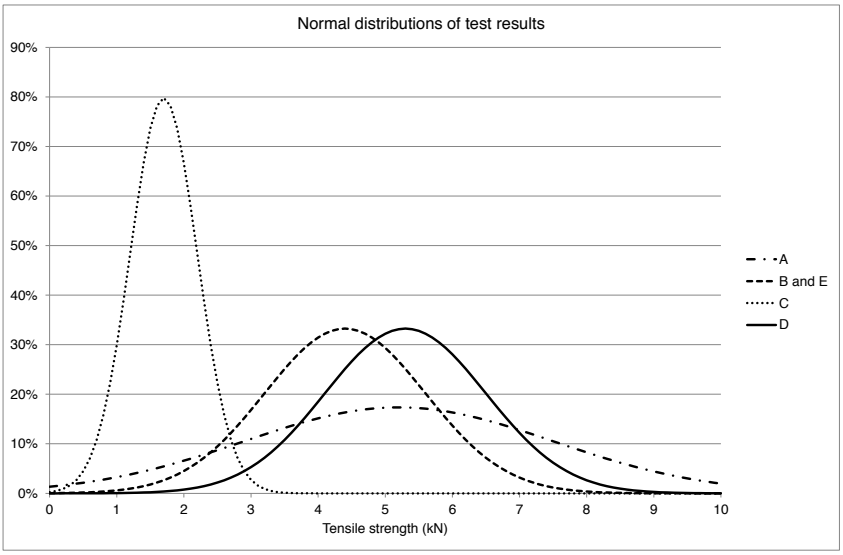

Figure 8 – Normal distributions of test results for different connection pin types.

The tensile strength values varied quite a lot for some types of connection pins (especially A, B, D and E). One reason for this was the way the connection pins were installed in concrete. They were just pressed into the concrete whereby they displaced concrete, which led to anchoring that was not sturdy enough. This can be clearly seen from the test specimens of Figure 9. The manufacturers of connection pins recommended that pins be moved back and forth in the concrete during installation [3, 14] or that they be installed by a vibrating tool [12]. Such installation methods would certainly provide better anchoring.

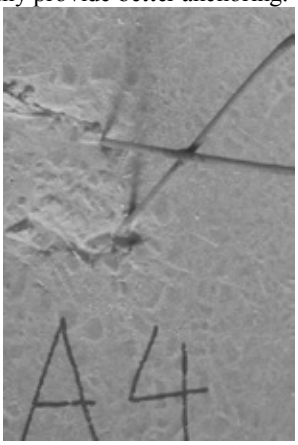

Figure 9 – Example of a poor installation method.

Another reason for the poor tensile strength results was the small installation depth: only about 20 mm for all trusses. The manufacturers of trusses recommended an installation depth of at least 40 mm [14], and at least 50 mm [13] for the truss types tested in this research.

The second part of tensile strength test was done only with trusses similar to type D. The second part focussed on tensile strength at 1 and 2 days after casting of the concrete. These strength values are important for concrete panel manufacturers as they allow speeding up production. Type D trusses were installed according to the manufacturer's instructions, which require installation by vibration [12].

Two tensile strength tests were carried out at the age of 24 hours (1 day) and ten at the age of 48 hours (2 day). Tensile strength was 3.4 kN at the age of 24 hours and 7.2 kN at the age of 48 hours. Compressive strength of concrete was tested in parallel with tensile strength and the results were 12.1 MPa (24 hours) and 17.9 MPa (48 hours). More details are shown in Table 3.

Table 3 – Statistics on different tests.

Number of tensile strength tests	Installation depth of trusses (mm)	Average ultimate tensile strength (kN)	Standard deviation of ultimate tensile strength (kN)	Properties of concrete			
				Age of concrete (days)	Number of test cubes	Average compression strength (MPa)	Standard deviation of compression strength (MPa)
2	47	3.4	2.1	1	3	12.1	1.6
10	49.7	7.2	1.3	2	6	17.9	1.2

The normal distribution of test results at the age of 48 hours is shown in Figure 10. With a 99.7% confidence level (same as 0.03 % fractile), the 48 hour test results indicate a tensile strength of 3.6 kN. The data are assumed to follow a normal distribution. It is important to note

that the results do not reflect the final tensile strength (i.e. at 28 days) of this connection pin, which is likely to be even higher. It rather tells the possibility of lift the panel safety up the moulds in the precast concrete panel factory.

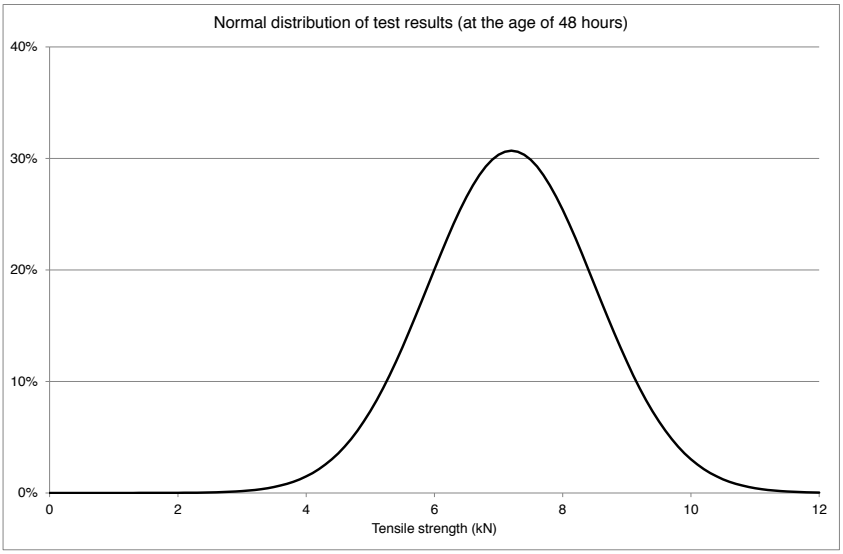

Figure 10 – Normal distribution at the age of 48 hours.

There are two loading conditions which must be paid attention to when designing concrete sandwich panels: lateral service load (e.g. wind pressure) and self-weight of structures or other vertical loads. The volume weight of reinforced concrete is about 25 kN/m³, which means that the vertical load from a 40 mm outer panel is 1 kN/m² (that from a 70 mm outer panel is 1.75 kN/m² and that from a 100 mm outer panel 2.5 kN/m²). The outer concrete panels commonly used in Finland are 70 mm or 85 mm thick. The vertical load caused by an 85 mm concrete panel is 2 kN/m².

The national instructions, RIL 201 Requirements for design and actions on structures [15], give a simplified method for the evaluation of wind pressure based on Eurocode 1 EN 1991-1-4 [16]. The typical prefabricated concrete structure in Finland is a 5- to 8-storey block of flats in a suburb. Thus, the typical terrain category is III.

Wind pressure in this terrain category at a height of 25 metres is 0.65 kN/m². The external pressure coefficient for the vertical walls of a rectangular building is 1.4 at the maximum. Thus, the dimensioning wind load is -0.91 kN/m². [15, 16] which makes the total load on the 85 mm outer concrete panel 2.2 kN/m², as shown in Figure 11.

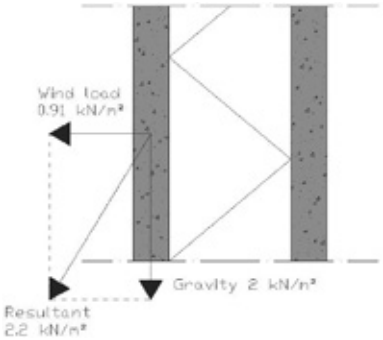

Figure 11 – Typical loading condition of concrete sandwich panels.

The test results clearly show that it is possible to support the typical outer layer of concrete panels (in Finland between 70 and 85 mm thick) with a small number of the described connection pins and still achieve sufficient total certainty.

4. CONCLUDING REMARKS

The results show that the shear stiffness of stone wool lamellas was extremely high and no significant depression occurred even at relatively high stress levels. Therefore, concrete sandwich panels can be made without diagonal trusses if the insulation layer is rigid enough and the safety of the structure is ensured with steel pins between the concrete layers.

The tensile strength tests, the second part of this study, showed that the safety of the structure can be ensured by a small number of stainless steel connection pins. The results indicate that the slenderness issues concerning the traditional diagonal trusses, a consequence of increasing thickness of the insulation layer, can be avoided. One possible solution, as the study shows, is a structure with insulation of sufficient shear stiffness and an outer concrete layer securely attached by connection pins.

The vertical loads of the outer layer of a concrete sandwich panel can be taken by thermal insulation of mineral wool lamellas without traditional trusses. However, the outer layer of a concrete sandwich panel will always be subject to some wind load in normal outdoor climate conditions which means that connection pins are required against wind loads. Handling of concrete sandwich panels, such as lifting them from a mould, transportation and installation, exerts various forces on the panel which must be taken by the connection pins.

REFERENCES

1. Ministry of Environment, “The National Building Code of Finland: Part C3 Thermal Insulation in a building, Regulations 2010”, 10 p.
2. Concrete codes of Finland. 2012. BY 50 Helsinki. Concrete Association of Finland. 251 p. (In Finnish)
3. Rantala, J., & Pentti, M., “Load Carrying Studies of Low Energy Concrete Sandwich Panel” Tampere University of Technology, Department of Structural Engineering. Research Report 1775/2009, 72 p. (In Finnish)

4. SFS-EN ISO 6946. 2008. Building components and building elements. Thermal resistance and thermal transmittance. Calculation method. Finnish Standard Association SFS. 31 p.
5. Salmon, D.C., Einea, A., Tadros M.K., Culp T.D. 1997. Full Scale Testing of Precast Concrete Sandwich Panels. ACI Structural Journal, V. 94, No. 4 pp. 354-362.
6. Oh, T-S., Jang S-J., Yun H-D. 2013A. Shear Reinforcing Influence of GFRP Shear Connectors in the Concrete Sandwich Wall Panel (CSWP) for Exterior Envelopes of Buildings. Advanced Materials Research Vol. 658 (2013) pp. 38-41.
7. Oh, T-S., Jang, S-J., Lee, K-M., Yun H-D. 2013B. Insulation Type Effect on the Direct Shear Behavior of Concrete Sandwich Panel (CSP) with Non-Shear Connectors. Advanced Materials Research Vol. 663 (2013) pp. 154-158.
8. Aitcin, P-C. & Mindess, S. 2011. Sustainability of concrete. Taylor & Francis. Oxon, UK. 301 p.
9. Holt, E. 2001. Early age autogenous shrinkage of concrete. Espoo 2001. Technical Research Centre of Finland, VTT Publications 446. 184 p. + app. 9 p.
10. Videla, C. & Aguilar, C. 2006. An updated look at drying shrinkage of Portland and blended Portland cement concretes. Magazine of Concrete Research 58(2006)7, pp. 459–476
11. Kovler, K. 1995. Interdepedence of Creep and Shrinkage for Concrete under Tension. Journal of Materials in Civil Engineering 7(1995)2, pp. 96–101
12. EK-Kaide Oy “Guideline for EK-connection pins”, 7.12.2011, 9 p. (In Finnish)
13. Peikko Group, “Guideline for trusses and connection pins”, 8/2010, 16 p. (In Finnish)
14. Taiter Oy, “Guideline for Taiter-connection pin and Taiter-triangle truss”, 17.3.2011, 8 p. (In Finnish)
15. RIL 201-1-2008 “Requirements for design and actions on structures”, 2008, 190 p. (In Finnish)
16. European Committee for Standardization 2010, “Eurocode 1: Actions on structures – Part 1-4: General actions – Wind actions”, SFS-EN 1991-1-4 +AC+A1, 254 p.

Heat Loss Compensation for Semi-Adiabatic Calorimetric Tests

Peter Fjellström
M.Sc., Ph.D. Student
Luleå University of Technology
Dept. of Structural Engineering
SE - 97187 Luleå
peter.fjellstrom@ltu.se

Dr. Jan-Erik Jonasson
Professor
Luleå University of Technology
Dept. of Structural Engineering
SE – 97187 Luleå
jan-erik.jonasson@ltu.se

Dr. Mats Emborg
Head of R&D, Betongindustri AB
Professor, Head of Department
Luleå University of Technology
Dept. of Structural Engineering
SE – 97187 Luleå
mats.emborg@ltu.se

Dr. Hans Hedlund
Adj. Professor
Skanska Sverige AB
Technology
Bridge and Civil Engineering
SE – 405 18 Göteborg
hans.hedlund@skanska.se

ABSTRACT

Heat of hydration has long been of importance since it affects the temperature levels within a concrete structure, and thus, potentially affects its durability. The only source of energy is the reaction between cement and water. This energy warms up the concrete sample and all the ambient materials. Therefore, in order to model these energies, the TSA (traditional semi-adiabat) setup is transformed into an associated sphere. By this, the temperature distribution and the energies within each layer of the TSA can be calculated. The sum of all energies gives the total heat of hydration. A refined model using a correction factor is introduced, which accounts for energies lost to the TSA setup materials. Results show that the effect of this factor cannot be disregarded, especially not for TSAs with low cooling factors.

Key words: concrete, heat of hydration, adiabatic calorimetry, semi-adiabatic calorimetry, heat flow, correction factor, cooling factor.

1. INTRODUCTION

1.1 General

The energy quantity of the exothermic reaction between cement and water has long been of importance since it affects the temperature levels within a concrete structure, which can, based on risks of thermal cracking, affect the durability. The temperature influences the development of the pore structure in concrete [1, 2] and naturally its mechanical properties, e.g. strength [3]. For building engineering purposes heat of hydration has commonly been determined by various versions of adiabatic calorimeters, see Figure 1.

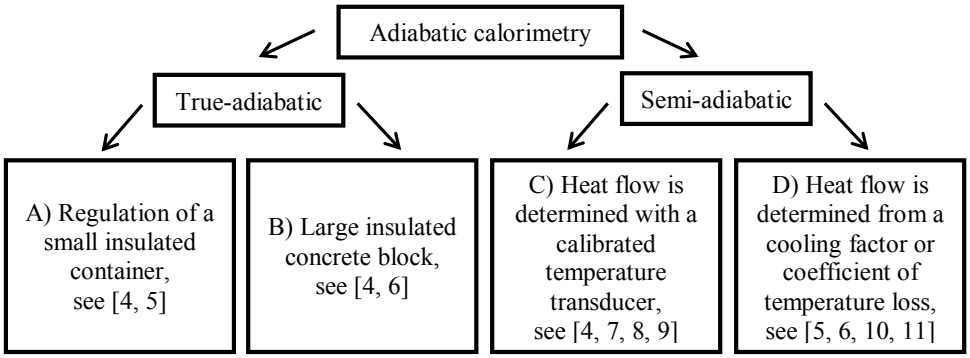

Figure 1 – Schematic presentation of adiabatic calorimetry.

In both the true-adiabatic and the semi-adiabatic setups the concrete temperature is registered as a function of time. The difference is that in the true-adiabatic setup no heat loss to the environment is supposed to be present. The semi-adiabatic setup allows for energy losses, which are accounted for in the evaluation process.

The true adiabatic measurement is in theory preferred, since it could give a correct value of heat of hydration direct from the test results. However, in A) it is hard to regulate the temperature, which can drift, and therefore the results are not always reliable [12]. In B) temperature measurement in the centre of a large concrete block is estimated to have true adiabatic temperature. However, in [6] they account for heat flow as in C) for better accuracy. In the semi-adiabatic methods, when heat flow is calculated from the temperature of the concrete sample, the following conditions have to be fulfilled

- The temperature in the concrete sample and the ambient air are equal when starting the semi-adiabatic measurement.
- The air temperature is constant during the test period.

To ensure these conditions limits are usually specified, e.g. the temperature of the fresh concrete mix should be within ±2°C of the calorimeter temperature [5], and the ambient temperature where the calorimeter is placed should be within the limit 20±1°C [5]. In [10] the laboratory, where the mixing of the constituents of the concrete occurs, the air temperature should be within 20±2°C. The room, where the test is conducted, have the corresponding limit 20±1°C, and the reference temperature should not differ more than ±0.5°C throughout the test [10].

When heat flow is directly measured with a calibrated temperature transducer, the points above are not that important. However, limits are still used, and in [7] the laboratory, where the test is conducted and where the mortar constituents are stored, the room temperature should be within 20±2°C. In this paper, heat flow is calculated from the sample temperature, and, our limits are the same as in [7].

1.2 Existing models and limitations

In order to determine the quantity of heat of hydration in a semi-adiabatic test, heat losses must be determined. In [11] a "traditional" semi-adiabatic (TSA) setup is presented, and the cooling factor were formally expressed as

$$a = \frac{\sum_i h_i \cdot A_i}{V_c \cdot c_c \cdot \rho_c} \tag{1}$$

Based on measured values of a [11] heat energy within the concrete sample, and heat losses based on heat flow, was expressed as

$$q_{cem} = \frac{\rho_c \cdot c_c}{C} \cdot \left(\left(T_c(t) - T_{air} \right) + a \cdot \int_0^t \left(T_c(t) - T_{air} \right) \cdot dt \right) \tag{2}$$

where a [1/s or 1/h] = cooling factor; h_i [W/m^2 °C] = heat transfer coefficient of the individual insulation material; A_i [m^2] = heat flow area of the individual insulation material; V_c [m^3] = volume of the concrete sample; c_c [J/kg °C] = heat capacity by weight of concrete; ρ_c [kg/m^3] = concrete density; q_{cem} [J/kg] = heat of hydration per kg of cement; C [kg/m^3] = cement content; $T_c(t)$ [°C] = concrete temperature; and T_{air} [°C] = air temperature.

When heat of hydration is determined by Eq. 2 the following conditions are usually stated.

- There should be small temperature gradients within the concrete sample. Then the average concrete temperature is easily measured and is representative when calculating energy stored in the concrete.
- A large temperature increase in the concrete sample is favourable, since the measured temperature hereby gives a reasonable picture of the energy involved.

The consequence of these conditions is that low values of the cooling factor or heat loss coefficients are needed. Recommended values are less than 100 J/h°C for the total heat loss coefficient in [5, 10] and for the cooling factor less than 0.035 h^{-1} in [13]. In [12] cooling factors between 0.020-0.025 h^{-1} are used, and lower values are recommended for reliable long term heat release measurements. However, when the amount of insulation is increased, more energy will be stored within the materials of the calorimetric setup during the test, and this is not accounted for by the traditional method using Eq. 2. For the thermos vessels in [5, 10] this is taken into account. However, these test setups are relatively complicated and expensive compared with TSAs. Therefore, this paper will focus on TSAs, and investigate the need of taking into account the energy stored within its relatively few parts.

2. AIMS AND PURPOSES

The TSA has the advantage that it can be built with inexpensive parts that are easily assembled. The temperature sensors are generally few, and the measurements can be performed quickly. The aims and purposes in this paper is to

- Demonstrate the existence and need of taking into account the energy that is heating up the equipment using a TSA.
- Develop a reasonable simple model for evaluation of the heat of hydration in concrete, which accounts for energy stored within the different parts of a TSA.
- Investigate how the different components of a TSA setup affect the amount of energy to be compensated for.

3. REFINED HEAT OF HYDRATION EVALUATION METHOD

3.1 Test preparation and procedure

First, concrete admixture proportions are determined in order to fulfil the specific recipes requirements, i.e. slump, air entrainment etc. Dry recipe constituents are mixed in the blender for 1 minute before adding water, and the total mixing time is 5 minutes. The concrete sample, of volume 4L is placed in a cylindrical metal bucket. The heating device, a Teflon carpet, is fixed around the bucket with a steel girdle and steel clamps. The mass of the sample is recorded before and after the semi-adiabatic test to ensure that no drying out has occurred. The concrete sample is put into the TSA about 15 minutes after mixing, and the temperature is recorded every 5 minute with sensors according to the numbers in Figure 2. In the square setup only sensors Nos. 1, 2 and 4 exist. Temperature sensors Nos. 1, 2 and 3 are placed in the concrete sample, and number 4 is located in the ambient air. In our laboratory, there exists two large (denoted A) and two small (denoted B) cylindrically shaped TSA, and three square (denoted C) TSAs.

The ambient air temperature in the laboratory varies very little and can be considered to be well within the range 20±2°C. Heat of hydration is measured until the concrete sample has approximately reached the temperature of the ambient air, which usually takes about 7 days. Then, without removing the concrete sample from the TSA, the concrete sample is heated to a level of maximum measured hydration temperature + 5°C. An empirical value of the cooling factor can then be determined by analysing the spontaneously cooling behaviour.

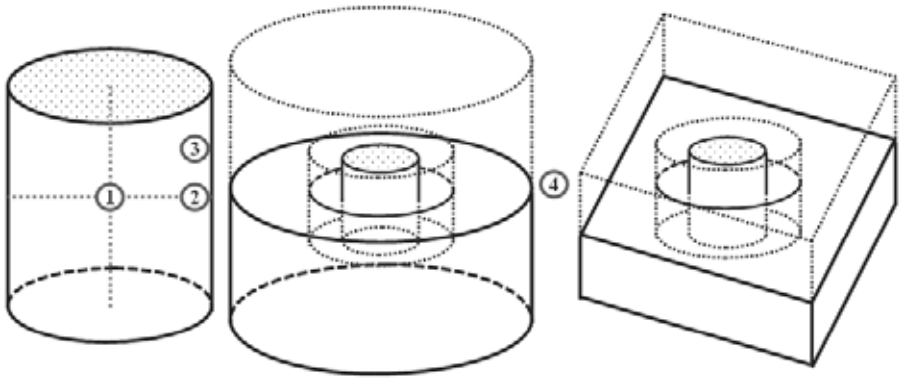

Figure 2 – Sample, cylindrical and square TSA units are shown in order from left to right. All TSAs use cellular plastic as insulation material. In addition, the square setup has an outer layer of plywood.

3.2 Empirical determination of the cooling factor

For a specific TSA setup with a constant volume of the concrete sample, the only variables should be the density and the thermal capacity of the concrete sample, see Eq. 1. However, other influencing factors may exist, e.g. aging of the TSA or some deviations in the placing of different components in the TSA setup. Therefore, to take possible variations into account, it is preferred to measure the cooling factor on each concrete sample before removing it from the test setup. A spontaneous cooling behaviour for a concrete sample is illustrated in Figure 3.

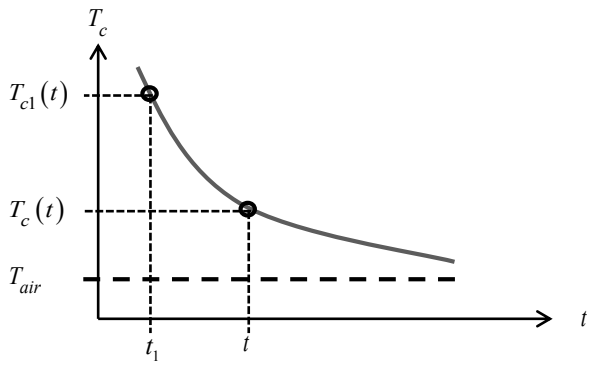

Figure 3 – Cooling behaviour for a mature concrete sample.

The common definition of the cooling factor is

$$\frac{dT}{dt} = a \cdot \left(T_c(t) - T_{air} \right) \tag{3}$$

Integrating this expression with the information given in Figure 3 results in Eq. 4, which can be fitted against empirical data with regression analysis. Here, the so called least square method is used.

$$a = \frac{\ln\left(\frac{T_c(t) - T_{air}}{T_{c1}(t) - T_{air}}\right)}{(t - t_1)} \tag{4}$$

where $T_c(t)$ [°C] = temperature in the concrete sample at time t [s or h]; $T_{c1}(t)$ [°C] = temperature in the concrete body at time t_1 [s or h].

3.3 Evaluation and modelling of heat of hydration

From the TSA measurement the evaluated heat of hydration produced per kg of cement can be determined by summation for each time step of the energy stored within the concrete sample, within the TSA components, and the energy loss due to heat flow from the concrete sample to the surrounding air, expressed by

$$q_{cem} = \frac{\rho_c \cdot c_c}{C} \cdot \left[\eta \cdot \left(T_c(t) - T_{air}\right) + a \cdot \int_0^t \left(T_c(t) - T_{air}\right) \cdot dt \right] \tag{5}$$

where η [-] = correction factor introduced in this paper accounting for heat energy used to warm up the TSAs components.

It must be noted that the model in [5, 10] could have been formulated in this way in order to fit both a thermos vessel and a TSA. Therefore, the model in this paper has been designed to suit any semi-adiabatic setup.

For normal weight concrete an approximate linear relationship exists between the water/cement ratio (w/C) of the concrete mixture and its thermal capacity [14]. However, it is quite cumbersome to determine the "correct" thermal capacity from material point of view. We calculate energies from measured temperatures, and then, before application in calculations, translate these energies back to temperatures. This is a "mathematical recirculation", which implies that information regarding concrete density and thermal capacity does not need to be known as "time" material properties. However, it is important to use the same values in the complete chain of methodology [15, 16], and acceptable constant values may be set to

$$\rho_c \cdot c_c = 2350 \cdot 1000 \text{ [J/m}^3\text{°C]} \tag{6}$$

It has been shown that the heat of hydration is approximately proportional to the degree of hydration [17]. The formulation for the degree of hydration in [15] and [18] is modified and fitted against the empirical heat data expressed by

$$q_{cem} = q_u \cdot \alpha^* = q_u \cdot \exp\left(-\left[\ln\left(1 + \frac{t_e}{t_1} \right) \right]^{-\kappa_1} \right) \quad (7)$$

where α^* [-] = is the "relative" degree of hydration; t_1 [s or h], κ_1 [-] and q_u [J/kg] are fitting parameters determined by the so called least square method; t_e [s or h] = equivalent time. The notation relative means that $\alpha^* = 1$ reflects the ultimate heat of hydration, q_u, at the individual final value for a tested concrete.

It should be noted that the heat of hydration in Eq. 7 gives about the same results as the commonly used Danish TPM (three point model) formulation in [19] for the "decisive" part of the heat of hydration description. However, Eq. 7 is favourable for predictions outside the most decisive interval, specialty for more mature concrete [16], and, besides, Eq. 7 is zero when $t_e = 0$, which is preferable in programming.

4. DEVELOPED MODEL FOR THE CORRECTION FACTOR

4.1 General

In order to get a reasonable estimation of the generated heat in concrete, hydration heat flow to the environment and heat energy stored in the involved materials must be determined. Thus, temperature measurement from initiation of the test until the system is in equilibrium "in practice" with the ambient air temperature is needed. The following observations are of importance for the presented model

- The exothermic reaction between cement and water is the only source of energy.
- The reaction energy heats up the concrete body and the ambient materials.
- Heat flow in the surrounding insulation materials can be described by Fourier's Law of conductive heat transfer.

4.2 Prerequisites for the model for the correction factor

- The TSA unit can be transformed into an associated sphere, where the concrete volume is retained, and the measured cooling factor is reflected by the actual amount of insulation in the associated sphere.
- There is good thermal contact between the materials involved. In reality, there is a small amount, less than 5L, of air between the concrete sample and the cellular plastic for the TSAs in Figure 2. This air volume is assumed to be quickly warmed up to the same temperature as the concrete. The thermal capacity by weight of air is high and its density is low. Thus, its stored energy can be neglected in relation to the other involved materials, see Table 1. Calculations have shown that the energy stored in the air affects the correction factor by less than one thousandth for TSAs evaluated in this paper. Therefore, in the presented model using an associated sphere the first layer of insulation (cellular plastic) starts where the concrete ends.

Table 1 – Chosen values for the components involved in our TSA tests. Values within brackets are currently not needed for the model in this paper. In literature, these values may vary.

	Concrete	Steel	Teflon	Air	Cellular plastic	Plywood
k [W/m °C]	(2.1-1.7)	60	(0.25)	(0.026)	0.036	0.18
c [J/kg °C]	1000	450	1000	(1000)	1500	1700
ρ [kg/m^3]	2350	7850	(2150)	(1.2)	25	800

- The thermal conductivity in the concrete is significantly higher than in the surrounding insulation materials, see Table 1. Thus, if enough insulation material is used, it is reasonable to assume that there are no, or neglectable, temperature gradients within the concrete body. For our TSAs presented in Figure 2 laboratory measurements show that the maximum temperature difference from the centre of the sample to its surface is within the accuracy of the temperature sensors (±0.5°C).
- The temperature changes in the concrete sample are relatively slow. Therefore a stationary heat flow is assumed for the associated sphere, which significantly simplifies the temperature calculations in the insulation materials. To verify this claim, a cylindrical TSA that corresponds to the approximate average cooling factor observed during laboratory tests, $a = 0,028\,[1/h]$ was simulated in 2D with ConTeSt Pro [20]. The resulting non-stationary temperature profiles were then compared with stationary 2D calculations for a cylinder, see Figure 4. The stationary estimation is based on the average concrete temperature and follows the same procedure as the 3D stationary calculations presented in this paper for the associated sphere.

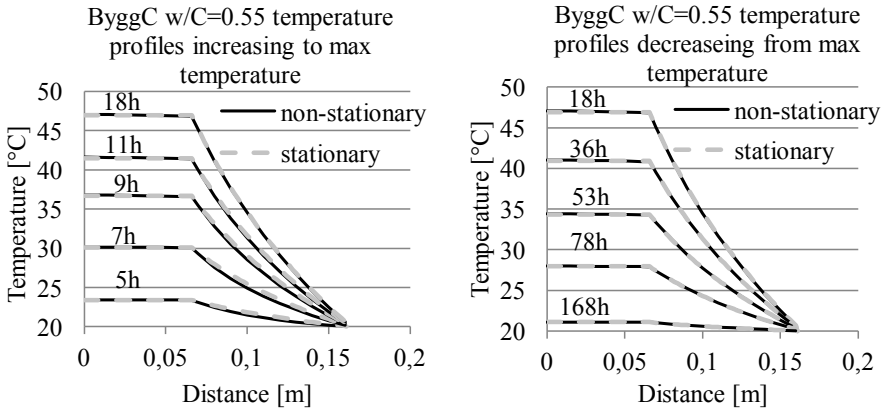

Figure 4 – Stationary and non-stationary temperature profiles in 2D simulations. The concrete radius r_c =0.066m and the insulation thickness is 0.094m. The chosen concrete mix is based on the "standard" cement used in this paper, see ByggC in Section 5.1.

A non-stationary behaviour can be observed for the hours that follow from start of the hydration process, where the stationary calculation shows a higher temperature within the insulation. This type of deviation increases for larger amount of insulation. The energy effect of this difference is illustrated by the correction factor for non-stationary and stationary conditions in Figure 5. Here, the correction factor is approximately equal after 10 hours. However, the consequences using a temporary "wrong" correction factor

during this "heat up" period is negligible in practice, as the total heat of hydration energy is very small in this period.

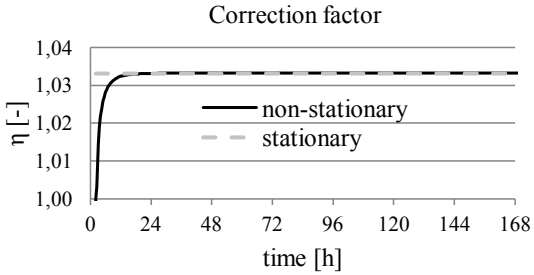

Figure 5 –The quotient between the energy stored within the insulation and the energy in the concrete when estimating the stationary and non-stationary correction factor.

4.3 Spherical heat transfer

In order to fit the model of an associated sphere to our laboratory setups, the concrete sample with radius r_c is surrounded by two materials, thicknesses l_{m1} and l_{m2}, see Figure 6.

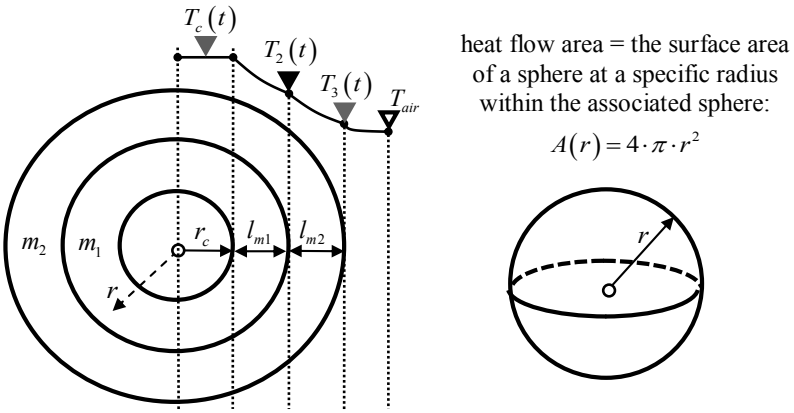

Figure 6 – A cross section of an associated sphere with a concrete sample surrounded by two layers of insulation materials. $A(r)\,[m^2]$ = heat flow area at any radius (r [m]).

Based on the information in Figure 6 the heat flow can be described by

$$\dot{Q}_{m1}(r,t) = -k_{m1} \cdot \frac{dT_{m1}(r,t)}{dr} \cdot 4 \cdot \pi \cdot r^2 \qquad \text{for} \qquad r_c \le r \le r_c + l_{m1} \tag{8}$$

$$\dot{Q}_{m2}(r,t) = -k_{m2} \cdot \frac{dT_{m2}(r,t)}{dr} \cdot 4 \cdot \pi \cdot r^2 \qquad \text{for} \quad r_c + l_{m1} \le r \le r_c + l_{m1} + l_{m2} \tag{9}$$

$$\dot{Q}_{air}(t) = h_{air} \cdot \left(T_3(t) - T_{air}\right) \cdot 4 \cdot \pi \cdot \left(r_c + l_{m1} + l_{m2}\right)^2 \quad \text{at} \quad r = r_c + l_{m1} + l_{m2} \tag{10}$$

$$\dot{Q}_{tot}(t) = h_{tot} \cdot \left(T_c(t) - T_{air}\right) \cdot 4 \cdot \pi \cdot r_c^2 \quad \text{at} \quad r = r_c \tag{11}$$

where $Q_i(r,t)$ [J] = energy in material i depending on time (t [s or h]) and radius (r [m]), and index i = m1 or m2; $\dot{Q}_i(r,t)$ [W] = $dQ_i(r,t)/dt$ = heat flow in material i; k_i [W/m °C] = thermal conductivity in material i; $T_i(r,t)$ [°C] = temperature in material i; l_i [m] = thickness of material i; $\dot{Q}_{air}(t)$ [W] = heat flow from the outer surface to air; h_{air} [W/m^2 °C] = heat transfer coefficient from the outer surface to air; T_3 [°C] = temperature at the outer surface; T_{air} [°C] = air temperature; $\dot{Q}_{tot}(t)$ [W] = heat flow from concrete to air; h_{tot} [W/m^2 °C] = heat transfer coefficient from concrete to air; $T_c(t)$ [°C] = temperature in the concrete body.

For a stationary heat flow Eqs. 8-11 describe the same flow formulated by

$$\dot{Q}_{m1}(r,t) = \dot{Q}_{m2}(r,t) = \dot{Q}_{air}(t) = \dot{Q}_{tot}(t) = \dot{Q}_{hf}(t) \tag{12}$$

where $\dot{Q}_{hf}(t)$ [W] = is the stationary heat flow at time t.

All equations concerning heat flow and temperature distribution in the subsequent text in this chapter are based on stationary heat flow conditions. In order to determine the temperature $T_{m1}(r,t)$ at specific point at time t within the material 1, the following integration needs to be performed

$$\frac{\dot{Q}_{hf}(t)}{k_{m1} \cdot 4 \cdot \pi} \cdot \int_r \frac{dr}{r^2} = \int_T -dT_{m1}(r,t) \tag{13}$$

if the boundary conditions are known it becomes

$$\frac{\dot{Q}_{hf}(t)}{k_{m1} \cdot 4 \cdot \pi} \cdot \int_{r_c}^{r} \frac{dr}{r^2} = -\int_{T_c(t)}^{T_{m1}(r,t)} dT_{m1}(r,t) \tag{14}$$

which gives

$$\frac{\dot{Q}_{hf}(t)}{k_{m1} \cdot 4 \cdot \pi} \cdot \left(\frac{1}{r_c} - \frac{1}{r}\right) = T_c(t) - T_{m1}(r,t) \tag{15}$$

The boundary temperature in the concrete sample, $T_c(t)$, can be measured at any time. Then, the temperature $T_{m1}(r,t)$ can be calculated for any point $r_c \le r \le r_c + l_{m1}$ at time t within the material 1 expressed by

$$T_{m1}(r,t) = T_c(t) - \frac{\dot{Q}_{hf}(t)}{k_{m1} \cdot 4 \cdot \pi} \cdot \left(\frac{r - r_c}{r_c \cdot r} \right) \tag{16}$$

At the end of material 1, where $r = r_c + l_{m1}$, we let $T_{m1}(r,t) = T_2(t)$, see Figure 6. Then, the corresponding expression for material 2 becomes

$$T_{m2}(r,t) = T_2(t) - \frac{\dot{Q}_{hf}(t)}{k_{m2} \cdot 4 \cdot \pi} \cdot \left(\frac{r - (r_c + l_{m1})}{(r_c + l_{m1}) \cdot r} \right) \tag{17}$$

At the end of material 2, where $r = r_c + l_{m1} + l_{m2}$, we let $T_{m2}(r,t) = T_3(t)$, see Figure 6.

Now, when the boundary conditions are known, T_2 and T_3 from Eqs. 16-17, by use of Eqs. 8-12 the temperature difference within each material is expressed as

$$T_c(t) - T_2(t) = \frac{\dot{Q}_{hf}(t) \cdot l_{m1}}{4 \cdot \pi \cdot k_{m1} \cdot r_c \cdot (r_c + l_{m1})} \tag{18}$$

$$T_2(t) - T_3(t) = \frac{\dot{Q}_{hf}(t) \cdot l_{m2}}{4 \cdot \pi \cdot k_{m2} \cdot (r_c + l_{m1}) \cdot (r_c + l_{m1} + l_{m2})} \tag{19}$$

$$T_3(t) - T_{air} = \frac{\dot{Q}_{hf}(t)}{h_{air} \cdot 4 \cdot \pi \cdot (r_c + l_{m1} + l_{m2})^2} \tag{20}$$

$$T_c(t) - T_{air} = \frac{\dot{Q}_{hf}(t)}{h_{tot} \cdot 4 \cdot \pi \cdot r_c^2} \tag{21}$$

Summation of the temperature differences from the concrete sample to the air gives

$$T_c(t) - T_{air} = \left(T_c(t) - T_2(t)\right) + \left(T_2(t) - T_3(t)\right) + \left(T_3(t) - T_{air}\right) \tag{22}$$

Substituting Eqs. 18-21 into Eq. 22 gives the total heat transfer coefficient from the concrete sample to the air expressed by

$$h_{tot} = \frac{1}{r_c^2} \cdot \left(\frac{l_{m1}}{k_{m1} \cdot r_c \cdot (r_c + l_{m1})} + \frac{l_{m2}}{k_{m2} \cdot (r_c + l_{m1}) \cdot (r_c + l_{m1} + l_{m2})} + \frac{1}{h_{air} \cdot (r_c + l_{m1} + l_{m2})^2} \right)^{-1} \tag{23}$$

Thus, the individual temperatures within each material, Eqs. 18-21, can be determined by the heat flow expression in Eq. 11.

4.4 Heat energy stored within the materials of the TSA

In order to account for the amount of energy heating up material 1 of the TSA, the average temperature within the material, T_{m1}^{ave}, is expressed as

$$T_{m1}^{ave} = \frac{1}{V_{m1}} \cdot \int_{r_c}^{r_c+l_{m1}} T_{m1}(r,t) \cdot 4 \cdot \pi \cdot r^2 \cdot dr \tag{24}$$

where $V_{m1}\,[\mathrm{m}^3] = \frac{4 \cdot \pi}{3} \cdot \left[\left(r_c + l_{m1} \right)^3 - r_c^3 \right]$ is the volume for material 1, which gives

$$T_{m1}^{ave}(t) = \frac{3}{\left(r_c + l_{m1} \right)^3 - r_c^3} \cdot \left\{ \begin{array}{l} \left(T_c(t) - \frac{h_{tot} \cdot \left(T_c(t) - T_{air} \right) \cdot r_c}{k_{m1}} \right) \cdot \left[\frac{\left(r_c + l_{m1} \right)^3 - r_c^3}{3} \right] \\ + \frac{h_{tot} \cdot \left(T_c(t) - T_{air} \right) \cdot r_c^2}{k_{m1}} \cdot \left[\frac{\left(r_c + l_{m1} \right)^2 - r_c^2}{2} \right] \end{array} \right\} \tag{25}$$

The corresponding expression for the average temperature in material 2, T_{m2}^{ave}, is expressed by

$$\begin{array}{l} T_{m2}^{ave}(t) = \frac{3}{\left(r_c + l_{m1} + l_{m2} \right)^3 - \left(r_c + l_{m1} \right)^3} \cdot \\ \left\{ \begin{array}{l} \left(T_2(t) - \frac{h_{tot} \cdot \left(T_c(t) - T_{air} \right) \cdot r_c^2 \cdot \left(r_c + l_{m1} \right)}{k_{m2}} \right) \cdot \left[\frac{\left(r_c + l_{m1} + l_{m2} \right)^3 - \left(r_c + l_{m1} \right)^3}{3} \right] + \\ \frac{h_{tot} \cdot \left(T_c(t) - T_{air} \right) \cdot r_c^2}{k_{m2}} \cdot \left[\frac{\left(r_c + l_{m1} + l_{m2} \right)^2 - \left(r_c + l_{m1} \right)^2}{2} \right] \end{array} \right\} \end{array} \tag{26}$$

Thus, the thermal energy in each of the materials are expressed as

Concrete $$Q_c(t) = \rho_c \cdot c_c \cdot V_c \cdot \left(T_c(t) - T_{air} \right) \tag{27}$$

Material 0 $$Q_{m0}(t) = \sum_j \left(\rho_j \cdot c_j \cdot V_j \right) \cdot \left(T_c(t) - T_{air} \right) \tag{28}$$

Material 1 $$Q_{m1}(t) = \rho_{m1} \cdot c_{m1} \cdot V_{m1} \cdot \left(T_{m1}^{ave}(t) - T_{air} \right) \tag{29}$$

Material 2 $$Q_{m2}(t) = \rho_{m2} \cdot c_{m2} \cdot V_{m2} \cdot \left(T_{m2}^{ave}(t) - T_{air} \right) \tag{30}$$

where $m0$ = material 0 reflects the stored thermal energy for materials in direct contact with the concrete sample, which are considered to have the same temperature as the concrete sample; j = index for individual materials within material 0. In the TSA setup presented here, material 0

consists of a steel bucket ($j=1$), a steel girdle ($j=2$), steel clamps ($j=3$) and a heating carpet of Teflon ($j=4$).

The heat of hydration energy stored within material 0, material 1 and material 2 are all proportional to the heat of hydration energy stored in the concrete sample. Therefore the energy correction factor is expressed by

$$\eta(t)=1+\frac{Q_{m0}(t)+Q_{m1}(t)+Q_{m2}(t)}{Q_c(t)} \tag{31}$$

Eq. 31 formally describes the correction factor as a function of time. However, the energy in each material is proportional to the energy stored in the concrete sample reflected by the term $\left(T_c(t)-T_{air}\right)$. Therefore, the correction factor is constant and can be evaluated for any time t.

In Figure 7 the total heat of hydration energy at any time t is the sum of the energy stored in the materials of the TSA, i.e. the sum of Eqs. 27-30, and the energy loss from the TSA due to the accumulated heat flow, see the second part of Eq. 2. Based on a measured value of the cooling factor, a in Eq. 4, the energy due to heat flow, $Q_{hf}(t)$, is expressed by

$$Q_{hf}(t)=\int_0^t \dot{Q}_{hf}(t)\cdot dt=\rho_c\cdot c_c\cdot V_c\cdot a\cdot\int_0^t\left(T_c(t)-T_{air}\right)\cdot dt \tag{32}$$

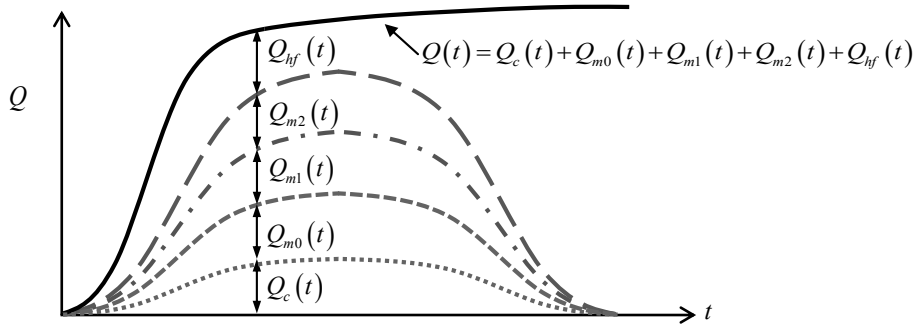

Figure 7 – The total energy is the sum of the energies stored in the concrete, the ambient materials and the energy loss to the surrounding air, see Eqs. 27-30 and 32. Note that this figure only illustrates the energies involved without respect to real size relations.

4.5 Determination of stationary heat transfer coefficient

In order to calculate the associated stationary temperature distribution the total heat transfer coefficient, h_{tot}, has to be calculated. The stationary heat flow based on the rate of temperature changes in the concrete sample is expressed by

$$\dot{Q}_{hf}(t)=\frac{dT_c(t)}{dt}\cdot V_c\cdot\rho_c\cdot c_c \tag{33}$$

Combining Eq. 11 with Eqs. 3 and 33 gives

$$h_{tot} \cdot \left(T_c(t) - T_{air}\right) \cdot 4 \cdot \pi \cdot r_c^2 = a \cdot \left(T_c(t) - T_{air}\right) \cdot \frac{4 \cdot \pi \cdot r_c^3}{3} \cdot \rho_c \cdot c_c \tag{34}$$

which results in

$$h_{tot} = \frac{a \cdot r_c \cdot \rho_c \cdot c_c}{3} \tag{35}$$

Eq. 35 expresses the parameter h_{tot} for an associated sphere with the same cooling factor as the real TSA.

4.6 Steps to determine the correction factor

1. Determine, or use Eq. 6, concrete density and heat capacity by weight. The volume of the concrete sample is known and is transformed into the associated concrete sphere with radius r_c. Heat capacity by weight for all materials in the TSA is also needed.

2. Determine, using data sheets or calibration, the thermal conductivity of all material layers, k_i, in the associated sphere.

3. The heat transfer coefficient from outer surface to air should be estimated. For our laboratory conditions h_{air} is approximately set to 10 W/m^2 °C.

4. Evaluate a cooling factor from the laboratory tests and calculate the total heat transfer coefficient, h_{tot} using Eq. 35.

5. The total heat transfer coefficient, h_{tot} in Eq. 35, reflects the real cooling factor. By using Eq. 23 and an iteration technique l_{m1} and l_{m2} can be determined. In cases with only one insulation material ($l_{m1} > 0$ and $l_{m2} = 0$) the use of Eq. 23 is straightforward. This is the case here for two cylindrical TSAs, see Figure 2.

6. The square TSA used here, see Figure 2, has an outer layer of plywood. The associated sphere is constructed with the condition that the relation between the stored energy per temperature unit is maintained between the two materials, which is expressed by

$$\delta_{m1,m2} = \frac{\rho_{m1} \cdot c_{m1} \cdot V_1}{\rho_{m2} \cdot c_{m2} \cdot V_2} \tag{36}$$

which gives

$$V_2 = \frac{1}{\delta_{m1,m2}} \cdot \frac{\rho_{m1} \cdot c_{m1} \cdot V_1}{\rho_{m2} \cdot c_{m2}} \tag{37}$$

where V_1 and V_2 are the real volumes of material 1 and material 2, respectively.

The volume of material 1 in the associated sphere is given by

$$V_{m1} = \frac{4 \cdot \pi}{3} \cdot \left[\left(r_c + l_{m1} \right)^3 - r_c^3 \right] \tag{38}$$

and the volume of material 2 in the associated sphere using Eq. 37 results in

$$V_{m2} = \frac{1}{\delta_{m1,m2}} \cdot \frac{\rho_{m1} \cdot c_{m1} \cdot V_{m1}}{\rho_{m2} \cdot c_{m2}} \tag{39}$$

and

$$V_{m2} = \frac{4 \cdot \pi}{3} \left[\left(r_c + l_{m1} + l_{m2} \right)^3 - \left(r_c + l_{m1} \right)^3 \right] \tag{40}$$

which gives

$$l_{m2} = \left[\frac{3 \cdot V_{m2}}{4 \cdot \pi} + \left(r_c + l_{m1} \right)^3 \right]^{1/3} - r_c - l_{m1} \tag{41}$$

7. The consequences of Eqs. 36-41 are that l_{m2} and V_{m2} are expressed as functions of l_{m1}. So, h_{tot} in Eq. 23 is solely a function of l_{m1}, and the size of l_{m1} is here determined by an iterative technique. l_{m2} is calculated using Eq. 41, and the size of the associated sphere is established. Now, the constant correction factor, Eq. 31, is determined for time t, see Figure 7.

5. EVALUATION OF THE EFFECT OF THE CORRECTION FACTOR

5.1 Tested concrete recipes

Here the purpose is to show how the correction factor affects the actual temperatures in a concrete structure. Two common Swedish cements are used, see Tables 2 and 3. AnlC is a "moderate heat" cement, that generally is used for civil engineering structures. ByggC is a "standard" cement causing higher concrete temperature than AnlC, and its application area is usually concerning housing.

Table 2 – Oxides, clinker minerals and specific surface of tested cements. ByggC is of type CEM II/A-LL 42,5 R containing about 13% LL, and AnlC is of type CEM I 42,5 N SR3 MH/LA produced by CEMENTA AB.

Cement	Oxides [%]					Clinker minerals [%]				Specific surface
	CaO	SiO_2	Al_2O_3	Fe_2O_3	SO_3	C_3S	C_2S	C_3A	C_4AF	[m^2/kg]
ByggC	61.4	18.7	3.9	2.8	3.5	54.1	8.9	5.1	7.8	460
AnlC	64.1	22.4	3.7	4.5	2.4	48.0	28.0	2.1	13.8	316

Table 3 – Main constituents of tested concretes.

Recipe	Cement	Cement content [kg/m^3]	w/C [-]
1	ByggC	360	0.55
2	AnlC	340	0.55

5.2 Calculated values of the correction factor

The materials in direct connection with the concrete sample in the TSAs are weighted in order to determine their stored energy, see Table 1 and 4.

Table 4 –Weighted components in direct connection with the concrete sample. The weight of the steel bucket includes the weight of a steel lid.

	Steel bucket [kg]	Steel clamps [kg]	Steel girdle [kg]	Teflon carpet [kg]
TSA A and B	0.427	0.164	0.069	0.099
TSA C	0.465			0.408

The heat of hydration for the recipes in Table 3 was evaluated from measurements performed in TSA A and B. The cooling factors and other parameters needed for the iteration process and their resulting correction factors are presented in Table 5.

Table 5 – Parameters used in the iteration process, and the resulting correction factor.

Recipe/ TSA	a [1/h]	h_{tot} [W / m^2°C]	h_{air} [W / m^2°C]	k_{m1} [W / m°C]	r_c [m]	l_{m1} [m]	V_{m1} [m^3]	η [-]
1/A	0.0237	0.5071	10	0.036	0.0985	0.2508	0.174	1.157
1/B	0.0327	0.7014	10	0.036	0.0985	0.1035	0.031	1.078
2/A	0.0259	0.5552	10	0.036	0.0985	0.1862	0.093	1.118
2/B	0.0324	0.6933	10	0.036	0.0985	0.1062	0.032	1.079

In the associated sphere the radius depends on the thickness of the concrete sample and the insulation, see Figure 6. A small decrease of the cooling factor gives a small increase of insulation thickness in material 1 (l_{m1}). However, the volume is significantly greater since it is a cubic function, see Eq. 38. Therefore, a small difference in cooling factor (a) for TSA A between recipe 1 and 2 in Table 5 results in a quite large difference in calculated volume (V_{m1}). The difference in energy stored within these insulation volumes are reflected by the correction factor in Table 5.

5.3 Evaluated heat of hydration

Both the traditional method, Eq. 2, and the refined method, Eq. 5, were used to evaluate heat of hydration (q_{cem}) for recipes 1 and 2 in Table 3. The parameters of Eq. 7 were fitted against the test results in Figure 8 from TSA A and B for each recipe, see Table 6.

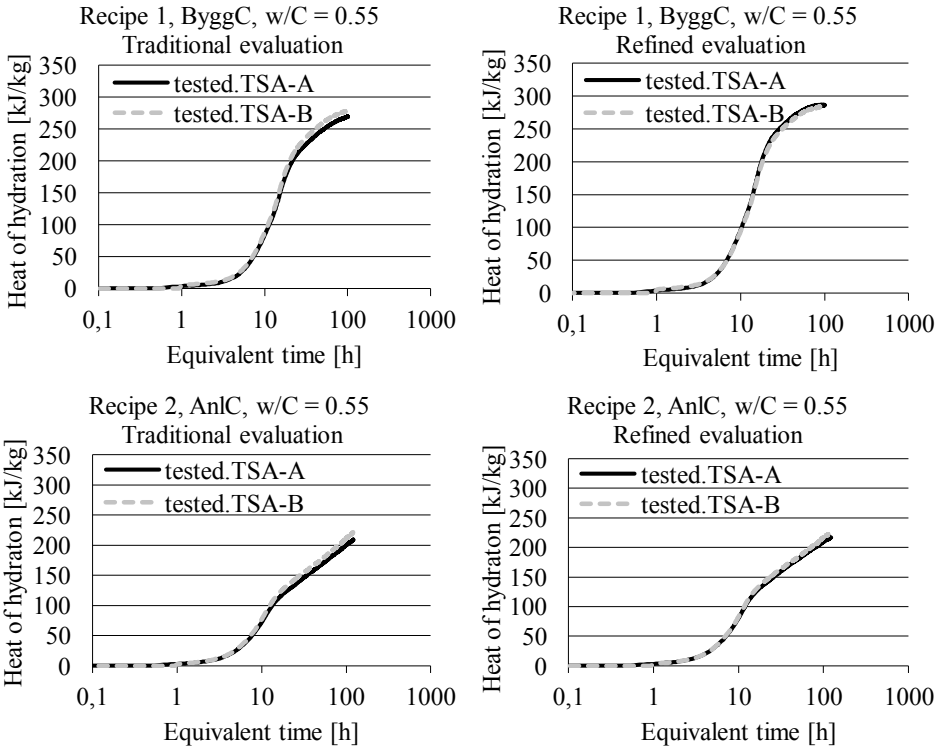

Figure 8 – Evaluated heat of hydration using the traditional method, Eq. 2, and the refined method, Eq. 5. Fitting parameters using Eq. 7 are presented in Table 6.

TSA A has a considerable lower value of the cooling factor compared to TSA B, see Table 5. This is caused by a higher amount of insulation material in TSA A. The energy stored in the insulation is reflected by the correction factor, which always is increased with decreased cooling factor. The consequence of not taking this energy into account using a larger TSA will result in a lower heat of hydration compared to a smaller TSA. This effect can be seen for the traditional evaluation in Figure 8 using the traditional evaluation, where TSA B is higher than TSA A. These results show that general recommendations concerning low cooling factors may result in too low heat of hydration using TSAs that are evaluated with the traditional method.

By using the refined evaluation the heat of hydration curves become approximately equal for the decisive part of the curves, see approximately equivalent time up to 100h in Figure 8. These results show that it is important to consider energies stored within the TSA materials.

Table 6 – Model parameters for evaluated heat of hydration results, see Eq. 7.

Recipe/TSA	Traditional evaluation (Eqs. 2 and 6)			Refined evaluation (Eqs. 5 and 6)		
	q_u [J/kg]	t_1 [h]	κ_1 [-]	q_u [J/kg]	t_1 [h]	κ_1 [-]
1/A	296000	6.54	2.28	300000	5.91	2. 27
1/B	309000	6.50	2.34	300000	6.23	2.96
2/A	420000	21.83	0.58	345000	11.01	0.85
2/B	358000	12.61	0.79	345000	10.39	0.87

5.4 Simulation of temperature development within walls

In order to determine the effect of the correction factor, the maximum temperature reached within a concrete structure was determined using the parameters in Table 6. This simulation was performed with ConTeSt Pro in 2D [20], where five concrete walls of different thicknesses with a formwork of plywood were studied. The air temperature was kept constant at 20°C, and the heat transfer coefficient from the outer surface to air (h_{air}) is set to 10 W/m^2 °C. The results are presented in Table 7 and 8

where ΔT_A and ΔT_B show the temperature difference between traditional and refined evaluation for TSA A and B, respectively; ΔT_{ABR} shows the temperature difference between the refined evaluation using TSA A and B.

Table 7 – Maximum temperature reached within a wall of different sizes, based on recipe 1.

Wall thickness [m]	Calculated temperatures, recipe 1, ByggC [°C]						
	1/A			1/B			1/(A+B)
	Traditional evaluation	Refined evaluation	ΔT_A	Traditional evaluation	Refined evaluation	ΔT_B	ΔT_{ABR}
0.1	36.6	40.7	-4.1	37.0	38.9	-1.9	1.8
0.2	42.9	47.4	-4.5	43.6	45.7	-2.1	1.7
0.4	49.3	53.6	-4.3	50.3	52.2	-1.9	1.4
0.8	55.3	58.9	-3.6	56.7	58.2	-1.6	0.7
1.6	60.0	62.4	-2.4	61.7	62.6	-0.9	-0.2

Table 8 – Maximum temperature reached within a wall of different sizes, based on recipe 2.

Wall thickness [m]	Calculated temperatures, recipe 2, AnlC [°C]						
	2/A			2/B			2/(A+B)
	Traditional evaluation	Refined evaluation	ΔT_A	Traditional evaluation	Refined evaluation	ΔT_B	ΔT_{ABR}
0.1	27.9	29.1	-1.2	28.9	29.7	-0.8	-0.6
0.2	31.7	33.2	-1.5	32.9	33.9	-1.0	-0.7
0.4	36.4	38.0	-1.6	37.7	38.8	-1.1	-0.8
0.8	41.8	43.4	-1.5	43.1	44.1	-1.0	-0.7
1.6	47.8	48.9	-1.1	48.7	49.4	-0.8	-0.5

The general behaviour for both ByggC and AnlC in Tables 7 and 8 are

- The maximum temperature level is higher for thicker walls for both traditional and refined evaluation.
- Traditional heat of hydration evaluation for TSA B gives a higher maximum temperature compared with TSA A, since less energy is lost to the smaller insulation material in TSA B.
- The temperature level is always higher for the refined evaluation compared to the traditional evaluation, since the energy in the surrounding materials are considered.
- ByggC is the “standard” cement with significantly higher heat of hydration during the decisive period and shows a higher maximum temperature compared to AnlC.
- ByggC shows a larger temperature difference between TSA A and B compared to AnlC, which is a consequence of that ByggC is the “faster” cement.
- The differences in ΔT_{ABR} are smallest for the refined evaluation and the largest wall. This indicates that the refined evaluation reflects the “true” material parameters, as the centre point of the thickest wall is most dependent on the heat of hydration.

The deviation of maximum temperatures between the traditional and the refined evaluation are of importance both for strength growth and crack risk calculations. For the larger TSA A and the faster cement ByggC the maximum difference in temperature is within 4.5°C, which for the estimation of strength growth can be regarded on "the safe side", i.e. too low strength values and too long hardening times are calculated, but this "extra margin" might not be wanted in practice. For the calculation of crack risks, and especially for risks of through cracking at high restraint, 4.5°C underestimates the crack risk substantially. This is explained by the maximum addition of the design strain ratio [= additional tensile strain/failure tensile strain] might be as big as $0.7 \cdot 4.5/10 = 0.32$ [21, 22]. Let us assume that the design strain ratio is calculated to be at most 0.7 (rather common requirement for civil engineering structures), the "true" strain ratio will be $0.7 + 0.32 = 1.02$. A strain ratio > 1 means obvious risk of cracking. Even a small temperature difference of about 2°C might result in an underestimation of the strain ratio with 0.14, which also is a too large difference in the calculations (0.7+0.14=0.84). Even if the underestimation in calculated strain ratios does not result in cracking, the margin in the safety factors are significantly reduced. Therefore, these results show that it is important to consider energies stored within the TSA materials.

5.5 Pre-calculated correction factors for TSAs at Luleå University of Technology

It has been shown that the correction factor will change due to the amount of insulation material in the TSA. For our cylindrical and square TSAs a normal span of cooling factors is between 0.023-0.034 1/h and 0.040-0.045 1/h, respectively. Therefore, an extended span with pre-calculated correction factors for corresponding cooling factors will simplify future evaluations, see Figures 9 and 10. In addition, a reasonable interval for normal weight concretes and their effect on the correction factor is shown. The thermal capacity by weight is kept constant at 1000 J/kg °C since it is cumbersome to establish in hydrating concrete.

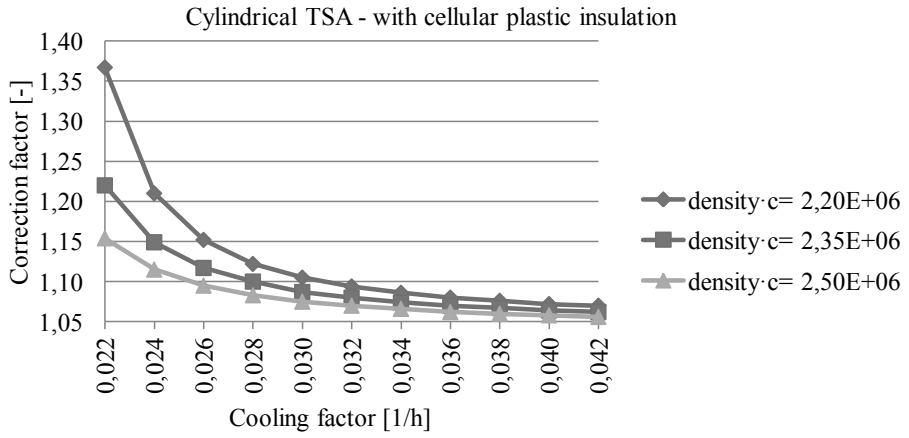

Figure 9 – Cooling and correction factor concerning TSA A and B.

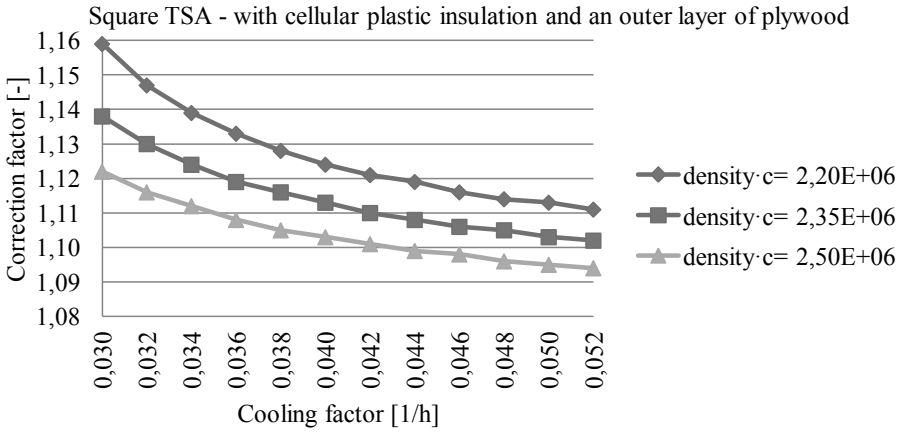

Figure 10 – Cooling and correction factor concerning TSA C.

In Figure 9 and 10 it can be seen that the higher the density, the lower cooling and correction factor. An increased amount of insulation gives a lower cooling factor, but a higher correction factor. Thus, it is again shown, that recommendations regarding low values of the cooling factor may result in too low hydration energy when evaluation is performed with the traditional method, Eq. 2.

6. SUMMARY AND CONCLUSIONS

The energy quantity of the exothermic reaction between cement and water has long been of importance since it affects the temperature levels within a concrete structure. Several adiabatic methods have been used to determine heat of hydration. The traditional semi-adiabat (TSA) has been popular to use for engineering purposes because of its simple construction with cheap parts.

The traditional evaluation method was presented in 1954 [11] and is still used today. Improvements to this evaluation method are found in [5] and [10], where energy stored in the semi-adiabatic setup is accounted for. However, the evaluation method in [5] and [10] only works for their specific semi-adiabatic setup using thermos vessels, and not for TSAs. Therefore, this paper presents a refined and general model that accounts for energies stored in the concrete sample and within all its surrounding materials, which is reflected by a correction factor formally increasing the energy in the concrete sample.

The concrete sample and the TSA are transformed into an associated sphere. The volume of the concrete sample is maintained in the associated sphere as the real volume in the TSA. The relative volume of the additional TSA materials within the associated sphere is determined by an iterative process, with the condition that the measured cooling factor is the same in the sphere. This paper presents a technique in which the only iterated parameter is the thickness of the first layer of insulation. Heat of hydration energy is calculated as the sum of energies in the concrete sample and all the surrounding materials. The correction factor reflects these additional energies in the surrounding materials. For our laboratory additional materials consist of a steel bucket, a

steel girdle, steel clamps, a heating carpet of Teflon and two layers of insulation. All these additional materials have a significant effect on the correction factor.

Two common Swedish cements are studied in this paper. ByggC is a "standard" cement and its application area is usually housing, and AnlC is a "moderate heat" cement generally used for civil engineering structures. The results from the heat of hydration evaluation using these concrete mixes show that TSA A has a considerable lower value of the cooling factor compared to TSA B. This is caused by the higher amount of insulation material in TSA A, as TSAs with lower cooling factors always store more energy in the surrounding material for a specific mix. Without compensation for this additional energy in the evaluation process, a lower cooling factor always results in a lower heat of hydration. Using the refined evaluation, i.e. including the energy compensation, the heat of hydration curves become approximately equal for TSA A and B. This shows that it is important to consider energies stored within the TSA materials, and that general recommendations concerning low cooling factors may result in too low heat of hydration using TSAs that are evaluated with the traditional method.

In order to investigate effects of the correction factor for our two mixes, the evaluated parameters were applied in 2D structural simulations. Five concrete walls of different thicknesses were used. The results show that temperatures are almost underestimated by 5°C for an "ordinary" cement, and 2°C for a "moderate heat" cement. The consequences for calculated strength development are that the lower strength causes longer hardening time than needed, which might be regarded as being "on the safe side", but this "extra margin" might not be wanted in practice. For crack risks, the calculated strain/stress ratios are underestimated with at most 0.32 (ordinary cement) and 0.14 (moderate heat cement). A rather common strain/stress ratio in design is 0.70, and based on that the "true" strain/stress ratio might be 1.02 and 0.84, respectively. For the true situation these underestimated temperatures may result in an obvious risk of cracking or at least a significant reduced safety factor. This confirms that it is important to consider energies stored within the TSA materials.

ACKNOWLEDGEMENTS

The authors of the paper acknowledge The Swedish Research Council Formas, Cementa AB and Betongindustri AB. The laboratory tests have been performed in cooperation with personnel from Complab at Luleå University of Technology, which is hereby acknowledged.

REFERENCES

1. Kjellsen, K.O., Detwiler, R.J., and Gjørv, O.E., "Pore Structure of Plain Cement Pastes Hydrated at Different Temperatures," *Cement and Concrete Research*, Vol. 20, No. 6, November 1990, pp. 927-933.
2. Kjellsen, K.O., Detwiler, R.J., and Gjørv, O.E., "Development of Microstructures in Plain Cement Pastes Hydrated at Different Temperatures," *Cement and Concrete Research*, Vol. 21, No. 1, January 1991, pp. 179-189.
3. Fjellström, P., Jonasson, J-E., Emborg, M., and Hedlund, H., "Model for Concrete Strength Development Including Strength Reduction at Elevated Temperatures," *Nordic Concrete Research*, Vol. 45, No. 1, June 2012, pp. 25-44.
4. Concrete: "Heat Development," Nordtest Method, NT BUILD 388, 1992, 4 pp.

5. RILEM Technical Committee 119-TCE, "Adiabatic and Semi-Adiabatic Calorimetry to Determine the temperature Increase in Concrete due to Hydration Heat of Cement," RILEM Report 15, Prevention of Thermal Cracking in Concrete at Early Ages, Edited by R. Springenshmid, E & FN Spon, London, 1998, pp. 315-330.
6. Ng, P.L., Ng, I.Y.T., and Kwan, K.H., "Heat Loss Compensation in Semi-Adiabatic Curing Test of Concrete," *ACI Materials Journal*, Vol. 105, No. 1, January-February 2008, pp. 52-61.
7. Concrete: "Heat Development," NordTest Method, NT BUILD 488, 1997, 6 pp.
8. Poole, J.L., Riding, K.A., Folliard, K.J., Juenger, M.C.G., and Schindler, A.K., "Hydration Study of Cementitious Materials using Semi-Adiabatic Calorimetry," *ACI Special Publication* 241CD Concrete Heat Development: Monitoring, Prediction & Management, Edited by K. Wang & A. Schindler, paper SP-241-5, Vol. 241, April 1 2007, pp. 59-76.
9. Riding, K.A., Poole, J.L., Juenger, M.C.G., Schindler, A.K., and Folliard, K.J., "Calorimetry Performed On-Site: Methods and Uses," *ACI Special Publication* 241CD Concrete Heat Development: Monitoring, Prediction & Management, Edited by K. Wang & A. Schindler, paper SP-241-3, Vol. 241, April 1 2007, pp. 25-38.
10. EN 196-9:2010, "Methods of Testing Cement – Part 9: Heat of Hydration – Semi-Adiabatic Method," European Committee for Standardization (CEN), 2010, Brussels.
11. Rastrup, E., "Heat of Hydration in Concrete," *Magazine of Concrete Research*, Vol. 6, No. 17, September 1954, pp. 79-92.
12. Helland, S., "Norwegian Standards on activation energy and heat release," IPACS report no. BE96-3843/2001:24-9, TU Luleå, Sweden, 2001, 27 pp.
13. NS 3657:1993, "Concrete Testing – Determination of Heat Release," Norwegian Standard, September 1993.
14. Whiting, D., Litvin, A., and Goodwin, S.E., "Specific Heat of Selected Concretes," *Journal of the American Concrete Institute*, Vol. 75, No. 7, July 1 1978, pp. 299-305.
15. Jonasson, J-E., "Slipform Construction – Calculations for Assessing Protection Against Early Freezing," Swedish Cement and Concrete Research Institute Report, no. 4:84, 1984, Stockholm, 70 pp.
16. Jonasson, J-E., "Modelling of Temperature, Moisture and Stresses in Young Concrete," Doctoral thesis 1994:153D, Luleå University of Technology, Luleå 1994, 225 pp.
17. Danielsson, U., "Conduction Calorimeter Studies of the Heat of Hydration of a Portland Cement," Swedish Cement and Concrete Research Institute Report, no. 38, 1966, Stockholm, 121 p. Cited from [19].
18. Byfors, J., Plain Concrete at Early Ages," Swedish Cement and Concrete Research Institute Report, no. 3:80, 1980, Stockholm, 464 pp.
19. Freiesleben Hansen, P., and Erik, J.P., "Curing of Concrete Structures," Danish Concrete and Structural Research Institute, Report prepared for CEM – General Task Group No. 20, Durability and Service Life of Concrete structures, December 1984, pp. 45.
20. ConTeSt Pro, "Användarhandbok – ConTeSt Pro (Users manual – Program for Temperature and Stress Calculations in Concrete)," Developed by JEJMS Concrete AB in co-operation with Luleå University of Technology, Cementa AB and Peab Öst AB, Danderyd, Sweden: Cementa AB, pp. 207. (In Swedish).
21. Larson, M., "Estimation of Crack Risk in Early Age Concrete: Simplified Methods for Practical Use," Licentiate thesis 2000:10, Luleå University of Technology, Luleå 2000, pp. 156.
22. Jonasson, J-E., Wallin, K., Emborg, M., Gram, A., Saleh, I., Nilsson, M., Larson, M., and Hedlund, H., "Temperature Cracks in Concrete Structures: Handbook with Diagrams for Crack Risk Estimation Including Measures for Typical Cases. Part D," Technical report 2001:14, Luleå University of Technology, Luleå 2001, pp. 107. (In Swedish)

Use of Limestone in Cement: The Effect on Strength and Chloride transport in Mortars.

Dimitrios Boubitsas
Lic.Eng., Ph.D. Student
University of Lund, Sweden
CBI Swedish Cement and Concrete Institute
Box 857, SE-501 15 Borås, Sweden
E-mail: dimitrios.boubitsas@cbi.se

ABSTRACT

This paper describes studies carried out to examine the influence on strength and chloride ingress when Portland cement is replaced with limestone filler. In the chloride ingress study both an accelerated method and field exposure measurements up to one year were employed. The results show that the method of measuring the resistance to chloride ingress can have a major influence on the assessment of the effect of different binders. Further, the effect on chloride resistance, when replacing Portland cement with limestone filler is strongly dependent of the replacement ratio. The effect on compressive strength when replacing Portland cement with limestone filler is also strongly dependent of the replacement ratio.

Key words: strength, chloride transport, limestone filler, cementitious efficiency, k-value.

1. INTRODUCTION

Different mineral additions for partial replacement of Portland cement (PC) in concrete and in other cement based materials are widely used, and will become more and more common as there are environmental, economic, and technical benefits of using mineral additions. Limestone is one of these mineral additions. The European standard EN 197-1[1] permits use of limestone as an ingredient in CEM II cements in two ranges: CEM II/A cements containing between 6% and 20% limestone (by mass) and CEM II/B cements containing between 21% and 35% limestone. From the data presented in [2] it can be concluded that Portland limestone cement (PLC) was the single largest type of cement used in 2004 in Europe.

The substitution of parts of the Portland cement by limestone filler has been shown to have several effects on the properties of cement-based materials. In studies of pure compounds of clinker, various authors have reported that the C_3S hydration rate is accelerated by limestone filler addition [3, 4], that the hydration rate of C_3A is also enhanced [5], and that calcium carboaluminates are formed [5,6]. Investigations on cements have also shown that the overall hydration rate of cement is accelerated with the incorporation of limestone filler [7]. The higher degree of hydration at an early age is also reflected by higher early age strength. It has been

shown that the use of limestone filler as a replacement for cement may improve or at least not affect significantly the strength of both mortars and concretes at early ages, but this improvement has been found to disappear at a later age [8, 9, 10, 11,12].

Limestone does not possess any hydraulic or pozzolanic properties and consequently it does not produce C-S-H. This means that a replacement of clinker with limestone gives an increased water to cement ratio (w/c-ratio). It is generally accepted that the durability of cement-based materials to a large extent is governed by their resistance to penetration of aggressive media [13, 14]. The most dominant parameter determining mass transport in cement-based materials is the w/c-ratio [15, 16], which also is given as a criterion in standards and regulations concerning durability aspects [17]. One of the major causes of deterioration of concrete structures is the ingress of chloride ions into the concrete initiating reinforcement corrosion [18]. Usually, chloride ions enter into concrete due to the application of de-icing salt or exposure to a marine environment.

The literature is found to be quite limited and sometimes conflicting about chloride ion penetration and Portland limestone cement. It has been stated that to achieve similar durability properties with a PLC as that of the corresponding PC, both cements must be in the same strength class [19, 20]. This is accomplished by grinding the PLC to a higher fineness. Chloride penetration studies have partially confirmed this statement, at least for a limestone replacement up to 15% [20, 21]. The results of Dhir et al. [22] showed a minor increase of chloride migration (potential diffusion index) for the limestone replacement rate of 15% compared with PC. For replacement ratios beyond this level a more progressive increase in chloride migration with limestone content and w/c-ratio was observed. Other studies have shown that limestone addition was associated with larger chloride penetration despite the fact that the compared cements were in the same strength class [23, 24]. It must be emphasized that conflicting results can originate due to different methods used in the cited literature and also to somewhat different testing ages. The testing took place within a month after casting in most studies, i.e. on rather young specimens.

This paper describes studies carried out to examine the influence on strength and chloride ingress when Portland cement is replaced with limestone filler. The laboratory tests were performed on one year old mortar specimens. In the chloride ingress study both an accelerated method (NT-BUILD 492) and field exposure measurements up to one year were employed. Additionally, the influence of limestone on the long-term (one year) strength was also investigated. Results from corresponding laboratory tests on 28 days old mortars have been previously published by the author [25].

2. EXPERIMENTAL

2.1 Materials

The physical and chemical properties of the cement and limestone fillers used throughout the experimental program as given by the producers are shown in Tables 1 and 2. The aggregate used was CEN standard sand in accordance with EN 196-1 [26], and the cement was a CEM I 52.5 R product conforming to EN 197-1 [1].
Limestone fillers, produced from three different qualities of natural calcium carbonate, were used in this study, see Table 2. Type LL is calcium carbonate filler manufactured from a high-purity white limestone from France, type MA is a white marble powder with high purity from

Austria, while type CH filler is a Danish calcium carbonate powder from a more recent origin than the two others, and can be defined as a fine microcrystalline sedimentary chalk. The calcium carbonate content of all three limestone qualities was ≥ 98% by mass. The limestone fillers also had different fineness, as can be seen in Table 2; CH has the highest specific surface area followed by MA and LL. All materials were obtained in single bulk deliveries and stored in airtight barrels to prevent deterioration with time.

Table 1 – Chemical composition of the cement.

Chemical composition	Cement (%)	Mineralogical composition of cement	(%)
CaO	64.1	C_3S	62.8
SiO_2	20.9	C_2S	12.4
Al_2O_3	3.8	C_3A	5.5
Fe_2O_3	2.7	C_4AF	8.3
SO_3	3.4		
MgO	2.8		
K_2O	1.1		
Na_2O	0.3		
Cl	0.02		

Table 2 – Physical characteristics of the cement and limestone fillers.

Material	Designation	Mean particle size (μm)	Specific surface, BET (m^2/kg)
Cement[1]	CEM	8	1760
Chalk	CH	2.3	2200
Limestone	LL	5.5	1000
Marble	MA	7.0	1500

(1) Blaine fineness of the cement: 550 m^2/kg.

Five different mortar mixtures were cast with pure Portland cement as binder, with water-binder ratios (w/b) ranging between 0.4 and 0.8. Another five different mortar mixtures were cast where a part of the Portland cement was replaced with limestone filler. The w/b is here defined as the water to [Portland cement + limestone] ratio. The mixture compositions for the mortars with pure Portland cement are shown in Table 3 and for mortars with limestone blended cements are shown in Table 4.

Table 3 – Mix proportions for Portland cement mortars.

Mortar mix	w/c	w/b	Cement (kg/m^3)	Water (kg/m^3)	Aggregate (kg/m^3)	Air (%)	Consistency (flow value) (mm)
PC04	0.40	0.40	702	281	1263	2.9	169
PC05	0.50	0.50	500	250	1500	4.9	170
PC06	0.60	0.60	413	248	1593	3.8	176
PC07	0.70	0.70	345	242	1666	7.5	168
PC08	0.80	0.80	319	255	1654	6.5	172

The limestone was added in the mixer, together with the cement and sand and was first dry mixed (1 min) to attain a homogeneous mixing, and then the water was added followed with additional mixing for 2 minutes.

The mortars where the w/b were 0.5 were proportioned as principally specified in the European Standard EN 196-1 [26], one part of cement, three parts of standard sand and one half part of water. One modification compared with the standard [26] was the batch size which in this case

was increased to 40 litres. In those cases where the w/b was not 0.5, the proportions by mass in the mix differed from those given in the standard. For all the mixes, the aim was to reach a flow value with the flow-table test for mortars (EN 1015-3 [27]) of about 170 mm. This was accomplished by keeping the water content more or less constant and altering the binder content.

The air content was measured in accordance with Swedish Standard SS 13 71 24 [28] on the fresh mortars. Relatively high air contents can be seen in Table 3 and 4 although no air entraining agents were used; for normal concrete without air entraining agent the air content is about 2%. This is probably a result of the high paste volume.

Table 4 - Mix proportions for limestone blended cement mortars.

Mortar mix	w/b	w/c	Cement (kg/m^3)	Limestone filler (kg/m^3)	Water (kg/m^3)	Aggregate (kg/m^3)	Air (%)	Consistency (flow value) (mm)
LL12%	0.50	0.57	440	60	250	1500	5.0	175
LL24%	0.50	0.66	380	120	250	1500	4.7	180
LL24%-07	0.70	0.92	262	83	242	1666	5.4	164
MA24%	0.50	0.66	380	120	250	1500	6.0	178
CH24%	0.50	0.66	380	120	250	1500	4.8	173

2.2 Methods

Compressive strength
The compressive strength test was performed in accordance with the European Standard EN 196-1[26], on one year old mortars. The test principle is that three prismatic mortar specimens (40 mm x 40 mm x 160 mm) are cast and water-cured until the time of testing, which in this investigation means one year. The prisms were then broken into two halves by flexure. Each half prism was then tested for compressive strength (each value is the mean result of six specimens).

Chloride migration
Chloride migration testing was performed in accordance with NT BUILD 492 [29], from which chloride migration coefficients can be obtained and used in defining the chloride penetration properties. The principle of the method is that an external electrical potential is applied across the specimen and forces the chloride ions on the outside to migrate into the specimen. After a certain test duration, specified in the standard, the specimen is split and a silver nitrate solution is sprayed on to one of the freshly split surfaces. The chloride penetration depth can then be measured from the visible white silver chloride precipitation, after which the chloride migration coefficient can be calculated from this penetration depth as specified in the standard. Cylinders 450 mm long with a diameter of 100 mm were cast in steel moulds. After demoulding, the cylinders were stored under water until the time for testing, i.e. one year. Immediately before testing, 50 mm thick specimens were sawn from the cylinders, with the 50 mm thick discs at each end of the cylinders being discarded.

Chloride diffusion (field exposure)
The specimens for field exposure were cast in plastic moulds with an inner diameter of 145 mm and a length of 250 mm. After one month of wet curing 20 mm thick slices were cut away from the end sides of the specimens. The specimens were then transported to the field exposure site and submerged in the sea in “open” plastic boxes, exposing the two newly cut surfaces to

seawater, see Fig. 1. The moulds were not removed at any time, which means that chloride penetration was one-dimensional when the specimens were submerged in the sea water.

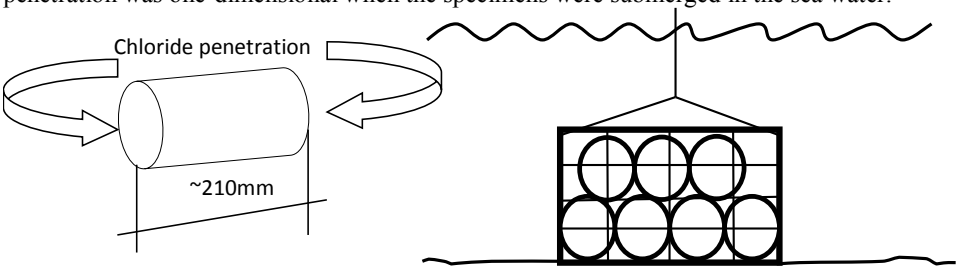

Figure 1 – Specimens, and the arrangement for immersing them in the sea.

The field exposure site is situated in the south-western part of Sweden (Träslövsläge). The exposure conditions at the field site are well documented in [30]. In general the chloride concentration in the seawater varies with time from 10 to 18 g per litre, and the water temperature has a normally annual variation between + 20 °C and + 2 °C.

After about one year submerged in the sea, one specimen of each kind of mortar was brought back to the laboratory for analysis. Each specimen was individually sealed in double, thick plastic bags, and stored at room temperature for no longer than three weeks prior to measurement of chloride profiles. The specimens were sawn in the middle, and one part was used for measurement of chloride profiles and the other piece was used for measurement of moisture profiles. The moisture profiles were measured by putting samples taken from several depths, in a test tube and inserting a Vaisala RH-probe into the test tube and sealing the whole arrangement as described in [31].

For the measurement of chloride profiles, powder samples were taken by dry-grinding with a drill gradually from the exposed surface to a certain depth. Powder from each millimetre was taken for the first 5 mm, and then powder was taken for every second millimetre until 20 mm, after which the distance between where powder samples were taken was increased gradually. The acid-soluble chloride content in each sample was determined principally in accordance with AASHTO T260 [32] using potentiometric titration on an automatic titrator (Metrohm Titranor 716). This method has shown good repeatability and reproducibility in round-robin tests [33]. After titration of chloride ions, the soluble calcium content of the same sample solution was determined, and recalculated to calcium oxide (CaO_{sample}) in order to estimate the binder content. The method for determining the soluble calcium content is described in detail in [34]. The following equation was used to estimate the binder content in each sample:

$$Binder_{sample} = \frac{CaO_{sample}}{CaO_{binder}} \tag{1}$$

where CaO_{binder} is the calcium oxide content of the binder. For the Portland cement used in this study the CaO_{PC} is 64.1% (see Table 1). When the binder consisted of Portland cement and limestone filler (PLC) the CaO_{binder} was calculated by the following expression:

$$CaO_{binder} = PC \cdot CaO_{PC} + LS \cdot CaO_{LS} \tag{2}$$

where *PC* and *LS* are the Portland cement and limestone filler as percent by weight of the binder, and CaO_{PC} and CaO_{LS} are the respectively calcium oxide amounts. The CaO_{LS} for limestone filler is 56.08% and was calculated by the following expression:

$$CaO_{LS} = \frac{(M_{CaO})}{M_{CaCO_3}} \tag{3}$$

where M_{CaO} and M_{CaCO3}, are the molar masses for calcium oxide and calcium carbonate. In the result section chloride content for the PLC-mortars are in some cases also given as the chloride percentage by mass of PC In those cases the following expression was used to estimate the PC content from the measured CaO_{sample}.

$$PC_{sample} = \frac{CaO_{sample}}{\left(CaO_{PC} + CaO_{LS}\frac{LS}{PC}\right)} \tag{4}$$

The chloride ingress model chosen to evaluate and describe the measured chloride profiles in this study is the frequently used semi-infinite solution to the empirical model based on Fick´s second law [35], expressed as:

$$C(x,t) = C_i + (C_s - C_i)\left(1 - erf\left(\frac{x}{2\sqrt{D_{F2}t}}\right)\right) \tag{5}$$

where $C(x,t)$ is the chloride concentration at depth x after an exposure period t, C_i is the initial concentration in the mortars (in this study measured at around 0.05 mass% of binder for all mixtures), C_s is the chloride concentration at the exposed surface, D_{F2} is the chloride diffusion coefficient, and *erf* is the error function. Curve-fitting of the measured chloride profiles to Eq. 5 was used to obtain the regression parameters D_{F2} and C_s. These two parameters should not be seen as direct material properties, but as regression parameters, describing the chloride ingress under a specific exposure condition and after a specific exposure time [30]. In this paper D_{F2} and C_s will be referred as the "apparent diffusion coefficient" (D_a) and the "apparent surface chloride content" (C_{sa}), respectively, as is suggested in reference [35].

Efficiency of limestone

The efficiency of limestone as replacement of Portland cement was evaluated by the methodology first suggested by Smith [36]. In this methodology, when mineral additions are used the water/cement ratio (*w/c*) is substituted with the equivalent water/cement ratio ($(w/c)_{eq}$) and an efficiency factor, called *k*-value, also referred to as the coefficient of efficiency, is introduced. The equivalent water-cement ratio is expressed as:

$$(w/c)_{eq} = \frac{w}{(c + kR)} \tag{6}$$

where *R* and *c* are the amount of mineral addition and Portland cement by mass, respectively. The *k*-value can be determined by taking the following steps:

1. Determine the relationship between the property to be studied (strength, permeability, etc.) and *w/c* for the Portland cement used.

2. Determine the value of the property to be studied for a given concrete mixture containing the mineral addition to be investigated.
3. Figure 2 illustrates how to determine the $(w/c)_{eq}$ by using the property/water cement relationship and the results from step 2.
4. By using the known values of c, R and w and the value of $(w/c)_{eq}$ determined in step 3, the k-value can be calculated using Eq. 2.

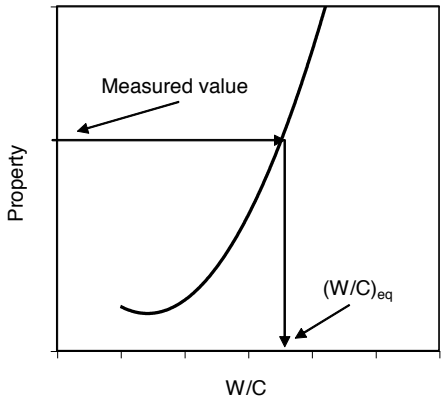

Figure 2 – Graphical illustration of the steps to be taken for determining the k-value for a mineral addition with regard to a certain property.

The k-value defines the cementitious efficiency of the mineral addition, i.e. to what amount by mass the mineral addition can be regarded as Portland cement.

3 RESULTS

3.1 Compressive strength

The results from the compressive strength tests for all mortars are shown in Fig. 3. The compressive strength is plotted versus the inverse of the w/b. The limestone replacement ratios are also given in Fig. 3. Each value is the mean result of six specimens; the standard deviations are also included. Fig. 3 shows linear relationships with good correlations for the PC-mortars between the compressive strength and the inverse of the w/b ratio, i.e. Bolomey's formula [37] is valid. The values for the PLC-mortars with 24% limestone filler replacement ratio are lower than the corresponding values for the PC-mortars with the same w/b, meanwhile the compressive strength does not seem to be appreciable affected by replacing Portland cement with 12% limestone filler.

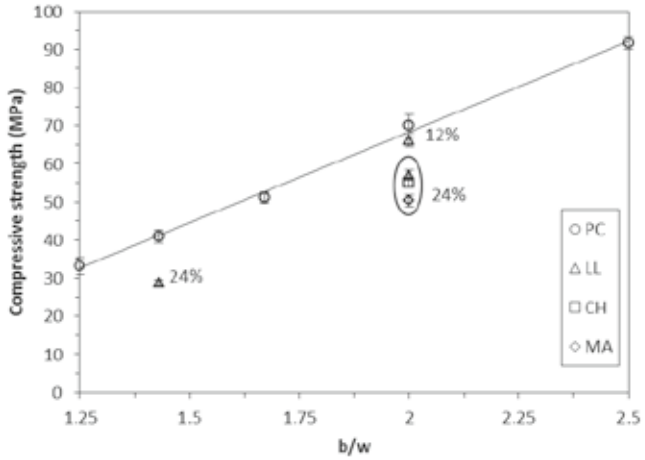

Figure 3 – The one-year compressive strengths as a function of binder/water ratio for all mixes.

3.2 Chloride migration

Fig. 4 shows the results from the chloride migration tests. The chloride migration coefficient (D_m) is plotted versus the w/b. Each value is the mean result of three tested specimens; the standard deviations and the limestone replacement rates are also included in Fig. 4. A linear relationship with good correlation is found in Fig. 4 between the migration coefficient and the w/b-ratio for the PC mortars. Close to linear relationship between D_m and the w/c has also been reported by Frederiksen et al. [38]. In relation to the PC-mortars the chloride migration coefficients of the LPC-mortars depend on the replacement ratio. For the lower replacement ratio (12%) the D_m is equal to that of the corresponding PC-mortar with the same w/b, while when the replacement ratio was doubled to 24%, the D_m increased. Due to technical problems no result is available for mix LL24-0.92.

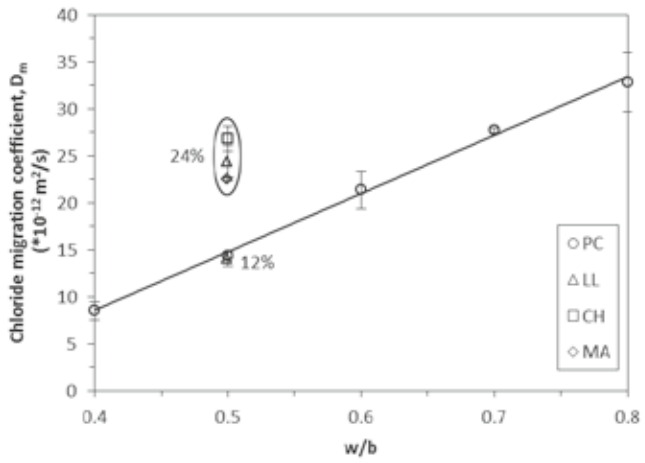

Figure 4. Chloride migration coefficient versus water/binder ratio tested at an age of one year.

3.3 Chloride diffusion (field)

The chloride profiles from the field exposure tests are summarized in Figs. 5 and 6. One chloride profile for each mix was determined and the chloride content is expressed as percentage by mass of binder for all mixes, for all samples the binder content was estimated according to the procedure described in section 2.2 (Eq. 1 and Eq. 2). The general trend in Fig. 5 is that an increased w/b-ratio results in more chlorides diffusing into the mortar. One exception from this trend is the mortar with w/b 0.50.

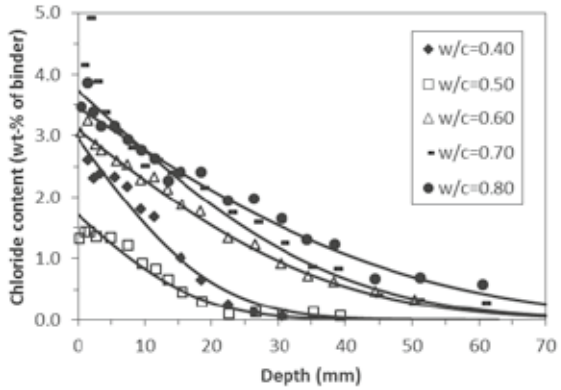

Figure 5. Chloride profiles after one year exposure time for the PC mortars.

Fig. 6 shows that both an increase in replacement ratio with limestone filler and increase of the w/b-ratio results in increased chloride ingress. However, in Fig. 6 it can also be observed from the measured chloride profiles that mortar mix LL24% shows lower chloride contents compared with mortar mixes MA24% and CH12%, which have the same replacement ratio and w/b.

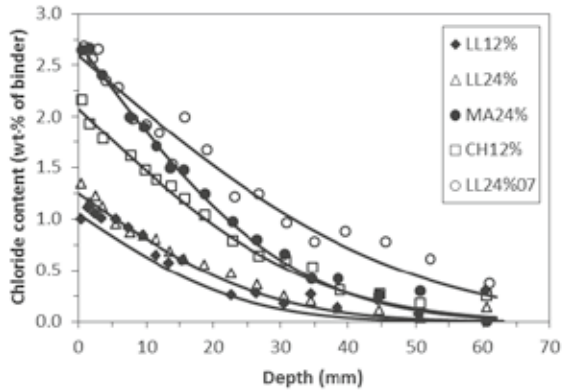

Figure 6 – Chloride profiles (where the chloride content is expressed as percentage by weight of binder (Portland cement + limestone filler))after one year exposure time for mortars with limestone blended cement.

In Figs. 5 and 6 the fitted curves to the error-function solution of the results are also included. The curve-fitting procedure of measured chloride profiles is a very subjective matter. One of the reasons for this is the often irregular behaviour observed close to the exposure surface on measured chloride profiles. This irregularity occurs as a deviation of the measured profile compare to the fitting curves obtained from Eq. 5. From the results in Figs. 5 and 6 this deviations between measured profiles and fitted curves exist, but are not so pronounced. Not showed here, but when the chloride profiles were expressed as chloride content by weight-% of sample the deviation of the measured profiles compare to the fitting curves was more pronounced. The point from where the curve-fitting is started, and the amount of accessible measured points in this critical area, will have a huge influence on the regression parameters, D_a and $C_{sa.}$ For most measured chloride profiles, the deviation from an expected diffusion profile seemed to occur at the same depth as that at which the parallel measured binder content had a tendency to decrease from the bulk quantity. The majority of the regression analyses were therefore made with this certain depth as starting point, which was around 2 mm from the exposed surface. For the chloride profiles which did not follow this pattern, the starting point was chosen by omitting the first one or two measuring points if the values significantly diverged from the expected diffusion profile. The coefficient of correlation, R^2, for all fitted chloride profiles was ≥ 0.96.

Fig. 7(a) shows the apparent diffusion coefficients (D_a) as a function of w/b. The D_a is evaluated by curve fitting the chloride profiles shown in Figs. 5 and 6. The w/b is as previous mentioned defined as water to Portland cement ratio for the PC-mortars, respectively water to Portland cement plus limestone filler ratio for the PLC-mortars.

Fig 7(b) shows the D_a as a function of the w/c. The evaluation of D_a is made by curve fitting the same chloride profiles as previous (Figs 5 and 6), but in this case the chloride content was expressed as percentage by mass of Portland cement for all mixes when the data were fitted to the error function solution. The estimation of Portland cement content from calcium measurements for the PLC-mortars is described in section 2.2 and Eq. 4. The procedure adapted in Fig. 7 (b) to estimate the D_a does not influence the results for the PC-mortars as the binder content and Portland cement content is the same. However, for the PLC-mortars when the chloride content was expressed as percentage by mass of Portland cement the curve fitting gave a small increase of D_a of about 2%. One exception is the LL24%-mortar where the increase was ~4% compared with the result in Fig. 7(a).

Fig. 7 (a) shows that despite some scatter in the results, an increase in the w/b for the PC-mortars generally results in an increased D_a. The D_a for the PC-mortar with w/b 0.50 deviates from what would have been expected, as it is lower than for the PC-mortar with w/b 0.40. A factor that to some degree could influence the results can be that after one year of marine exposure, growth of algae to various extents was found on the specimen surfaces. Despite the occurring uncertainties in the results, the results for the PC-mortars were fitted to a linear regression line in Figs 7(a) and 7(b). Close to linear relationship between the D_a and the w/c has previous been reported by Frederiksen et al. [38].

In Fig. 7(a) the response of the PLC-mortars with the alternation of the w/b is not straightforward. A lower limestone replacement ratio (12%) seems to have a beneficial effect on the D_a (lowering it) compared to the expected value for a corresponding PC-mortar, while the opposite is true for the PLC-mortars with higher replacement ratio. These results conform to the results from the migration test (see Fig. 4). However, when the D_a for the PLC-mortars is plotted as a function of the water-Portland cement ratio (w/PC) the response is similar to that of the PC-

mortars (see Fig. 7(b)), i.e., an increase in the w/PC results in higher D_a. It can also be noticed in Fig. 7(b) that the D_a for all PLC-mortars is lower than the expected value of a PC-mortar with the same water-Portland cement ratio.

Figs. 8(a) and 8(b) show the apparent surface chloride content (C_{sa}) as percentage by mass of binder respectively as percentage by mass of Portland cement. The C_{sa} is the other regression parameter obtained from the curve fitting procedures described in section 2.2 (Eq. 5). As in Figs. 7(a) and 7(b) the results for the PC-mortars does not change in Figs. 8(a) and 8(b), while for the PLC-mortars the difference in the results when comparing Figs. 8(a) and 8(b) is obvious. For the PLC-mortars the absolute value of C_{sa} is about 30% higher when it is expressed as percentage by mass of Portland cement instead of as percentage by mass of binder. One exception is the LL12%-mortar where the C_{sa} is about 14% higher when expressed as percentage by mass of Portland cement.

The C_{sa} has been suggested to give an indication of the chloride binding capacity [39]. The chloride concentration of the exposure solution (in this case chloride ion concentration in the sea water) represents the free chloride concentration and together with C_{sa} one point in the binding isotherm could be estimated. The value of C_{sa} depends primarily on the concentration of the exposure solution, on the porosity and on the binding capacity of the cement gel [38]. In Figs. 8(a) and 8(b) the mean value of C_{sa} for the PC-mortars is plotted. This value is 3.3 ± 0.4% Cl^- by weight of binder (or weight of Portland cement, which is the same). The value of PC05-mortar is not included in this mean value as it seems to deviate from the rest of the results without any conceivable explanation.

In Figs. 8(a) and 8(b) also the mean value of C_{sa} for the PLC-mortars with higher replacement ratio (24%) is plotted. In this case the value of LL24% is excluded from the mean value for the same reason as the PC05-mortar. The C_{sa} mean value in this case is 2.5 ± 0.3% Cl^- by weight of binder (Portland cement + limestone filler) and 3.3 ± 0.5% when expressed as Cl^- by weight of Portland cement. This means that the lines representing the mean values of the C_{sa} coincide in Fig. 8(b). The lowest value of C_{sa} was measured for the LL12%-mortar. The reason for this is somewhat ambiguous whether it depends on material properties or natural scatter found in field data.

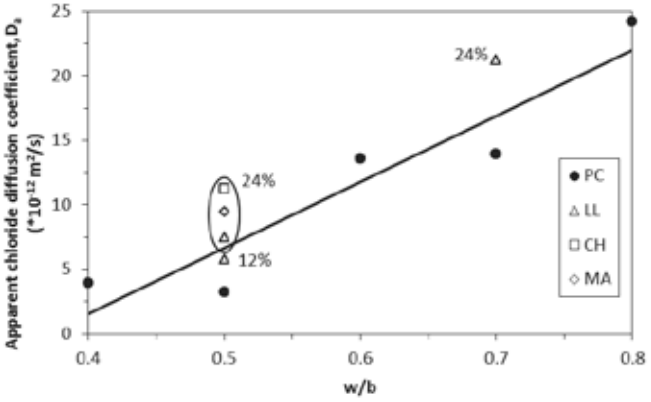

(a)

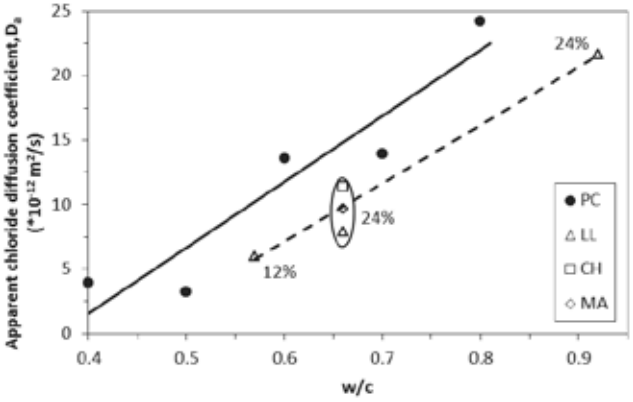

(b)

Figure 7 – Apparent chloride diffusion coefficient as function of (a) w/b-ratio and (b) w/c-ratio after 370 days of field exposure.

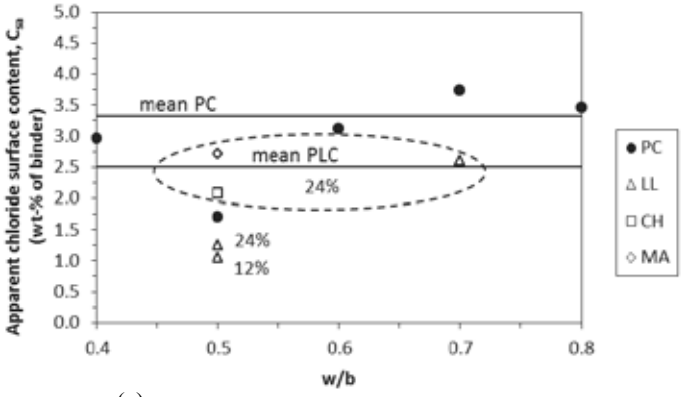

(a)

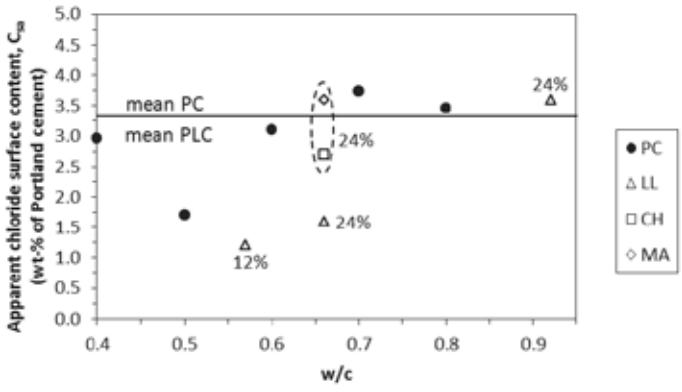

(b)

Figure 8 – Apparent surface chloride content as function of (a) w/b-ratio and (b) w/c-ratio after 370 days of field exposure.

Fig. 9 shows the results of the moisture measurements after one year of submerged exposure. All mortar qualities except one were almost saturated, showing an RH ≥ 95% (RH 95% is the upper limit of the calibration of the RH-probes) throughout the specimen depth. The Portland cement mortar with w/c 0.4 deviates from the general results (see Fig. 9). For a depth larger than 10 mm a continuous decreasing RH profile was measured.

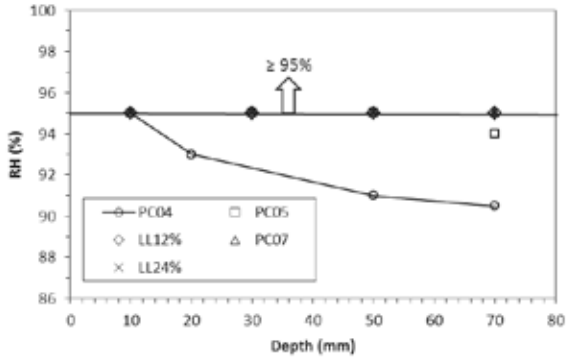

Figure 9 – Moisture profiles from samples after one year of exposure in sea water.

3.4 Efficiency of limestone

By following the concept for evaluating the coefficients of efficiency (*k*-values) described in section 2.2 the cementitious efficiency of limestone filler was determined regarding compressive strength chloride migration and chloride diffusion, the results are presented in Table 5. The *k-values* with regard to chloride diffusion were determined from the curve fitting results where the chloride profiles were expressed as percentage by mass of binder (Fig. 7(a)). Because the *k*-values with respect to chloride diffusion presented in Table 5 are based on one measured chloride profile for each mortar quality the uncertainties of those values are difficult to foresee.

Table 5 – k-values for limestone filler based on different properties.

Mortar mix	*k*-values		
	Compressive strength	Migration	Diffusion
LL12%	0.8	1.2	1.3
LL24%	0.5	0	0.9
LL24%-07	0.3	-	0.6
MA24%	0.2	0.2	0.6
CH24%	0.4	-0.2	0.4

However, apart for the LL12%-mortar when comparing the calculated *k*-values from the migration test with the corresponding values from the natural diffusion test in Table 5 it is obvious that limestone filler seem to be less efficient as replacement of Portland cement when tested with the accelerated migration method. A possible explanation to the discrepancy between the *k*-values determined with the different chloride ingress methods is illustrated in Fig. 10, where the ratio between the D_m and the D_a for the different mortar qualities is shown. In Fig. 10 the mean values of this ratio for PC-mortars respective PLC-mortar is also given, the results for PC05-mortar and LL24% -mortar are considered as outliers and therefore excluded from the mean values shown in Fig 10.

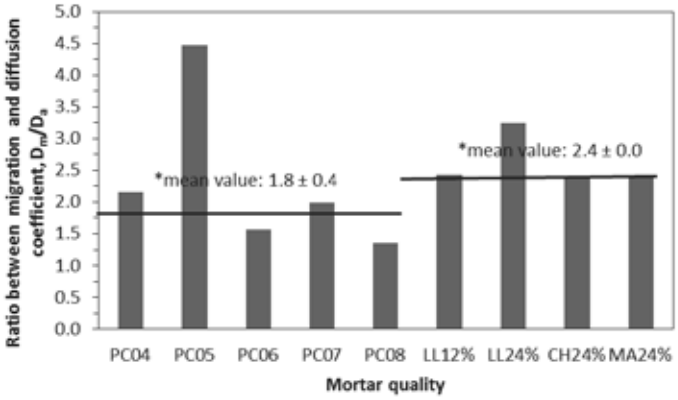

Figure 10 – The ratio between the migration coefficient and the diffusion coefficient for the different mortar qualities, also the mean values of this ratio for PC-mortars respective PLC-mortar are given. The mean values do not include PC05 and LL24%, which are considered as outliers.

The mean value of the D_m/D_a-ratio for the PC-mortars is lower than for the PLC-mortars, implying deeper chloride ingress in the accelerated migration test than in the natural diffusion test for the PLC-mortars compared to the PC-mortars. This is apparent when comparing Fig.4 with Fig. 7(a).

In Table 5 the *k*-values from the compressive strength seem to be of the same magnitude as the *k*-values from the natural diffusion for the higher replacement ratio, while for the lower replacement ratio *k*-value is lower.

4 DISCUSSION

Limestone can be regarded as inert concerning the ability to form C-S-H. There is, however, much agreement that limestone reacts with the aluminate phases producing monocarbonate [40]. Other effects observed when inert (don´t form C-S-H) mineral additions are used as cement replacement are: cement dilution, modification of the particle size distribution and heterogeneous nucleation [41, 42]. The dilution effect is connected with the replacement ratio of cement with the mineral addition, and equivalent to an increase in water-cement ratio. The effect of particle size distribution depends on the fineness and amount of the mineral addition, and is related to the modification of the initial porosity of the mix, concerning mostly the fresh properties. The heterogeneous nucleation is a physical process enhancing the cement hydration by providing nucleation sites (on the mineral addition) for the cement hydrates.

The influence of the dilution effect will be an increase of the total porosity resulting in a lower compressive strength and higher chloride ingress coefficient, which is quite obvious in Figs. 3, 4 and 7 for the mortars with the higher replacement of Portland cement with limestone filler. Porosity measurements were made for some of the PLC-mortars used in this study and a higher porosity was confirmed [43]. Further, from mercury intrusion studies Pipilikaki et al. [44] reported that an increased limestone addition gave an increased intruded mercury volume indicating an increasing porosity. However, in the same study [44] a decreased threshold

diameter (d_{th}) with increased limestone addition was also reported. The threshold diameter corresponds to the narrowest path in the interconnected pore, and it has been found that permeability of cement paste to be more sensitive to the d_{th} than the total porosity [45]. The dilution effect and the effect of a microstructural refinement (due to heterogeneous nucleation and/or the filler effect) can be seen as two antagonistic effects concerning chloride ingress. In this study, for the mortar with lower replacement of Portland cement with limestone the effect of a microstructural refinement predominate the dilution effect as can be seen in Table 5, while the opposite is true for the higher replacement ratio.

In Table 5 it can also be observed that for the higher replacement ratio the efficiency of limestone filler concerning the resistance to chloride ingress also depends on the test method. Fig.10 shows the D_m/D_a-ratio for the different mortar, where for all mortars this ratio is higher than one. This is reasonable as the driving force for the chloride ingress is different for the two methods. An external electrical field can be expected to cause deeper chloride ingress than the movement of ions as the result of a concentration gradient. It has also been suggested that interaction with seawater can improve the microstructure of concrete surface during field exposure and consequently block chloride ingress [46]. That the D_m/D_a-ratio is higher than one can also be found in data reported in [30, 47].

Fig. 10 reveals also that the mean value of the D_m/D_a-ratio for the PC-mortars is lower than for the PLC-mortars, implying deeper chloride ingress in the accelerated migration test than in the natural diffusion test for the PLC-mortars compared to the PC-mortars. This can be due to two conceivable explanations; one is that the microstructural refinement of the PLC-mortars is less beneficial in the migration test than in natural diffusion and the other is differences in the binding capacity for the different binders.

Some kind of microstructural change other than the dilution effect is also evident in Fig. 7(b). The diffusion coefficient is in fact increased with increased limestone filler replacement ratio. However, the D_a is lower for the PLC-mortars than the corresponding PC-mortars with the same water-Portland cement ratio. If this effect is thought as the result of a microstructural refinement such as narrowing of paths to the interconnecting porosity, then the movement of ions though natural diffusion ('random walk') can be expected to be more prohibited by this refinement than the movement of ions through an external imposed electrical field.

Two main mechanisms are general accepted to be responsible for chloride binding, those are, physical adsorption to C-S-H surfaces and chemical reaction with the aluminate phases [48, 49]. As an external electrical field is applied in the migration test forcing chloride ion to penetrate it is possible that the part of chloride binding associated to physical adsorption on the C-S-H surface will decrease, so the remaining chloride binding capacity will mostly be attributed to the chemical reaction with the aluminate phases. When Portland cement is replaced with limestone filler less aluminate phases will be available for chloride binding. Further, as limestone filler has been identified to react to some extend with the aluminate phases, this can further decrease the available aluminate phases for binding chlorides. Some indication for the effect on chloride binding capacity for the different binders can be found in Figs. 8(a) and 8(b). In Fig 8(a) where the C_{sa} is expressed as percentage by mass of binder the PC-mortars have generally a higher C_{sa} than the PLC-mortars implying a higher binding capacity. In Fig. 8(b) the C_{sa} is expressed as percentage by mass of Portland cement, here the mean values of C_{sa} for the both binders coincide, which suggest that the chloride binding capacity is determined by the Portland cement content. The consequence of this is that in the migration test the chloride binding capacity for

the PLC-mortars will be exhausted both by the nature of the test and also by the less available clinker aluminate phases.
Similar tendency as for chloride ingress can be observed in the result for compressive strength when Portland cement is replaced by limestone filler. When compared with PC-mortars with the same w/b a higher replacement ratio results in a clear reduction of the compressive strength, while the lower replacement ratio results in a marginal reduction (Fig. 3). However, one difference do exist between the effect on chloride ingress and compressive strength, that is, for chloride ingress a small replacement of Portland cement with limestone filler is beneficial, while for compressive strength even if small the effect is negative (Table 5). This is not surprising as compressive strength is a property mainly governed by total porosity while chloride ingress is also strongly influenced by the pore structure.

In this study also moisture profiles for the different mortars were measured which showed that all mortars except one were almost capillary saturated. The PC-mortar with a w/c 0.4 (PC04) showed close to saturation at 10 mm depth, thereafter the RH decreased likely due to self-desiccation. These results are in agreement with the results reported in [31]. An implication of the RH result for the PC04-mortar is the chloride transport process differs compared to the rest of the mortars that are saturated.

5 CONCLUSIONS

The following conclusions can be drawn from the results obtained in this investigation:

The method of measuring the resistance to chloride ingress can have a major influence on the assessment of the effect of different binders.

The effect on chloride resistance when replacing Portland cement with limestone filler is strongly dependent of the replacement ratio. Compared to neat Portland cement moderate replacing ratio (12%) shows decreased chloride ingress, while the opposite is true for a higher replacement ratio (24%).

The effect on compressive strength when replacing Portland cement with limestone filler is strongly dependent of the replacement ratio. A moderate replacing ratio (12%) shows marginal decrease in compressive strength, while the decrease is more pronounced for a higher replacement ratio (24%).

REFERENCES

1. EN 197-1, Cement-Part 1: “Composition, specification and conformity criteria for common cements”, *European standard,* 2000.
2. Hooton, R.D., Nokken, M., Thomas, M.D.A., “Portland–limestone cement: State-of-the-art report and gap analysis for CSA A 3000”, Cement Association of Canada, Ottawa, Canada, 2007, 59 pp.
3. Ramachandran, V.S., Chun-Mei, Z., “Dependence of Fineness of Calcium Carbonate on the Hydration behavior of Tricalcium Silicate,” *Durability of Building Materials*, Vol. 4, 1986, pp. 45-66.
4. Pera, J., Husson, S., Guilhot, B., “Influence of finely ground limestone on cement hydration”, *Cement and Concrete Composites*, Vol. 21, 1999, pp. 99-105.

5. Ramachandran, V.S., Chun-Mei, Z., "Hydration kinetics and microstructural development in the $3CaAl_2O_3$-$CaSO_4.2H_2O$-$CaCO_3$-H_2O system", *Materials and Structures,* Vol. 19, No. 114, 1986, pp. 437-444.
6. Ohba, Y., Nakamura, A., Lee, J.K., Sakai, E., Daimon, M., "Influence of $CaCO_3$ on the hydration of various types of calcium aluminates with anhydrite", Proceedings, 10th International Congress on the Chemistry of Cement, Gothenburg, Sweden, June 1997, Vol. 2, pp.2ii022, 8-15.
7. Sharma, R.L., Pandey, S.P., "Influence of mineral additives on the hydration characteristics of ordinary Portland cement", *Cement and Concrete Research,* Vol. 29, 1999, pp. 1525-1529.
8. Soroka, I., Stern, N., "Calcareous fillers and the compressive strenth of portland cement", *Cement and Concrete Research,* Vol. 6, 1976, pp. 367-376.
9. Menendez, G., Bonavetti, V., Irassar, E.F., "Strength development on ternary blend cement with limestone filler and blast-furnace slag", *Cement and Concrete Composites,* Vol. 25, 2003, pp. 61-67.
10. Vuk, T., Tinta, V., Gabrovsek, R., Kaucic, V., "The effect of limestone addition, clinker type and fineness on properties of Portland cement", *Cement and Concrete Research,* Vol. 31, 2001, pp 135-139.
11. Kenai, S., Soboyejo, W., Soboyejo, A., "Some Engineering Properties of Limestone Concrete", *Materials and Manufacturing Properties,* Vol. 19, No. 5, 2004, pp. 949-961.
12. Lawrence, P., Cyr, M., Ringot, E., "Mineral admixture in mortars effect of type, amount and fineness of fine constituents on compressive strength", *Cement and Concrete Research,* Vol. 35, 2005, pp. 1092-1105.
13. Taylor, H.F.W., "Cement Chemistry", second ed., Thomas Telford, London, 1997.
14. Hilsdorf, H.K. "Introduction and problem statement", Chapter in:, Performance Criteria for Concrete Durability, J. Kropp, H.K. Hilsdorf (Eds.) RILEM Report 12, E & SPON, London, 1995, pp 1-3.
15. Powers, T.C., Copeland, L.E., Hayes, J.C., Mann, H.M. "Permeability of Portland cement paste", Research and Development Laboratories of the Portland Cement Association, Bulletin 53, Chicago, 1955, 13 pp.
16. Ollivier, J.-P., Massat, M., Parrott, L., "Parameters influencing transport characteristics" Chapter in: Performance Criteria for Concrete Durability, Kropp, J., Hilsdorf, H.K. (Eds.), RILEM Report 12, E & SPON, London, 1995, pp 15-32.
17. EN 206-1, Concrete-Part 1: "Specification, performance, production and conformity", *European standard,* 2000.
18. Hobbs, D.W., "Concrete deterioration: causes, diagnosis, and minimising risk", *Int. Materials Reviews*, Vol. 46, 2001, pp.117-143.
19. Ranc, R., Moranville-Regourd, M., Cochet, G., Chaudouard, G., "Durability of cements with fillers", Proceedings, 2nd Inter. Conf. Durability Concrete., Montreal, Canada, ACI SP 126,1991, Vol. II, pp. 1239-1257.
20. Cochet, G., Jesus, B., "Diffusion of chloride ions in portland cement-filler mortars", Proceeding,. Inter. Conf. Blended Cement in Construction, Swamy R. N. (Eds.), Sheffield, UK, 1991, pp. 365-376.
21. Tsivilis, S., Batis, G., Chaniotakis, E., Grigoriadis, G., Theodossis, D., "Properties and behaviour of limestone cement concrete and mortar", *Cement. Concrete. Research*, Vol. 30, 2000, pp. 1679-1683.
22. Dhir, R.K., Limbachiya, M.C., McCarthy, M.J., Chaipanich, A., "Evolution of Portland limestone cements for use in concrete construction", *Materials & Structures*, Vol. 40, 2007, pp. 459-473.

23. Bonavetti, V.L, Donza, H., Rahhal, V., Irassar, E.F, "Influence of initial curing on the properties of concrete containing limestone blended cement", *Cement Concrete Research*, Vol. 30, 2000, pp.703-708.
24. Irrasar, E.F., Bonavetti, V.L., Menendez, G., Donza, H., Cabrera, O., "Mechanical properties and durability of concrete made with Portland limestone cement", Proceedings 3rd CANMET/ACI Int. Symp. Sustainable Development of Cement and Concrete, V.M. Malhotra (Eds), Detroit, USA, 2001, pp. 431-450.
25. Boubitsas, D., "Replacement of cement by limestone filler: The effect on strength and chloride migration in cement mortars", *Nordic Concrete Research, no*. 32, 2005, pp. 31-44.
26. EN 196-1, "Methods for testing cement-Part 1: Determination of strength", *European standard,* 1994.
27. EN 1015-3, "Methods of test for mortar for masonry- Part 3: Determination of consistency of fresh mortar (by flow table)", 1999.
28. SS 13 71 24, "Concrete testing-Fresh concrete-Air content (pressure method)", Swedish standard, 1989.
29. NT BUILD 492, "Concrete, Mortar, and Cement-based Repair Materials: Chloride Migration Coefficient from Non-steady-state Migration Experiments". *Nordtest methods,* 1999.
30. Tang, L., "Chloride ingress in concrete exposed to marine environment-Field data up to 10 years exposure", SP Swedish National Testing and Research Institute, SP Report 2003:16, Borås, Sweden, 2003, 62 pp.
31. Nilsson, L.-O., "Moisture in marine concrete structures-studies in BMB-project 1992-1996", Chapter in: Durability of Concrete in Saline Environment, Almqvist & Wiksell, Uppsala, 1996, pp. 23-47.
32. AASHTO T 260, "Standard Method for Sampling and Testing for Total Chloride Ion in Concrete and Concrete Raw Materials", American Association of State Highway and Transportation Officials, 1997.
33. Tang, L., "Measurement of chloride content in concrete with blended cement –An evaluation of the repeatability and the reproducibility of the commonly used test methods", NORDTEST Project No. 1410-98, SP Swedish National Testing and Research Institute, SP Report 1998:27, Borås, Sweden, 1998, 26 pp.
34. Tang, L., "Estimation of cement/binder profile parallel to the determination of chloride profile in concrete", NORDTEST Project No. 1581-02, SP Swedish National Testing and Research Institute, SP Report 2003:07, Borås, Sweden, 2003, 30 pp.
35. Tang, L., Nilsson L.-O., Basheer, P.A.M, "Resistance of concrete to chloride ingress", Spon Press, Abingdon, 2012, 238 pp.
36. Smith, I.A., "The design of fly ash concrete", Proceedings, Inst. Civ. Eng., London, UK, Vol. 36, 1967, pp. 769-790.
37. Odler, I., "Strength of cement (final report)", Materials & Structures, Vol. 24, 1991, pp. 143-157.
38. Frederiksen, J.M., Sørensen, H.E., Andersen, A., Klinghoffer, O., "The effect of the w/c ratio on chloride transport into concrete", Danish Road Directorate, 1997, 35 pp.
39. Nilsson, L.-O., Poulsen, E., Sandberg, P., Sørensen, H.E., Klinghoffer, O, "HETEK, Chloride penetration into concrete, State of the Art, Transport processes, corrosion initiation, test methods and prediction models", Danish Road Directorate, 1996, 151 pp.
40. Hawkins, P., Tennis, P., Detwiler, R. "The use of limestone in Portland cement: A state-of-the-art review", EB227, Portland Cement Association, Skokie, Illinois, USA, 2003, 44 pp.

41. Moosberg-Bustness, H., Lagerblad, B., Forssberg, E., "The function of fillers in concrete", *Materials & Structures*, Vol. 36, 2004, pp. 74-81.
42. Lawrence, P., Cyr, M., Ringot, E., "Mineral admixtures in mortars. Effect of inert materials on short-term hydration", *Cement Concrete Research*, Vol. 33, 2003, pp. 1939-1947.
43. Boubitsas, D., Nilsson, L.-O., "Replacement of Cement by Limestone Filler: the Effect on Chloride Diffusion in Cement Mortars", **to be submitted**, 2013.
44. Pipilikaki, P., Beazi-Katsioti, M., "The assessment of porosity and pore size distribution of limestone Portland cement pastes", *Construction Building Materials*, Vol. 23, 2009, pp. 1966-1970.
45. Aligizaki, K.K., "Pore structure of cement-based materials", Taylor & Francis, Abingdon, 2006, 388 pp.
46. Mohammed, T.U, Yamaji, T., Hamada, H., "Chloride Diffusion, Microstructure, and Mineralogy of Concrete after 15 Years of Exposure in Tidal Environment", *ACI Mater. Jour.*, Vol. 99, 2002, pp. 256-263.
47. Salta, M.M., Melo, A.P., Garcia, N., Pereira, E.V., Ribeiro, A.B., "Chloride transport in concrete from lab test to in situ performance", Proceedings, RILEM Pro 47, Andrade, C., Torrent, R., Scrivener, K. (Eds.), 2006, pp. 229-240.
48. Yuan, Q., Shi, C., Schutter, G.D., Audenart, K., Deng, D., "Chloride binding in cement-based material subjected to external chloride environment – A review", *Construction Building Materials*, Vol. 23, 2009, pp. 1-13.
49. Justnes, H., "A review of chloride binding in cementitious systems", SINTEF, Trondheim, Norway, 1996, 16 pp.

Laboratory testing of early age bond strength between concrete for shotcrete use and rock

Lars Elof Bryne
Lic. Eng., Ph.D. Student
KTH Royal Institute of Technology
Division of Concrete Structures
SE-100 44 Stockholm, Sweden
E-mail: lars-elof.bryne@byv.kth.se

Anders Ansell
Professor
KTH Royal Institute of Technology
Division of Concrete Structures
SE-100 44 Stockholm, Sweden
E-mail: anders.ansell@byv.kth.se

Jonas Holmgren
Professor em.
KTH Royal Institute of Technology
Division of Concrete Structures
SE-100 44 Stockholm, Sweden
E-mail: jonas.holmgren@byv.kth.se

ABSTRACT

Shotcrete (sprayed concrete) is, together with rock bolts, the most important material used for reinforcement in hard rock tunnelling. Sprayed concrete differs from ordinary concrete through the application technique and the addition of accelerators which give immediate stiffening. The bond between sprayed concrete and rock is one of the most important properties in the quality assessment of shotcreted concrete. During the very early age after spraying the physical properties of the concrete and the bond to the rock depend on the accelerator and the micro structure that is formed. In this work a laboratory test method for measuring early bond strength for very young shotcrete is presented.

Key words: Shotcrete, sprayable, rock, bond strength, testing.

1. INTRODUCTION

Shotcrete (sprayed concrete) is a very important material for rock reinforcement and repair work. It is either used in combinations with rock bolts or other mechanical connectors or as a shell or lining that bond directly to the substrate, which e.g. can be rock or concrete. The ability to bond strongly to the substrate is one of the most important material properties of shotcrete. This is particularly important in tunnelling through hard rock using shotcrete linings not secured by rock bolts. A fast developing shotcrete strength is often a high priority in tunnelling since displacements in the rock mass may occur soon after the excavation of the rock. By immediately spraying the tunnel walls and the roof with shotcrete loosening of smaller blocks will be prevented which secures the arch shape of the tunnel and its load carrying capacity. Bond failure can occur already at deformations of about a few millimetres which can lead to catastrophic failures for un-reinforced linings. If the shotcrete is reinforced with e.g. fibres or steel mesh it can maintain its functionality also when bond failure has occurred partly over the concrete–rock interface [1]. When shotcrete interacts with rock bolts in the rock mass surrounding a tunnel, or other shotcreted underground openings, the lining may be subjected to concentrated punch loads from the bolts, or from loose rock blocks. In such cases the supporting function of the shotcrete lining will be maintained through three stages [2]. During the first stage, the bond along the concrete–rock interface will be dominant. After primary bond failure flexural resistance from bending in the undamaged lining will carry the load, during continuous crack growth. Then, during the third and final stage, the lining acts as a membrane before totally losing its supporting effect. The importance of the rock-shotcrete bond was demonstrated during in situ testing of young shotcrete subjected to vibrations from blasting [3]. It was concluded that shotcrete, up to 24 hours old, can withstand vibration levels at which a cracked rock mass is seriously damaged and that the main failure mode is loss of the bond between shotcrete and rock. During the evaluation of the test results (see e.g. [4] and [5]) it became evident that accurate estimations of the early bond strength are needed as input to numerical models. It was also found that different rates of growth for material parameters such as tensile strength, elastic modulus and bond strength will lead to stress concentrations during certain periods of the shotcrete hardening process. It is not possible to analyse these phenomena using known material data for ordinary, cast concrete. Shotcrete has basically the same material composition as cast concrete but the method of placement, also including the use of set accelerators, gives a material with unique properties and performance.

The bond strength, or adhesive strength, between two materials in contact is determined by a combination of mechanisms, where mechanical interlocking and adsorption can be mentioned among others [6]. Other factors, such as the material microstructure and interface surface geometry, also contribute to the overall strength and reliability of a bonding situation. The bond strength of shotcrete can thus be defined as the ability to adhere to a particular surface, which often is rock or concrete. The bond strength possible to obtain on hard rocks surfaces is governed by type of rock, the condition of the rock surface and the method of spraying, i.e. using wet-mix or dry-mix method, see [7]. In the following, conditions that primarily applies to wet-mix shotcrete are assumed, unless otherwise stated. In the case of wet-mix shotcrete, care

must be taken when using accelerators since these will, apart from accelerating the rate of strength growth, also affect the rate of shrinkage which may lead to severe loss of bond [1]. Therefore the skill and accuracy of the operator handling the spraying equipment are of vital importance. Thus, there is a need for data on the early age bond strength development for shotcrete and this also requires reliable test methods. In this paper a new laboratory test method that can be used immediately after shotcreting, or casting, is presented and evaluated. Results from tests with cement mortar and concrete, cast not sprayed but bonding to concrete and rock, are given. These results will be used as reference for future tests that will be performed with shotcreted samples. By comparing the results obtained in the two types of test the effect of the shotcreting process, also including the set accelerators, will be possible to evaluate.

2. BOND STRENGTH

Sections of shotcrete with partial loss of bond to the rock substrate can usually be detected in situ with the simple and fast method of manual hammer soundings, where drummy sound is the indicator. The bond strength between shotcrete and rock, or other substrates, is usually determined by pull-out tests directed perpendicularly to the rock wall. A variety of testing techniques exists but most of these methods are intended for testing of fully hardened shotcrete and are not suitable for very young and un-hardened shotcrete. The following section discusses existing methods for bond strength measurements. The knowledge of the bond strength which is possible to obtain for fully hardened shotcrete on various types of rock, and concrete, is then summarized, followed by comments on strength levels which can be expected for young shotcrete.

2.1 Bond strength testing

The most common technique for bond strength testing of shotcrete is to pull cores, pre-drilled through the concrete and the outer layer of the rock, see e.g. [1]. As schematically shown in Figure 1(a) there are three failure modes possible; complete bond failure, shotcrete tensile failure and rock failure. It is also possible that combinations of these modes will occur. The technique is well adapted for use in situ but can also be suitable for laboratory testing, also on horizontal surfaces. One drawback of the method is that friction may occur between the test core and the cylinder casing of the drill which may damage the bond at the shotcrete-rock interface. The method cannot be used with very young shotcrete which is not hard enough for drilling. Also, it must be possible to support the pull-out device on the shotcrete surface. An alternative technique is to pull steel discs through the shotcrete lining [8], as shown in Figure 1(b). The discs, mounted on the rock surface prior to spraying, will displace a conical piece of concrete with a failure mode that is a mix of bond loss and tensile failure. This method will not give a direct measure of the bond strength but can, however, be used immediately after the concrete has been sprayed.

This paper suggests and evaluates a new approach intended for laboratory testing with cast or sprayed specimens, possible to use immediately after applying the material on the substrate. The principle of the method is schematically described in Figure 1(c) where it can be seen that the direction of pull is reversed compared to the other two methods. This is possible since the method is intended for laboratory work where the substrate is represented by a slab of finite thickness, of e.g. rock or concrete. The slab will be prepared with a pre-drilled hole in which a solid, cylindrical core is placed and fixed in position prior to application of the test material. This can be shotcrete or concrete cast on top of the slab, covering the core and bonding to its cross section surface and the surrounding slab. Since the core is pre-drilled there will be no disturbance on the shotcrete-rock bond prior to the pull-out and as there is no contact between core and slab, due to the gap, there will be no friction losses. The test set-up can be arranged either with the shotcrete side facing downwards, as in the figure, or upwards.

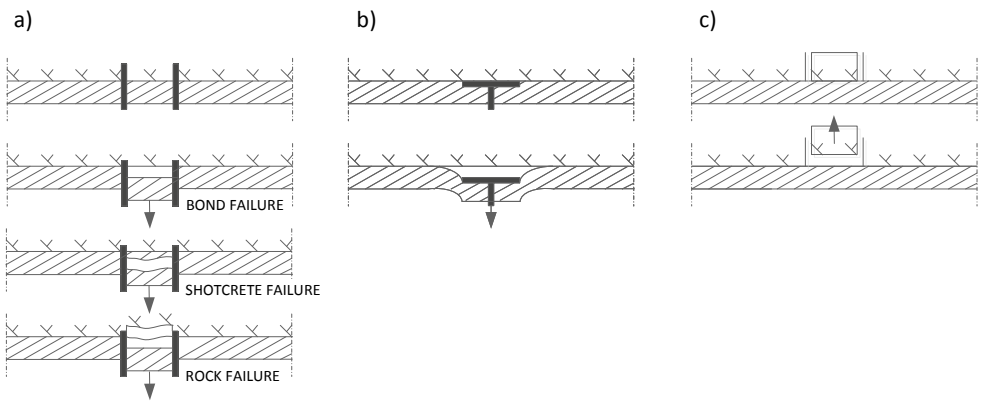

Figure 1 – Methods for bond strength testing. Pull-out of drilled test cores (a), pull-out of shotcrete covered steel discs (b) and pull-out in the reversed direction of a substrate core (c).

2.2 Fully hardened shotcrete on rock or concrete

Examples of documented bond strength values, from laboratory testing and in situ measurements, are presented and compared in Table 1, from a compilation published by Bryne et al. [9]. Each of these tests is briefly summarized and commented in the following. First, measured values for shotcrete on concrete surfaces are given. These are of interest as reference values since a concrete surface is plane and more even than most in situ rocks, and with a mineralogical composition nearly identical to that of shotcrete. Tests with shotcrete on a well-cleaned concrete wall were performed by Malmgren et al. [10] presenting values within 0.6–2.0 MPa. The concrete surface had been sandblasted prior to spraying. The results are similar to those presented by Silfwerbrand [11] who presents results from test carried out with shotcrete sprayed on old concrete that had been tooled with a jackhammer. The results from these pull-out tests show values between 1 and 2 MPa and it is interesting to note that torsional testing in the same material gave higher values for the bond shear strength. Bond strength values possible to

obtain on different types of rock are presented by Hahn & Holmgren [12]. The tests were conducted in a tunnel under well controlled conditions with shotcrete older than 28 days that had been sprayed on rock panels with different surface configuration. The variation in results depending on if the rock surface was smooth or rough is shown in Figure 2. It is concluded that the type of rock mineral is more important than the roughness of the surface and that the increase in bond strength due to surface roughness is mainly caused by the surface magnification gained compared to a smooth surface. Results obtained with shotcrete on sandstone and shale are also presented by Kumar et al. [13], who show results within 0.1–0.5 MPa, comparable to those put forth by Hahn & Holmgren [12]. The influence of surface roughness was observed and it is also concluded that there is no effect on the bond strength from an increase in tensile strength of the rock. As a conclusion from laboratory testing, Saiang et al. [14] comment that the bond strength between shotcrete and rock is almost similar in size to the tensile strength of the shotcrete.

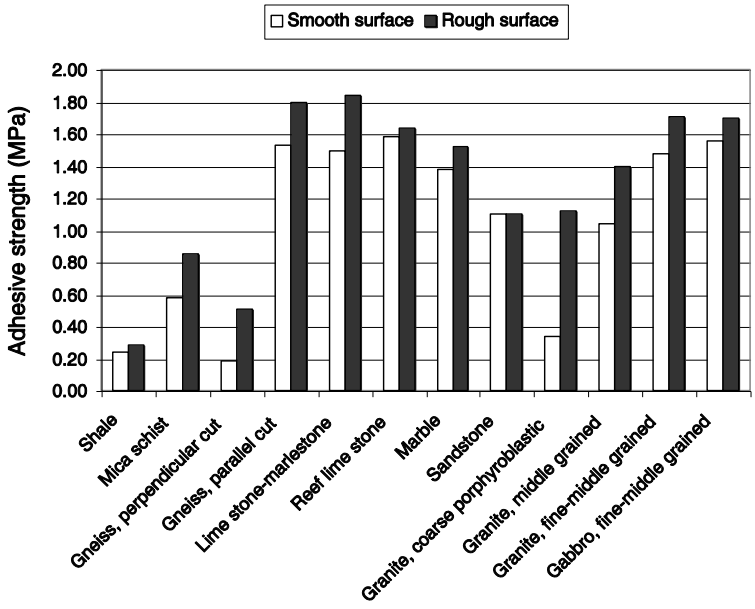

Figure 2 – Obtained bond strength between sprayed concrete and various types of rock, from testing by Hahn & Holmgren [12]. Figure from [4].

Table 1 – Examples of bond strength obtained from pull-out testing of fully hardened shotcrete, sprayed on different substrates. From Bryne et al [9].

Bond strength (MPa)	Surface	Reference
0.6–2.0	Concrete	Malmgren et al. [10]
1.0–2.0	Concrete	Silfwerbrand [11]
0.1–0.3	Shale	Kumar et al. [13]
0.2–0.3	Shale	Hahn & Holmgren [12]
0.6–0.9	Mica schist	Hahn & Holmgren [12]
0.1–0.5	Sandstone	Kumar et al. [13]
1.1	Sandstone	Hahn & Holmgren [12]
0.3–0.4	Magnetite (iron ore)	Malmgren et al. [10]
0.7–1.1	Magnetite (iron ore)	Ansell [3]
1.4–1.5	Marble	Hahn & Holmgren [12]
0.3–1.7	Granite	Hahn & Holmgren [12]
1.6–1.7	Gabbro	Hahn & Holmgren [12]
0.2–1.8	Gneiss	Hahn & Holmgren [12]
1.5–1.8	Lime stone	Hahn & Holmgren [12]
1.0–3.0	Quartz diorite	O'Donnell & Tannant [8]
0.0–2.0	Usual results	Holmgren [2]
>0.5	At normal tunnelling conditions	Holmgren [2]
≤0.5	Recommendation, hard granite	Vandewalle [7]
1.4 (mean)	Tunnelling, wet-mix method	Ellison [15]
1.0 (mean)	Tunnelling, dry-mix method	Malmberg [16]
0.9 (mean)	Tunnelling, wet-mix method	Malmberg [16]

Pull-out tests in situ usually give results between 0 and 2 MPa, depending on the conditions. For tunnelling in hard rock, values higher than 0.5 MPa are realistic [2]. This should be compared to the in situ mean values measured during tunnelling work, [15] and [16], listed in Table 1 that are within 0.9–1.4 MPa. However, relatively low values are often used for practical design work due to uncertain rock performance and lack of knowledge. E.g. for shotcrete on hard granite a recommended design value of 0.5 MPa is often given, see e.g. Vandewalle [7]. Tests conducted

in a Canadian mine, where the rock type was quartz diorite of good quality [8], showed results within 1–3 MPa. It should be noted that these results in some cases exhibited higher values than the results presented by Hahn & Holmgren [12]. However, in this case the bond strengths were obtained by calculation from measured pull-out forces using the method with a pull-out disc, see Figure 1(b). It is well known that a clean rock surface is of outmost importance if a good bond to the shotcrete is to be reached. This was pointed out already by Barbo [17], who showed that surfaces polluted by diesel exhausts reduce the bond strength. It is also well known that free water on the rock surface has a negative effect, [18]. The effect from various types of surface treatment was investigated by Malmgren et al. [10]. Three different methods of surface preparation on iron ore (Magnetite) were tested; mechanical scaling, scaling and high-pressure water washing and water-jet scaling. The results show that for areas with only mechanical scaling over one third of the samples indicated no bond between rock and shotcrete. For the other two methods only 7–17 % of the tests resulted in zero bond strength, which demonstrates the importance of spraying on a well-cleaned rock surface. The results showed an overall poor bond strength of 0.3–0.4 MPa but another, smaller test series carried out in the same mine gave values within 0.7–1.1 MPa [3].

2.3 Early age shotcrete

Due to the practical problems associated with pull-out testing of very young shotcrete there are few documented test results available. Most results that can be seen as relevant and of interest deal with shotcrete older than 48 hours. The tests reported by Malmgren et al. [10], with shotcrete on a well-cleaned concrete wall, show 0.3–0.6 MPa bond strength after 2 days and 0.6–1.0 MPa after 7 days. At 28 days the corresponding strength is 0.8–1.4 MPa, finally reaching up to 2.0 MPa as seen in Table 1. The results had a significant scatter, which is thought to be due to the variation in distance between nozzle and substrate rather than variation in concentration of the set accelerator used. The results indicate that there is a correlation between the growth of compressive and bond strengths, respectively. Results for shotcrete ages of 1–90 days are presented by Seymour et al. [19]. The pull-out tests with shotcrete on concrete test panels showed a bond strength of 0.4 MPa at 24 hours of shotcrete age and 1.1 MPa at 72 hours. When fully hardened, in this case defined as 90 days of age, the bond strength was 1.6 MPa. It was concluded that this is within the normal range of bond strengths specified for shotcrete sprayed on concrete substrates. The test series with shotcrete on sandstone and shale presented by Kumar et al. [13] also contain values for 2–7 days old shotcrete. For sandstone the bond strengths, at 2, 3, 4, 5 and 7 days, are approximately 0.03, 0.13, 0.21, 0.29 and 0.30 MPa. This should be compared with 0.50 MPa at 28 days, which is listed in Table 1. For shale a bond strength value of only 0.03 MPa was reached after 7 days, which should be compared with 0.30 MPa at 28 days. From tests using a method with a pull-out slab, see Figure 1(b), similar to what was used by O´Donnell and Tannant [8], strength values from testing at the first few hours after shotcreting are presented by Bernard [20]. The focus was, however, not primarily on the bond strength but on the load resistance associated with shear or flexural failure in the concrete lining.

The bond strength of shotcrete on rock for age of 24 hours was observed to be as low as 0.2 MPa in this case.

3. MATERIALS AND TEST METHOD

In this initial study no sprayed shotcrete samples were tested, instead samples cast from cement mortar and concrete with a composition equal to that of shotcrete were used. The suggested test method can be adopted for use with both cast and sprayed samples and the focus of this part of the investigation was on the practical aspects of the bond strength testing procedure and to compile reference data to be used for comparison with future results obtained with shotcreted samples. For this reason the compressive strength development was also investigated.

3.1 Tested materials

For this laboratory investigation shotcrete was substituted with cast concrete with a composition comparable to standard concrete used for spraying, with a water-cement ratio of 0.45. Earlier results from tests with cement mortar are also included for comparison. The two materials are sprayable but contain different types of cement, thereby demonstrating the different rates of strength growth that is obtained with the two most common Swedish cement types. The composition of the cement mortar is given in Table 2. This material contains the cement type "Byggcement" which is of quality CEM II/A-LL 42.5 R, a "cement for housing", [21]. Preliminary results from tests with this material are presented by Bryne et al. [9] and Bryne & Ansell [22].

Table 2 – Composition of cement mortar used in the earlier tests. The cement is Swedish type "Byggcement" (cement for housing, CEM II/A-LL 42.5 R). From [9].

Composition	
Cement type	CEM II/A-LL 42.5 R
Cement content	427 kg/m^3
Water content	192 kg/m^3
Aggregates, 0–6 mm	1923 kg/m^3
Density	2542 kg/m^3

The composition of the tested concrete is given in Table 3. The cement used is Swedish type "Anläggningscement" (CEM I 42.5 N – SR 3 MH/LA), which is a slower reacting cement for "civil engineering use", [21]. The maximum aggregate size is here restricted to 8 mm, which

often is the norm for standard wet-mix shotcrete. To investigate the effect on the bond strength from set accelerators used in shotcrete two series of bond strength tests were performed, first with non-accelerated concrete and then with addition of an alkali-free set accelerator, at 3% of the cement weight. The set accelerator was mixed in by hand and the mix then had to be applied quickly for bond strength testing. No concrete cubes including accelerators for compressive strength testing were cast for this investigation. This was mainly due to the practical problems with quickly mixing and casting homogeneous volumes of accelerated concrete. The effect of the set accelerator inside a concrete cube is probably also different from that in a thin shotcrete shell, since the early cement hydration reactions will take place in a stiff structure produced by the set accelerator, see [23]. Preliminary results, and comments, from compressive strength testing of the concrete described in Table 3 are given by Hedenstedt & Ryberg, [24].

Table 3 – Composition of the concrete used in the tests. The cement is Swedish type "Anläggningscement" (cement for civil engineering use, CEM I 42.5 N – SR 3 MH/LA).

Composition	
Cement type	CEM I 42.5 N –SR 3 MH/LA
Cement content	495 kg/m^3
Silica U	19.8 kg/m^3
Water content	221 kg/m^3
Glenium 51	3.5 kg/m^3
Aggregates, 0–2 mm	394 kg/m^3
Aggregates, 0–8 mm	1183 kg/m^3
Density	2316 kg/m^3

3.2 Compressive strength

The two tested materials (Tables 2–3) were cast as 150 mm cubes, tested to determine the growth in compressive strength. Tests were performed according to standard [25], which was possible from 6 hours of age for the mortar (Table 2) and from 10 hours for the concrete (Table 3). The cube strength results are shown in Figure 3, where curves fitted to the results, using the method of least squares, also are shown. For the mortar, the equation of the curve is as follows:

$$f_{cc} = 139.5 e^{-1.706/t^{0.821}} \text{ (MPa)} \quad \text{for} \quad 0 \le t \le 24 \text{ hrs.} \tag{1}$$

and for the concrete the corresponding equation is:

$$f_{cc} = 28.4\,e^{-0.661/t^{1.653}} \quad \text{(MPa)} \quad \text{for} \quad 0 \le t \le 48 \text{ hrs.} \tag{2}$$

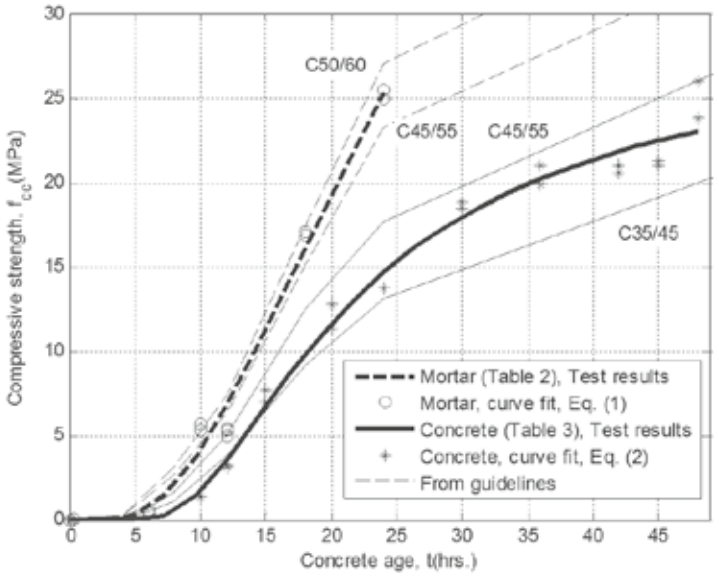

Figure 3 – Compressive cube strengths vs. age of concrete from laboratory tests for cement mortar and concrete, compared with the strength growth curves specified in guidelines [26].

The equations are on the form suggested by Byfors [27] and it should be noted that they are valid within the time intervals specified for *t*, which should be given in hours. The mortar was only tested up to 24 hours of age, see [9, 22], while the concrete was tested up to 48 hours, see [24]. As can be seen in Figure 3 the initial strength growth rate for the mortar is almost twice as that for the concrete, which is due to the slower hardening cement type "Anläggningscement" (CEM I). It should, however, also be noted that the mortar was tested at a temperature of +22 °C and the concrete at +20 °C, which may contribute somewhat to the more rapid hardening of the mortar. The relative humidity was held constant at 50% during the tests presented in [9,22] and 30 % during the tests in [24], respectively. As a comparison, the average strength growth curves for concrete with Swedish types of cement according to the guidelines [26] are also shown. As seen, the test results for the mortar is between the curves for C45/55 and C50/60 while the corresponding curves for the concrete are C35/45 and C45/55, respectively. Since the composition of the tested concrete (Table 3) is intended for shotcrete use, slump testing [28] was also carried out in this case. The results showed slump values within 210–245 mm, thus indicating a sprayable concrete.

3.3 Test procedure

The test method schematically described in Figure 1(c) is intended for use with shotcrete sprayed on different types of rock materials, or concrete. The initial tests were, however, performed with cast concrete and mortar, bonding to granite and concrete, respectively. For the cast test specimens a 450×450 mm^2 mould was used, as seen in Figure 4. The concrete, or mortar, was cast to a level of 40 mm, in line with the wooden blocks at each corner of the mould. On these blocks precast C25/30 concrete slabs 350×350×40 mm^3 were then placed. Through the centre of the slabs a circular ϕ100 mm hole had been drilled which was later covered by a ϕ95 mm core, with a coupling steel ring on its upper surface, fixed with a hardened adhesive (glue), see Figure 5. For the initial tests using cement mortar (see Table 2) the concrete cores from the slabs were used and for the later test series with concrete (see Table 3) these were replaced by granite cores. To get a proper wetting of the mortar (or concrete) to the core a 1–2 cm layer of concrete was applied on the surface before the core was mounted back in the hole and pushed into the fresh cast material. The gap between slab and core was sealed with wetted paper, allowing the core to be pulled out without friction resistance. The bond strength tester was then applied and mounted to the test disc concentrically, as seen in Figure 6. Then, the entire equipment was covered by a plastic sheet in order to prevent drying shrinkage before testing. The testing device was driven manually but instrumented with a load cell and a strain gauge (LVDT) connected to a PC.

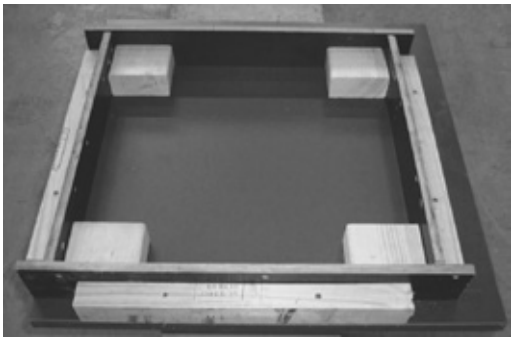

Figure 4 – Casting mould with wooden block supports for precast concrete slabs.

When used for shotcrete testing the cores will be fixed centrally in the holes of the slabs and the gap sealed prior to spraying. The testing device can also be positioned in the reverse direction, so that the cores can be pulled downwards. In the case of shotcreting the material will be compacted during spraying. In the case with cast specimens there will be a minimum of compacting pressure at the contact interface between the core and the newly cast material and, thus, these bond strength results will not be affected by the impact from spraying. Also, the surface of the test cores are plane and therefore more even than rock in situ. The surface texture was un-polished but fine grained for the concrete cores, while the granite cores were sawn or ground.

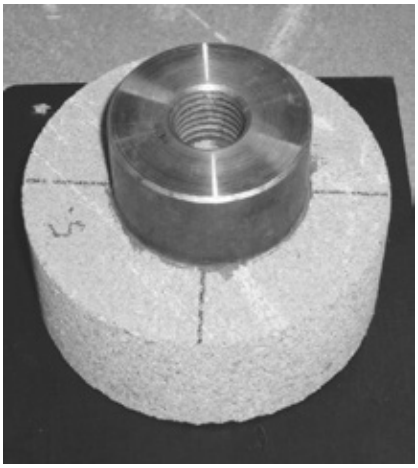

Figure 5 – Core of concrete adhered to a steel disc to be mounted to the testing device.

Figure 6 – Precast concrete slab on top of newly cast concrete and bond strength testing device with load cell and strain gauge (LVDT).

4. TEST RESULTS

The results from bond strength testing of the cement mortar described in Table 2 are shown in Figure 7. The test series was used as a pilot test including mortar 6–24 hours old with concrete cores used for the pull-out, see [9]. Two samples (each time) were tested at 6, 10, 12, 18 and 24 hours. Only one measurement at the age of 10 hours was successful since the second test failed due to delamination between the steel coupling disc and the concrete core. The high value of 1.15 MPa at 24 hours was actually a tensile failure in the concrete core and not a bond failure between mortar and core, thus indicating a possibly even higher strength value at this age. The failure was superficial and could have been caused by low quality in the concrete slab from which the core was taken. A curve of the same type as given by Eqs. (1)–(2) has been fitted to the results, also in this case using the method of least squares, giving:

$$f_{cb} = 1.68 e^{-0.571/t^{1.230}} \text{ (MPa)} \quad \text{for} \quad 0 \le t \le 24 \text{ hrs.} \tag{3}$$

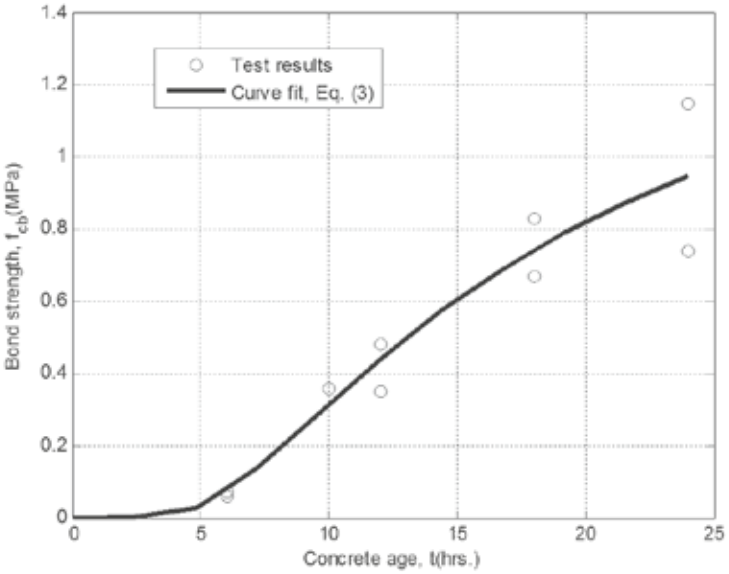

Figure 7 – Bond strength test results vs. age of cement mortar (Table 2).

The concrete defined in Table 3 was tested at 4, 8, 12, 18, 24, 36, 48 and 72 hours, also in this case using two samples at each age. The cores used for these tests were of granite while the surrounding slabs were of precast concrete, as in the first test series. The concrete was mixed with and without set accelerator, giving two separate series. With the addition of the alkali-free set accelerator it was possible to get measurable bond strength results already after two hours. The results are shown in Figure 8 where it can be seen that the bond strength development is faster for the accelerated concrete within the first 10 hours but after this lower values are

obtained compared to the non-accelerated samples. For values over 0.7 MPa, failures frequently occurred in the adhesive between the granite core and the steel coupling ring. These tests have been excluded in Figure 8 and the test cores were later replaced by ϕ100 mm steel discs, for comparison with the smaller ϕ50 mm ones previously used, thus reducing the tensile stress in the adhesive between steel disc and granite core that could be well over 1.5 MPa, in this case enough to cover concrete ages up to 72 hours. It should be noted that in both series there is a comparatively large scatter in the results at 48 hours. As for the cement mortar in Figure 7, curves have been fitted also to these results. For the non-accelerated test series the curve is as follows:

$$f_{cb} = 1.30\,e^{-0.690/t^{1.250}} \text{ (MPa)} \quad \text{for} \quad 0 \le t \le 72 \text{ hrs.} \tag{4}$$

for the accelerated series a less convex shape is given below as:

$$f_{cb} = 3.64\,e^{-2.154/t^{0.447}} \text{ (MPa)} \quad \text{for} \quad 0 \le t \le 72 \text{ hrs.} \tag{5}$$

The failure types that were observed during the tests were perfect delamination, i.e. full bond failure, and tensile material failures close to the bonding interface. In the latter case areas of concrete, or mortar, remained on the surface of the test cores. The two types of failures occurred with the same frequency and the results have not been separated. Examples of the two failure types are shown in Figure 9.

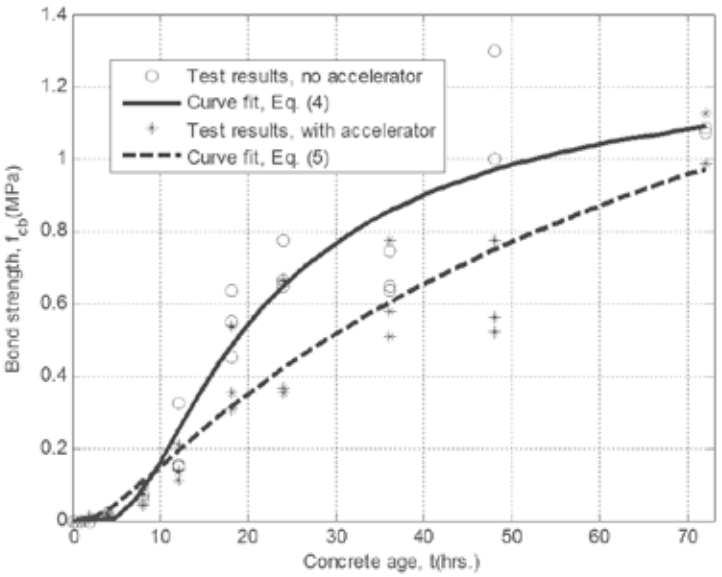

Figure 8 – Bond strength test results vs. age of concrete (Table 3). Results obtained with and without set accelerator.

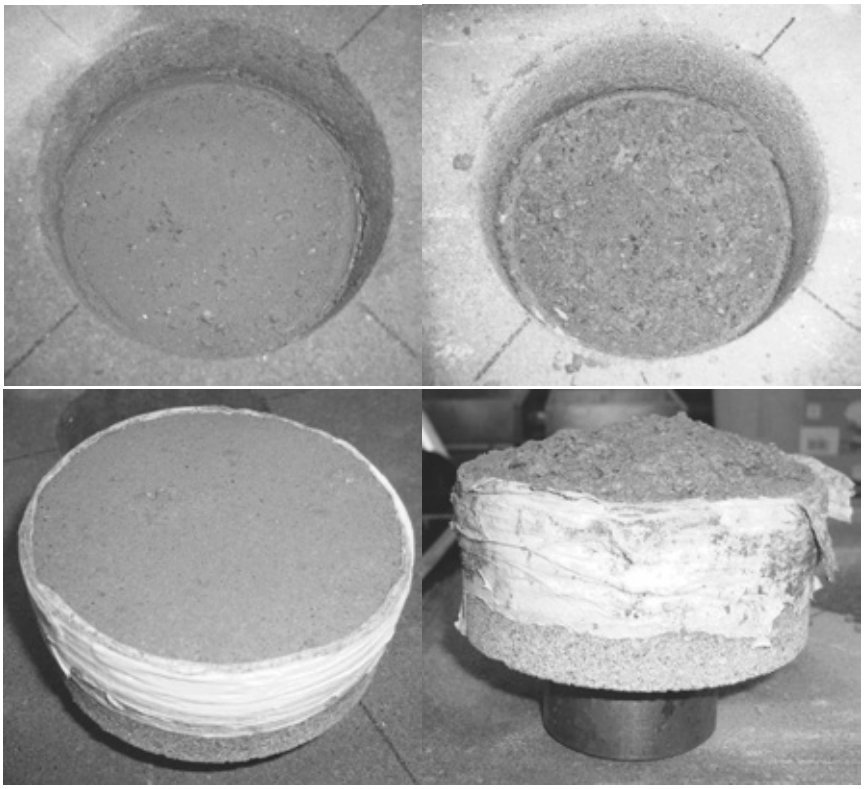

Figure 9 – Typical failure surfaces, delamination (left) and tensile, material failure (right).

5. CONCLUSIONS

The new laboratory test method was tested and evaluated and it was shown that the method can be used for bond testing in laboratory, from a couple of hours after the placement of cast cement based specimen. The test results presented can be used as reference for the evaluation of future tests with shotcreted samples.

5.1 Test method

The newly developed test method proved to be well suited for use in laboratory environments and reliable for testing of cast samples. Experiences from the trials with the new method will be of great importance when it is adapted for use with shotcreted test samples. Steel discs with a larger diameter were used from 24 hours hardening time, capable of higher pull-out forces since adhesive failures could be prevented. It should be mentioned that the difference in weight of the different sized steel discs is 1.3 kg. The type of adhesive between the test cores and the steel coupling rings has been upgraded for larger pull-out forces. The tests also showed that the used

concrete cores were of low strength which resulted in some concrete tensile failures for bond stresses over 1.2 MPa. For further testing with concrete cores a higher strength class must therefore be used for tests with shotcrete older than 24 hours. It should be pointed out that the method is intended for use with rock cores of high quality. Other details that must be adjusted before shotcreting is possible are to arrange a practical re-fixation of the cores to the slabs and to seal the gap between core and slab. The latter must withstand the pressure from the impacting shotcrete without disturbing the pull-out by inducing friction resistance. The precast concrete slabs will be replaced by larger, more rigid slabs of granite in which several holes will be drilled in each slab. The pull-out cores will be the drilled out parts of the slabs. In the case with sprayed samples the pull direction will be upwards as shown schematically in Figure 1(c).

5.2 Early age bond strength

The pull-out test method resulted in a combination of bond and tensile failure, as shown in Figure 9. However, for concrete samples older than 24 hours pure bond or delamination failures occurred. The pull-out test method resulted in pure bond strength failures until about 1.1 MPa was reached and after this a combination of bond and tensile failures occurred in some cases. However, some material failures also occurred during the first 8 hours, especially in the test series with the granite cores, which probably is due to low tensile strength for the cast mortar or concrete. The results shown in Figures 7–8 cover the bond strength growth up to 1 MPa. For the cement mortar, containing the faster cement type “Byggcement” (cement for housing, CEM II/A-LL), this level is reached in 24 hours while for the concrete, based on the slower “Anläggnings-cement” (cement for civil engineering use, CEM I), it takes almost 72 hours to reach this strength. By comparing the curves in Figure 8 it is evident that the set accelerator after about 10 hours has a negative effect on the rate of the bonding strength growth. The curves have started to converge at 72 hours but the largest difference that occurs is 0.2 MPa at approximately 36 hours of concrete age. In comparison to other work, e.g. the study presented by Malmgren et al. [15] who show 0.3–0.6 MPa bond strength after 2 days and 0.6–1.0 MPa after 7 days, the bond strength in the present study has developed faster. This is probably due to the climate conditions which in the latter case were +12 °C with a relative humidity of 80 %, in underground environment, in comparison with the laboratory environment with +20–22 °C and 30–50 % relative humidity. Comparing the rate of bonding strength growth with that of compressive strength in Figure 3 is of great interest for future modelling of the stresses that occur in hardening shotcrete on rock. The direct relation between bonding and compressive strengths for the presented test results is shown in Figure 10. It can be seen that the accelerated concrete shows significantly lower bond strength than the other two materials, for the same compressive strength. The exception is for the lowest strength levels where the bond strength of the accelerated concrete shows a rapid development. A comparison between material age and the rate of strength growth is made in Figure 11.

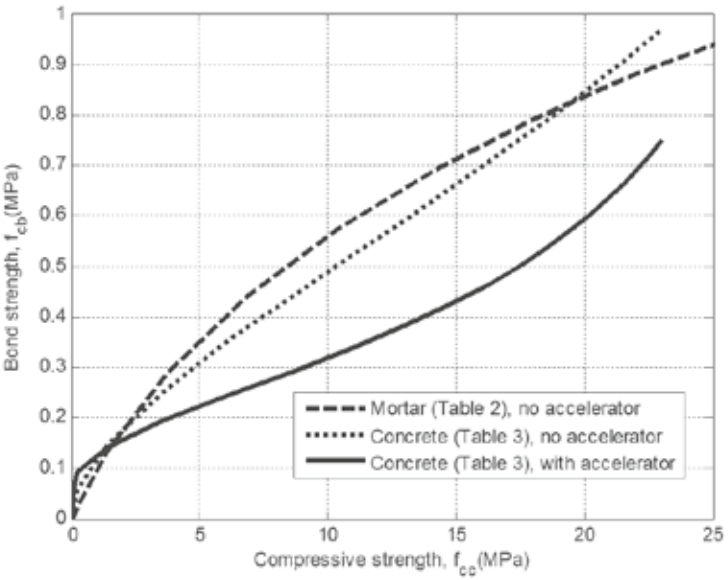

Figure 10 – Compressive strength vs. bond strength of cement mortar and concrete.

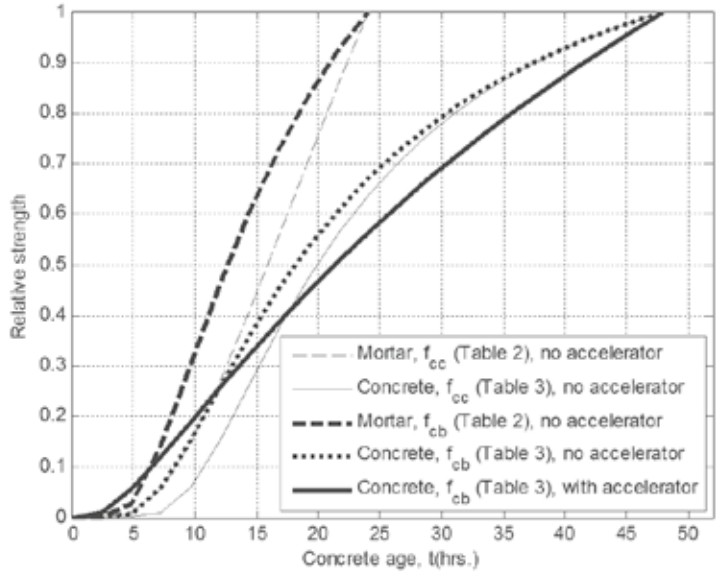

Figure 11 – Compressive (f_{cc}) and bond strengths (f_{cb}) vs. age of cement mortar and concrete. Values given in relation to the 24 and 48 hour strengths, respectively.

5.3 Further research

The material properties of shotcrete sprayed on rock need to be further investigated in order to provide values representative for in situ conditions. Next step in the investigation of the bond strength for hardening shotcrete will be laboratory investigations using sprayed test samples. This test series should focus on the development during the first 3–4 days after shotcreting. The effects of set accelerators are of special interest. Microstructural studies will be made in connection with the pull-out tests in order to investigate e.g. the formation and development of ettringite in the interfacial zone of hard rock. Surface chemical studies of the hard rock surface will also be carried out, together with investigations of the surface roughness on microscale. It is also of interest to study the development of shotcrete material properties under different climate conditions, i.e. temperature and humidity conditions other than in the indoor laboratory. The laboratory test results will provide a reference basis for comparison with future in situ tests, where a great scatter is always found and which are difficult to analyse due to variations in rock quality, rock wall geometry and the shotcreting process.

ACKNOWLEDGEMENTS

The presented laboratory investigations constitute part of a project that studies the material properties of young and hardening shotcrete. The project is supported by *BeFo*, The Rock Engineering Research Foundation, *Formas*, the Swedish Research Council for Environment, Agricultural Sciences and Spatial Planning, *SBUF*, the Development Fund of the Swedish Construction Industry and *Trafikverket*, the Swedish Transport Administration. Their support is hereby greatly acknowledged!

REFERENCES

1. Holmgren, J., Alemo, J., Skarendahl, Å., “Stålfiberbetong för bergförstärkning – provning och värdering” (In Swedish, “Steel fibre sprayed concrete for rock strengthening – testing and evaluation), CBI rapport 3:97, Swedish Cement and Concrete Research Institute, Stockholm, Sweden, 1997.
2. Holmgren, J., “Bergförstärkning med sprutbetong” (In Swedish, “Rock reinforcement with shotcrete”), Vattenfall, Vällingby, 1992.
3. Ansell, A., “In situ testing of young shotcrete subjected to vibrations from blasting”, *Tunnelling and Underground Space Technology*, Vol. 19, 2000, pp. 587–596.
4. Ansell, A., “Recommendations for shotcrete on rock subjected to blasting vibrations, based on finite element dynamic analysis”, *Magazine of Concrete Research*, Vol. 57, 2005, pp. 123–133.
5. Ansell, A., “Dynamic finite element analysis of young shotcrete in rock tunnels”, *ACI Structural Journal*, Vol. 104, 2007, pp. 84–92.

6. Kinloch, A.J., "The science of adhesion. Part 1 – Surface and interfacial aspects", *Journal of Materials science*, Vol. 15, 1980, pp. 2141–2166.
7. Vandewalle M., "Dramix – Tunnelling the World. With 7 Reference Projects", 6th edn. N.V. Bekaert S.A., Zwevegem, Belgium, 1998.
8. O'Donnell, J.D.P. Sr., Tannant, D.D., "Pull tests to measure the in situ capacity of shotcrete", CIM-AGM, Montreal, Canada, 1997.
9. Bryne L.E., Holmgren J., Ansell A., "Experimental investigation of the bond strength between rock and hardening sprayed concrete", Proceedings, 6th International Symposium on Sprayed Concrete, Tromsö, Norway, September 2011, pp. 77–88.
10. Malmgren, L., Nordlund, E., Rolund, S., "Adhesion strength and shrinkage of shotcrete", *Tunnelling and Underground Space Technology*, Vol. 20, 2005, pp. 33–48.
11. Silfwerbrand, J., "The influence of traffic-induced vibrations on the bond between old and new concrete", Bulletin 1992 No.158. Dept. of Structural Mechanics and Engineering, KTH, Stockholm, Sweden, 1992.
12. Hahn, T., Holmgren, J., "Adhesion of shotcrete to various types of rock surfaces and its influence on the strengthening function of shotcrete when applied on hard jointed rock", Procedings, 4th International Congress on Rock Mechanics, International Society for Rock Mechanics Montreux, Switzerland, 1979, Vol. 1, pp. 431-440.
13. Kumar, D., Behera, P.K., Singh, U.K., "Shotcreting and its adhesion strength", *Electronic Journal of Geotechnical Engineering*, Vol. 7A, 2002, 12 pp.
14. Saiang D., Malmgren L., Nordlund E., "Laboratory tests on shotcrete–rock joints in direct shear, tension and compression", *Rock Mechanics and Rock Engineering*', Vol. 38, 2005, pp. 275–297.
15. Ellison, T., "Vidhäftningsprovning Södra länken Stockholm" (In Swedish, "Bond strength testing at Södra länken Stockholm"), Test report, Besab, Gothenburg, Sweden, 2000.
16. Malmberg, B., "Sprutbetong – uppföljning av sprutbetongprovningar på Grödinge-banan" (In Swedish, "Shotcrete – evaluation of shotcrete testing at Grödingebanan"), No. T93-913/34, Banverket, Borlänge, Sweden, 1993.
17. Barbo, T., "Sprøytebetong – betongteknologi. Heftfasthet" (In Norwegian, "Sprayed concrete – concrete technology. Bond strength"), Kontor for fjellsprengningsteknikk, Oslo, Norway, 1964.
18. Karlsson, L., "Sprutbetong mot olika bergytor" (In Swedish, "Shotcrete on various rock surfaces"), Byggforskningsrådet, Stockholm, Sweden, 1980.
19. Seymour, B., Martin, L., Clark, C., Stepan, M., Jacksha, R., Pakalnis, R., Roworth, M., Caceres, C., "A practical method of measuring shotcrete adhesion strength", Proceedings, SME Annual Meeting and Exhibit 2010, Phoenix, USA, pp. 1–9.
20. Bernard, E.S., "Early-age load resistance of fibre reinforced shotcrete linings", *Tunnelling and Underground Space Technology,* Vol. 23, 2008, pp. 451–460.
21. "Glossary of Concrete Terms, Swedish-English", Betongrapport nr 17, Swedish Concrete Association, Stockholm, Sweden, 2012.

22. Bryne L.E., Ansell A., “Laboratory testing of the bond strength between shotcrete and rock”, Proceedings, fib Symposium - Concrete Structures for Sustainable Community, Stockholm, Sweden, June 2012, pp. 433–436.
23. Lagerblad B., Fjällberg B, Vogt C., “Shrinkage and durability of shotcrete”, Proceedings, 3rd International Conference on Engineering Developments in Shotcrete, Queenstown, New Zealand, 2010, pp. 173–180.
24 Ryberg J., Hedenstedt J., “Laborativ utvärdering av utrustning för bestämning av tryckhållfasthet hos sprutbetong” (In Swedish, “Laboratory investigation of equipment for compressive strength testing of shotcrete”), Master Thesis 356, KTH Concrete Structures, Stockholm, Sweden, 2012.
25. SS-EN 12390-3:2009, “Testing hardened concrete - Part 3: Compressive strength of test specimens”, Swedish Standards Institute, Stockholm, Sweden, 2009.
26. “Svenska Betongföreningens handbok till Eurokod 2” (In Swedish, “The Swedish Concrete Association Handbook to Eurocode 2”), Betongrapport nr 15, Swedish Concrete Association, Stockholm, Sweden, 2010.
27. Byfors, J., “Plain concrete at early ages”, Research Fo 3:80, Swedish Cement and Concrete Research Institute, Stockholm, Sweden, 1980.
28. SS-EN 12350-2, “Testing fresh concrete - Part 2: Slump test”, Swedish Standards Institute, Stockholm, Sweden, 2009.

Research Council and Editorial Board for Nordic Concrete Research

Prof. Dr. Olafur H. Wallevik, Chairman for the Research Council
Dr. Dirch H. Bager, Editor of Nordic Concrete Research

28 April 2013

Active reviewers for Nordic Concrete Research as per May 2013

DENMARK	
Dr.	Dirch H. Bager
Prof., Dr.	Lars Damkilde
Dr.	Mette Glavind
Prof., Dr.	Per Goltermann
Mr.	Oscar Klinghoffer
Prof., Dr.	John Forbes Olesen
Mr	Claus Pade
Prof., Dr.	Eigil V. Sørensen
Prof., Dr.	Jens Peder Ulfkjær
FINLAND	
Dr.	Klaus Juvas
Dr.	Matti V. Leskala
Prof., Dr.	Jussi Mattila
Mr.	Erik Nordenswan
Dr.	Jouni Punkki
Mr	Juha Valjus
ICELAND	
Mr.	Einar Einarsson
Mr.	Haukur J. Eiriksson
Dr.	Gisli Gudmundsson
Mr.	Karsten Iversen
Mr.	Torfi G. Sigurdsson
Mr.	Sveinbjörn Sveinbjörnsson
Dr.	Jon E. Wallevik
Prof., Dr.	Ólafur H. Wallevik
Prof., Dr.	Børge J. Wigum
NORWAY	
Dr.	Helge Brå
Ms.	Danielle Bosnjak
Mr.	Anton Gjørven
Mr.	Steinar Helland
Dr.	Bernt Jacobsen
Prof., Dr.	Terje Kanstad
Dr.	Terje F. Rønning
Mr.	Tor Kristian Sandaker
Mr.	Sverre Smeplass
Mr.	Hans Stemland
SWEDEN	
Prof., Dr.	Anders Ansell
Dr.	Thomas Blanksvärd
Prof.	Lennart Elfgren
Prof., Dr.	Mats Emborg
Prof., Dr.	Kent Gylltoft
Prof., Dr.	Mikael Hallgren
Prof., Dr.	Jan-Erik Jonasson
Prof., Dr.	Björn Lagerblad
Prof., Dr.	Karin Lundgren
Prof., Dr.	Tang Luping
Prof., Dr.	Per-Erik Petersson
Prof., Dr.	Johan Silfwerbrand
Dr.	Peter Simonsson
Dr.	Peter Utgenannt